STRUCTURAL AND DYNAMICAL PROPERTIES OF CENTRAL NERVOUS SYSTEM PROTEINS WITH PHARMACEUTICAL AND BIOTECHNOLOGICAL POTENTIAL

Francesca Stanzione

Dottorato in Scienze Biotecnologiche XXIII ciclo
Indirizzo Biotecnologie Industriali e Molecolari
Università di Napoli Federico II

Dottorato in Scienze Biotecnologiche XXIII ciclo
Indirizzo Biotecnologie Industriali e Molecolari
Università di Napoli Federico II

STRUCTURAL AND DYNAMICAL PROPERTIES OF CENTRAL NERVOUS SYSTEM PROTEINS WITH PHARMACEUTICAL AND BIOTECHNOLOGICAL POTENTIAL

Francesca Stanzione

Dottoranda:	Francesca Stanzione
Relatore:	Prof. Ettore Benedetti
Correlatore:	Dr. Luigi Vitagliano
Coordinatore:	Prof. Giovanni Sannia

Ai miei genitori
che mi hanno
sostenuto sempre
e comunque.

INDEX

RIASSUNTO pag. 1

SUMMARY pag. 6

ABBREVIATIONS pag. 8

1. INTRODUCTION pag. 10

1.1. Neurotrophins: structure, functions and therapeutic applications pag. 10

1.1.1. Neurotrophins pag. 10

1.1.2. Biological partners of Neurotrophins pag. 11

1.1.3. Structural characteristics of Neurotrophins pag. 12

1.1.4. Therapeutic applications of Neurotrophins pag. 13

1.2. Amyloid fiber and amyloidogenic peptides pag. 14

1.2.1. Neurodegenerative diseases and Amyloid fiber pag. 14

1.2.1.1. Misfolded protein deposition pag. 15

1.2.2. Amyloid fiber: properties and structural characteristics pag. 15

1.2.3. Amyloid fiber: dynamical properties pag. 18

1.2.4. Amyloid fibers: from diseases to devices pag. 18

1.3. Objectives of present PhD project pag. 19

2. ROLE OF THE CONFORMATIONAL VERSATILITY OF THE NEUROTROPHIN N-TERMINAL REGIONS IN THEIR RECOGNITION BY TRK RECEPTORS pag. 20

2.1. Background pag. 20

2.2. MATERIALS AND METHODS pag. 21

2.2.1. Peptide synthesis pag. 21

2.2.2. CD spectroscopy pag. 21

2.2.3. MD simulations pag. 21

2.3. RESULTS AND DISCUSSION pag. 22

2.3.1. CD spectroscopy pag. 22

2.3.2. MD simulations pag. 23

2.3.2.1. NT4 N-terminal peptide pag. 23

2.3.2.2. MD simulation on the NGF N-terminal peptide pag. 26

2.4. Implications for the molecular recognition of neurotrophins by receptors pag. 27

2.5. Conclusions pag. 28

3. INTRINSIC FLEXIBILITY OF THE NERVE GROWTH FACTOR ANALYZED BY ESSENTIAL MOLECULAR pag. 29

3.1. Background pag. 29

3.2. MATERIALS AND METHODS pag. 30

3.2.1. System pag. 30
3.2.2. Molecular Dynamics parameters pag. 30
3.2.3. Essential dynamics pag. 31
3.4. RESULTS pag. 32
3.4.1. Structural stability of NGF in the simulation pag. 32
3.4.2. NGF fluctuations in MD simulation pag. 34
3.4.3. Essential dynamics and concerned motion pag. 35
3.5. DISCUSSION pag. 37

4. DYNAMICS AND STABILITY OF AMYLOID-LIKE STERIC ZIPPER ASSEMBLIES WITH HYDROPHOBIC DRY INTERFACES pag. 39
4.1. Background pag. 39
4.2. MATERIALS AND METHODS pag. 39
4.2.1. Systems pag. 39
4.2.2. Molecular dynamics parameters and protocols pag. 40
4.3. RESULTS AND DISCUSSION pag. 41
4.3.1. Model peptides with apolar aliphatic interfaces: the case of SSTSAA pag. 41
4.3.2. Model peptides with apolar aliphatic interfaces: the case of VQIVYK pag. 43
4.3.3. Structural stability of the HET-s (218-289) pentamer evaluated by MD simulations pag. 47
4.4. Conclusions pag. 49

5. DYNAMICAL PROPERTIES OF STERIC ZIPPER POLYMORPHS FORMED BY A IAPP-DERIVED PEPTIDE pag. 51
5.1. Background pag. 51
5.2. MATERIALS AND METHODS pag. 51
5.2.1. Models pag. 51
5.2.2. MD parameters and protocols pag. 52
5.3. RESULTS AND DISCUSSION pag. 52
5.3.1. Description of the two SSTNVG polymorphs pag. 52
5.3.2. Molecular dynamics simulations on the 3DG1 model pag. 53
5.3.3. Molecular dynamics simulations on the 3FTR model pag. 56
5.3.4. Molecular dynamics simulations on single ten-stranded sheet of SSTNVG pag. 58
5.4. Conclusions pag. 60

6. INSIGHTS INTO STABILITY OF SYMMETRY-RELATED HPRP MOLECULES BY REPLICA EXCHANGE MOLECULAR DYNAMICS ANALYSES pag. 61
6.1. Background pag. 61

6.2. MATERIALS AND METHODS pag. 62
6.2.1. System setup pag. 62
6.2.2. Replica exchange molecular dynamics pag. 63
6.3. RESULTS AND DISCUSSION pag. 65
6.3.1. System and overall REMD features pag. 65
6.3.1.1. AB 2-stranded β-sheet pag. 65
6.3.1.2. BB' 2-stranded β-sheet pag. 67
6.3.1.3. ABB'A' 4-stranded β-sheet pag. 69
6.3.1.4. M129V and G131V mutants pag. 70
6.4. Conclusions pag. 72

7. CONCLUSIONS AND FUTURE PERSPECTIVES pag. 73

APPENDIX pag. 75

ACKNOWLEDGEMENTS pag. 80

REFERENCES pag. 80

PUBBLICATIONS pag. 90

ORAL PRESENTATIONS pag. 90

POSTER PRESENTATIONS pag. 90

ATTENDED COURSES ANS SCHOOLS pag. 91

RESEARCH ACTIVITY IN SCIENTIFIC INSTITUTIONS ABROAD pag. 91

RIASSUNTO

Le patologie del sistema nervoso centrale comprendono una vasta gamma di malattie ad elevato impatto sociale, causate da disturbi che interessano i neuroni o le altre cellule del tessuto nervoso. Tra queste patologie, un'attenzione sempre crescente è rivolta alle malattie neurodegenerative che includono: le malattie prioniche, il morbo di Parkinson, le malattie di Alzheimer e di Huntington e la sclerosi laterale amiotrofica. Tali patologie sono caratterizzate dalla formazione di depositi fibrillari insolubili di particolari peptidi o proteine che, a causa di uno scorretto *folding* (*misfolding*), acquisiscono la capacità formare aggregati all'interno di specifiche cellule neuronali. L'elevato interesse verso le malattie neurodegenerative è dettato a)dal progressivo aumento della loro diffusione b) dalla scarsa conoscenza dei meccanismi molecolari ad esse associati e (c) dalla conseguente inefficacia degli approcci diagnostici e terapeutici disponibili. In questo scenario, le attività di ricerca per la prevenzione e la cura di tali patologie si muovono su due distinte direttici volte al potenziamento dei fattori in grado di favorire la sopravvivenza e il mantenimento delle cellule nervose e alla definizione dei processi molecolari che portano alla loro insorgenza. In linea con tali esigenze, il presente progetto di dottorato è stato focalizzato sull'analisi dei determinanti strutturali e dinamici dei meccanismi di azione di proteine ad azione neuroprotettiva, (neurotrofine) e sullo studio delle proprietà strutturali di aggregati amiloidi e dei loro precursori tossici che caratterizzano lo stato patologico dei neuroni affetti da patologie di tipo neurodegenerativo.

Le neurotrofine (NTs) sono proteine che giocano un ruolo fondamentale nella differenziazione, sopravvivenza e mantenimento delle cellule nervose. Di questa classe di proteine sono stati identificati cinque membri: il fattore di crescita nervoso (NGF) (Levi-Montalcini, 1964), il Brain-*Derived Neurotrophin Factor* (BDNF) (Barde et al., 1982), la neurotrofina 3 (NT3) (Maisonpierre et al., 1990), la neurotrofina 4 (NT4) (Ip et al., 1991), e la neurotrofina 6 (NT6) (Gotz et al., 1994). Le neurotrofine nella loro forma attiva agiscono come proteine omodimeriche e interagiscono con uno specifico recettore tirosinchinasico (Trk) di cui sono state descritte tre isoforme: TrkA, TrkB, TrkC. (Neet and Campenot, 2001). L'attivazione di questi recettori avviene nella loro porzione extracellulare, con la conseguente dimerizzazione del dominio citoplasmatico che porta alla trasduzione di una serie di segnali indispensabili per la sopravvivenza delle cellule neuronali. Le neurotrofine mostrano una specifica selettività per i recettori tirosinchinasici in particolate, NGF interagisce ad alta affinità con il recettore TrkA, il BDNF e l'NT4 attivano invece il TrkB e infine l'NT3 lega il recettore TrkC. Oltre al recettore tirosinchinasico, tutte le neurotrofine interagiscono con minore affinità con un altro recettore, il $p75^{NTR}$, appartenente alla famiglia dei *Tumor Necrosis Factor Receptor* (TNF), la cui attivazione porta ad apoptosi e conseguente morte delle cellule neuronali (Zampieri et al., 2004).

Numerosi studi hanno mostrato il notevole potenziale terapeutico delle neurotrofine (Saragovi et al., 2009), sebbene le effettive applicazioni siano limitate dalle loro scarse proprietà farmacologiche. Non sorprende, quindi, che particolare attenzione sia dedicata allo sviluppo di nuove molecole dotate di azione NT-agonista o antagonista (Colangelo et al., 2008) (Peleshock and Saragovi 2006). A tal fine è richiesta una profonda conoscenza dei determinanti strutturali, della loro funzione e della loro specificità. Studi cristallografici hanno fornito un'immagine dettagliata delle neurotrofine nei loro stati non legati e in complesso con i recettori (Trk e $p75^{NTR}$) (Wiesmann and de Vos. 2001) (Gong et al., 2008) (Wehrman et al., 2007) (He et al., 2004). D'altra parte, solo dati molto limitati sono disponibili sulle loro proprietà

dinamiche. In questo contesto, nel corso del dottorato è stata condotta una dettagliata indagine delle proprietà dinamiche di diverse regioni delle neurotrofine, mediante tecniche di dinamica molecolare.

In primo luogo è stato condotto uno studio mirato all'identificazione delle preferenze conformazionali intrinseche della regione N-terminale delle NTs, importanti per il riconoscimento e la specificità NT-Trk. Infatti, la regione N-terminale dell'NGF in complesso con TrkA presenta una conformazione di tipo α-elica (Wiesmann and de Vos 2001), mentre quella dell'NT4 in complesso con il TrkB è in elica di tipo 3_{10} (Banfield et al., 2001). Tuttavia, entrambe le regioni N-terminali delle due neurotrofine sono assenti nei modelli cristallografici dei dimeri isolati e nel complesso con il recettore $p75^{NTR}$, lasciando trasparire la loro flessibilità in assenza del recettore e una loro transizione conformazionale nell'interazione con il recettore Trk. Gli studi di dinamica molecolare hanno chiaramente indicato che preferenze conformazionali intrinseche delle regioni N-terminali giocano un ruolo rilevante nel processo di riconoscimento tra neurotrofine e recettori chinasici. Le simulazioni condotte sui modelli rappresentanti la sola regione N-terminale delle neurotrofine NGF e NT4, hanno rivelato che per la regione N-terminale dell'NT4, e in misura minore per quella dell'NGF, la conformazione elicoidale associata all'interazione con i rispettivi recettori tirosinchinasici è già presente tra gli stati energicamente accessibili della proteina. E' stato inoltre possibile assegnare precisi ruoli strutturali ai residui presenti nella sequenza di queste proteine, infatti, l'isoleucina in posizione 6 di NGF data la sua scarsa propensione a formare strutture di tipo elicoidali, potrebbe essere responsabile della ridotta percentuale di strutturazione in α-elica della regione N-terminale dell'NGF in assenza del recettore (Stanzione et al., 2010). Sulla base di queste osservazioni sono state proposte strategie innovative per la progettazione e lo sviluppo di nuovi peptidi con attività agonista per NGF.

In parallelo, nel corso del dottorato, studi di dinamica molecolare sono stati successivamente estesi all'analisi delle proprietà conformazionali del NGF, la cui stechiometria di legame al recettore $p75^{NTR}$ è alquanto controversa. Esistono, infatti, indicazioni contrastanti che supportano una stechiometria NGF:$p75^{NTR}$ 2:2 (Feng et al., 2010) o alternativamente un complesso asimmetrico 2:1 (He and Garcia 2004). Il complesso asimmetrico è di particolare interesse alla luce della perfetta simmetria del dimero di NGF. Studi recenti hanno inoltre mostrato che NT3 lega $p75^{NTR}$ con una stechiometria 2:2 (Gong et al., 2008). Al fine di valutare eventuali dissimmetrie nelle proprietà dinamiche di NGF che possano essere in qualche modo collegate al complesso asimmetrico, è stata effettuata una lunga simulazione (200 ns) della proteina. I risultati, analizzati anche mediante tecniche di dinamica essenziale, indicano chiaramente che la maggior parte dei moti della proteina è caratterizzata da un'elevata simmetria. Ciononostante, per alcune regioni di loop, è stato possibile evidenziare moti lievemente dissimmetrici tra le due subunità. Alla luce di questi risultati, si può concludere che probabilmente il legame del recettore $p75^{NTR}$ a NGF induca un rilevante "*induced-fit*" da strutture simmetriche verso strutture asimmetriche.

Come descritto in precedenza, l'insorgenza di varie malattie neurodegenerative è frequentemente associata alla formazione di depositi fibrillari insolubili denominati fibrille amiloidi. Tali fibrille sono strutturalmente ben definite e costituite da proteine specifiche che, a causa di una loro scorretta strutturazione (*misfolding*), acquisiscono la capacità di aggregarsi in diversi tessuti e organi. La caratterizzazione strutturale di queste fibrille è stata a lungo ostacolata dalla ridotta solubilità e dalla natura parzialmente disordinata di questi aggregati. Alla luce di queste considerazioni, una

caratterizzazione della struttura e delle proprietà dinamiche di questi aggregati è comunque necessaria per poter definire i meccanismi molecolari di queste malattie con importanti ricadute nella messa a punto di efficaci strategie terapeutiche. Inoltre, la notevole resistenza delle fibrille amiloidi, combinata alla loro flessibilità, alla versatilità e alla capacità di auto-assemblarsi ha stimolato un crescente interesse sulle potenzialità di tali fibre anche in campi non strettamente farmaceutici come nella produzione di nanobiomateriali. In questo contesto sono state proposte possibili applicazioni delle fibre amiloidi nello sviluppo di nuovi conduttori (Reches and Gazit 2003), ligandi bioattivi, materiali biodegradabili e *scaffolds* per promuovere l'adesione cellulare e la crescita in tessuti ingegnerizzati (Holmes et al., 2000).
La risoluzione della struttura del peptide modello con sequenza GNNQQNY, della proteina prionica di lievito Sup35, ha fornito un primo modello atomico per le fibre amiloidi, denominato *cross-β-spine steric zipper* (Nelson et al., 2005). Recentemente, è stato dimostrato che questo motivo strutturale è adottato anche da frammenti peptidici isolati da proteine coinvolte in malattie neurodegenerative. Diversi studi di dinamica molecolare condotti su modelli di aggregati di tipo amiloide hanno mostrato che tali modelli possono assumere, in ambienti non cristallini, strutture significativamente differenti da quelle osservate in fase cristallina (De Simone et al., 2008) (Esposito et al., 2008) (Vitagliano et al., 2008) (Esposito et al., 2006). Più recenti applicazioni hanno in aggiunta mostrato che studi di dinamica molecolare, possono fornire indicazioni anche sulle caratteristiche strutturali di forme oligomeriche protofibrillari che sembrano essere le specie tossiche associate all'insorgenza delle patologie (De Simone et al., 2008).
In questo scenario e alla luce del duplice interesse, farmaceutico e biotecnologico, rivestito da tali strutture fibrillari, un'ampia parte delle attività di ricerca programmate durante il dottorato sono state dedicate alla caratterizzazione di strutture amiloidi e dei loro precursori tossici. In particolare, mediante simulazioni di dinamica molecolare e applicazioni sofisticate di *replica exchange molecular dynamics* (REMD), sono state condotte analisi delle proprietà strutturali e dinamiche di vari analoghi di proteine e peptidi amiloidogenici recentemente determinati.
Inizialmente, sono stati caratterizzati una serie di aggregati caratterizzati da un'interfaccia dello *steric zipper* formata essenzialmente da residui apolari e alifatici. Queste analisi sono state condotte su un frammento della regione "Hinge" delle ribonucleasi (SSTSAA) e su un frammento della proteina Tau (VQIVYK) coinvolta nella patogenesi del morbo di Alzheimer (Sawaya et al., 2007). Le simulazioni, condotte su aggregati composti da 10 *strand* di coppie di foglietti β, hanno mostrato elevate fluttuazioni e una significante distorsione della struttura cristallografica. Per il segmento della proteina Tau è stato anche valutato l'impatto dell'addizione di un ulteriore foglietto β che avrebbe potuto avere effetti stabilizzanti sulla struttura cristallina. Queste analisi però non hanno mostrato un evidente incremento della stabilità dell'aggregato. Paragonate a studi precedenti, condotti su peptidi aventi nell'interfaccia residui aromatici e/o polari, le analisi condotte, hanno messo in evidenza l'importanza della natura dei residui direttamente coinvolti nel motivo *steric zipper.* Infatti, i residui alifatici non sono in grado di formare forti interazioni *intra-sheet* ed *inter-sheet* che sono invece stabilite dai residui aromatici e polari e possono quindi, contribuire alla stabilizzazione dello *steric zipper*. Questi risultati suggeriscono quindi che l'impacchettamento dei peptidi amiloidi allo stato cristallino è determinato da un delicato equilibrio di diversi fattori (associazioni di coppie di *sheet*, i contatti elettrostatici tra coppie di simmetria, la presenza di controioni e solvente, ecc.), e che la loro rilevanza biologica sia alquanto limitata.

Alla luce delle osservazioni fatte, lo studio dell'interfaccia con residui apolari è stato esteso alla proteina prionica fungina HET, che presenta un'interfaccia apolare con una superficie più ampia (Wasmer et al., 2008). Tale simulazione, in contrasto con quelle condotte sulla regione Hinge delle ribonucleasi e sul frammento della proteina Tau, ha mostrato una notevole stabilità di questa struttura, suggerendo quindi che una superficie maggiore all'interfaccia possa avere un effetto stabilizzante sulla struttura fibrillare, favorendo quindi la formazione di aggregati molto più stabili (Vitagliano et al., 2009).
In un recente lavoro Eisenberg e collaboratori hanno messo in evidenza la capacità di uno stesso peptide amiloide di formare più strutture alternative, caratterizzate dalla presenza di distinti *steric zipper* (polimorfi) (Wiltzius et al., 2009). Questa osservazione ha suggerito che tali strutture alternative possano essere coinvolte nei processi molecolari associati alla trasmissione dei prioni. Tale processo, prevede la possibilità che una stessa proteina possa formare entità infettive distinte, i cosiddetti *"prion strains*". Allo scopo di analizzare la stabilità strutturale dei polimorfi identificati da Eisenberg e collaboratori al di fuori del contesto cristallino, sono stati effettuati studi di dinamica molecolare su aggregati costituti dai due distinti polimorfi. In particolare, le simulazioni di dinamica molecolare sono state condotte sulle due strutture polimorfiche di un segmento, con sequenza SSTNVG, dell'amilina (IAPP), ormone di 37 amminoacidi che forma depositi fibrillari insolubili tra le cellule β del pancreas nei pazienti affetti da diabete di tipo II. Il primo polimorfo del segmento in questione è caratterizzato dalla presenza nella regione centrale dello *steric-zipper* di 2 residui di serina, mentre nel secondo polimorfo tale regione è occupata da due asparagine. L'analisi delle simulazioni condotte ha mostrato che entrambi gli aggregati sono stabili, tuttavia il polimorfo con le asparagine nel *core* centrale dello *zipper* subisce una più alta fluttuazione se comparato con il polimorfo avente nell'interfaccia le due serine. La simulazione ha suggerito inoltre una possibile associazione tra la rigidità del polimorfo con le serine all'interfaccia e la presenza di legami idrogeno *inter-sheet* tra le catene laterali delle due serine stesse. Tali interazioni sono presenti nell'impacchettamento cristallino del peptide modello e restano preservati durante la simulazione di dinamica molecolare, mostrando quindi un effetto stabilizzante sull'associazione fibrillare. In conclusione, la stabilità dei due polimorfi durante la simulazione supporta l'ipotesi che questi modelli strutturali possano essere rappresentativi dei diversi *strains* riscontrati in alcune patologie neurodegenerative.
L'ultimo argomento trattato nell'attività di ricerca del dottorato riguarda la proteina prionica umana. Questi studi sono stati effettuati in collaborazione con l'Università di Cambridge. Tale collaborazione nasce dall'esigenza di studiare le caratteristiche strutturali e la stabilità della proteina prionica umana (HPrP) coinvolta in numerose patologie. Studi cristallografici indipendenti hanno evidenziato il coinvolgimento del foglietto β di questa proteina in interazioni intermolecolari tra due diverse molecole di HPrP (Antonyuk et al., 2009). L'associazione di due foglietti β, ciascuno costituito da due *strand*, porta alla formazione di un foglietto β costituito quindi da quattro *strand*.
Sulla base di queste osservazioni è stato ipotizzato che tale associazione possa essere rappresentativa delle fasi iniziali del processo di aggregazione del prione. Allo scopo di valutare la stabilità di questo frammento strutturale e di supportare un suo ruolo nel meccanismo di aggregazione della proteina, sono stati condotti studi di REMD sul foglietto formato da quattro *strand*. Le simulazioni sono state ripetute tenendo conto di mutazioni presenti in queste regioni che sono associate a diverse patologie prioniche (Santini et al., 2003) .

La procedura REMD consiste nel considerare inizialmente tante copie identiche del sistema (repliche); per le diverse repliche vengono effettuate simulazioni di dinamica molecolare a diverse temperature. A intervalli regolari si permette ad una coppia di repliche di scambiare la temperatura con una probabilità che dipende dalla differenza di temperatura tra le due repliche. Il risultato di questo tipo di simulazione è quello di ottenere le proprietà di equilibrio a tutte le temperature simulate, compresa l'energia libera di interazione tra i quattro *strand*.
Queste analisi indicano che il foglietto formato da quattro *strand* non è particolarmente stabile, esso, infatti, tende a dissociarsi nel corso delle simulazioni. E' però interessante osservare che la dissociazione del frammento porta sempre alla formazione di due foglietti ciascuno formato da due *strand* di HPrP, corrispondenti alla struttura β osservata nella proteina prionica. Simulazioni indipendenti effettuate sul foglietto formato da due *strand* hanno confermato la notevole stabilità di questo elemento strutturale. Alla luce di queste osservazioni, si può concludere che la struttura β della proteina prionica umana è dotata di una rilevante stabilità strutturale intrinseca con importanti implicazioni sul processo di aggregazione della proteina. Infatti, la struttura β del prione, la cui stabilità è indipendente dal contesto, si estende anche a stati non strutturati della proteina e potrebbe essere un elemento essenziale del processo di aggregazione. Le informazioni strutturali derivanti da queste analisi hanno portato alla progettazione di peptidi sintetici potenzialmente in grado di inibire il processo di aggregazione della proteina prionica umana.

SUMMARY

Neurodegenerative diseases are widespread pathologies of large social impact that include: prion, Alzheimer and Parkinson disease, Huntington chorea and amyotrophic lateral sclerosis. The onset of such diseases is commonly associated with the accumulation of insoluble amyloid plaques in specific neuronal population. In this scenario, research activities for the prevention and the treatment of these diseases are focused on two distinct directions: (a) the enhancement of factors that promote the survival and maintenance of nerve cells and (b) the definition of the molecular processes that lead to onset of neurodegenerative diseases. In this framework, the main scopes of the present PhD project have been the analysis of structural/dynamic determinants of the function of neuroprotective proteins (neurotrophins) and the study of structural properties of amyloid aggregates and their toxic precursors.

Neurotrophins (NTs) are homodimeric proteins that play a key role in the differentiation, survival and maintenance of nerve cells. This class of proteins include: nerve growth factor (NGF), Brain-Derived Factor (BDNF), neurotrophin 3 (NT3), neurotrophin 4 (NT4), and neurotrophin 6 (NT6). NTs act by binding to two distinct classes of transmembrane receptors. One is the $p75^{NTR}$ neurotrophin receptor and the other is the Trk family of tyrosine kinase receptors, which includes TrkA, TrkB, and TrkC. All mature NTs bind to $p75^{NTR}$, but Trks are more selective. NGF interacts selectively with TrkA receptors, NT4 and BDNF selectively with TrkB receptors, and NT3 interacts with TrkC receptors.

During the PhD, a detailed investigation of the dynamical properties of different regions of NTs was carried out by molecular dynamics techniques. Initially, these studies were focussed on the intrinsic conformational preferences of N-terminal region of the NTs. These N-terminal regions are important for the recognition and the specificity of NT-Trk binding. Indeed, N-terminal region of NGF in complex with TrkA has an α-helical conformation, whereas the NT4 in complex with TrkB receptor is in 3_{10} helix conformation. However, both N-terminal regions of the two NTs are absent in the crystallographic models of isolated dimers and in complex with the $p75^{NTR}$ receptor, revealing their flexibility in the absence of receptor and a conformational transitions in the interaction with the Trk receptor. Our calculations unveil that for NT4-Nter, and to a lesser extent for NGF-Nter, the conformation of the peptide that is prone to the Trk binding is already present among the states that are energetically accessible to the isolated peptide. This consideration has suggested feasible strategies for the design of effective NT agonist/antagonists. Indeed, variants of these peptides with an increased helical propensity will better mimic the NT functions. Successive simulations carried out on the main body of NGF have provided a detailed picture of mechanisms of interaction with the $p75^{NTR}$ receptor, whose stoichiometry of binding is controversial. These results provided important information on the correlated motions of distant region of the protein. Moreover, essential dynamics analyses clearly indicate that most of the motions of the protein are highly symmetrical. On the basis of results, it has been concluded that the binding of $p75^{NTR}$ to NGF induces a significant "induced-fit" from symmetric structures to asymmetric structures.

In the last years, enormous efforts have been made to obtain insights into the structure of the amyloid-like forms of proteins and peptides involved in the insurgence of neurodegenerative diseases. A characterization of the structure and dynamic properties of these aggregates is required to define the molecular mechanisms underlying these diseases for the development of effective therapeutic

strategies. In addition, the considerable resistance of amyloid-like fibrils, combined with their flexibility, versatility and ability to self-assemble has stimulated a growing interest in the potential of these fibers in biotechnological fields as nanobiomaterials. Previous MD simulations have shown that some steric zipper models are endowed with a remarkable stability also in a crystal-free context. However, MD simulations were limited to peptides with polar and/or aromatic dry interfaces. In this scenario, a section of my PhD project was focused on MD simulations of various amyloidogenic structures recently determined. Primarily, were carried out MD studies of steric zipper assemblies whose dry interface involves exclusively aliphatic residues. These simulations have highlighted the key role of residues involved in the steric zipper interface. Indeed, aliphatic residues are not able to form the intra-sheet and inter-sheet interactions formed by polar and aromatic residues that likely provide a strong contribution to the steric zipper motif stability. Along this line, amyoid-like assemblies endowed with hydrophobic residues presumably require larger interfaces, as it is shown by the stability of MD simulation of HET-s protein with a larger steric zippers interface.

Very recent crystallographic studies have shown that the same amyloidogenic peptide can adopt distinct steric zipper assemblies (polymorphs). Intriguingly, it has been postulated that the different polymorphs of the same polypeptide sequence may be representative of distinct strains. In this framework, a detailed analysis of dynamical properties of two polymorphic structures formed by a segment of the islet amyloid polypeptide (IAPP) was carried out during the PhD. The analyses of the MD simulations show that the two IAPP distinct polymorphs are stable in a crystalline-free environment. This finding supports the hypothesis that the occurrence of strains in neurodegenerative diseases may be related to the possibility that a single peptide/protein chain may self-associate in alternative steric zipper-based assemblies.

The last section of present thesis was dedicated to the studies of human prion protein (HPrP) properties. These studies were conducted in collaboration with the University of Cambridge. Independent crystallographic studies have shown the involvement of the β-sheet of the HPrP in intermolecular interactions that lead to the association of two different molecules HPrP in the crystalline state. These observations suggest that this association may be representative of the early stages of aggregation of HPrP. In this framework, during the PhD project detailed replica exchange molecular dynamics (REMD) studies on the intrinsic stability of HPrP β-structure were conducted. In particular, simulations were conducted on different β-strand combinations taken either from HPrP monomer or dimeric crystalline assemblies. The REMD simulations conducted on the isolated two stranded β-sheet of the protein monomer indicate that this structure is remarkably stable. The stability of larger aggregates formed by the juxtaposition of two of these sheets, as detected in the crystalline state, is very limited stability. Interestingly, additional simulations indicate that these aggregates are stabilized by mutations linked to the insurgence of pathological states. The observation that the two stranded β-sheet of the prion monomer are intrinsically stable hold important implications for prion polymerization process and for the design of synthetic peptides that potentially can inhibit the aggregation process of human prion protein.

ABBREVIATIONS

Å	Angstrom (10^{-10} m)
AMBER	Assisted Model Building with Energy Refinement
BDNF	Brain Derived Neurotrophic Factor
CD	Circular Dichroism
CRD	cysteine-rich domains
ED	Essential Dynamics
Fs	Femtosecond (10^{-15} s)
G131V AB	Mutant G131V 2-stranded β-sheet AB
G131V ABB'A'	Mutant G131V 4-stranded β-sheet ABB'A'
G131V BB'	Mutant G131V 2-stranded β-sheet BB'
GROMACS	GROningen MAchine for Chemical Simulations
GROMOS	Groningen Molecular Simulation
HPrP	Human Prion Protein
HSPs	Heat-Shock Proteins
IAPP	Islet Amyloid Polypeptide
Ig	Immunoglobluin
K	Kelvin
L	Loop
LINCS	LINear Constraint Solver
M129V AB	Mutant M129V 2-stranded β-sheet AB
M129V ABB'A'	Mutant M129V 4-stranded β-sheet ABB'A'
M129V BB'	Mutant M129V 2-stranded β-sheet BB'
MD	Molecular Dynamics
NGF	Nerve Growth Factor
NGF-Nter	N-terminal region of NGF
Nm	Nanometre (10^{-9} m)
NMR	Nuclear Magnetic Resonance
Ns	Nanosecond (10^{-9} s)
NT	Neurotrophin
NT4-Nter	N-terminal region of NT4
NVE	Microcanonical ensemble
NVT	Canonical ensemble
OPLS-AA	All atoms Optimized Potentials for Liquid Simulations
$p75^{NTR}$	p75 Neurotrophin receptor
PCA	Principal Component Analysis
PDB	Protein Data Bank
PME	Particle Mesh Ewald
Ps	Picosecond (10^{-12} s)
PSIPRED	Protein Structure Prediction Server
RE	Replica Exchange
RMSD	Root Mean Square Deviation
RMSF	Root Mean Square Fluctuation
RMSIP	Root Mean Square Inner Product
SA	Surface Areas
Sc	Shape complementarity
SPC	Simple Point Charge
SPCE	Extended Simple Point Charge
TNF	Necrosis Factor Receptors

TIP3P	Transferable intermolecular potential with three interaction sites
Trk	Transmembrane Tyrosine Kinase receptor
Trk-d4	Fourth extracellular domain of Trk
Trk-d5	Fifth extracellular domain of Trk
UPS	Ubiquitin-proteosome system
UV	Ultraviolet
VMD	Visual Molecular Dynamics
VQIVYK-dP	VQIVYK-polar interface
VQIVYK-dA	VQIVYK-apolar interface
VQIVYK-T1	VQIVYK-polar interface
VQIVYK-T2	VQIVYK-apolar interface
Wt ABB'A'	Wilde type 4-stranded β-sheet
Wt AB	Wilde type 2-stranded β-sheet AB
Wt BB'	Wilde type 2-stranded β-sheet BB'

1. INTRODUCTION

The diseases of nervous system include a wide range of pathologies with high social impact caused by disorders affecting neurons or other cells in the nervous tissue. Among the pathologies of the nervous system, neurodegenerative diseases have recently attracted the interest of the scientific community. These include prion diseases, Parkinson disease, Alzheimer disease, Huntington chorea and amyotrophic lateral sclerosis. The neurodegenerative diseases are characterized by molecular changes that lead to nerve cell degeneration, to nerve dysfunction, to cell death, and, in extreme cases, to dementia. The number of people suffering from neurodegeneration is dramatically high. Alzheimer disease affects about over 5 million in the world and this number is expected, in the absence of effective treatments, to drastically increase because of the raising of the population average age. Patients with Alzheimer disease have an average life of 10 years, during which their autonomy decreases, thus requesting commitment and increasing costs by the family. These sick persons are almost never hospitalized and more than 75% of their treatments and care is provided by families, who live the daily drama of an healthy emergency still unresolved. The pathogenesis of neurodegenerative diseases remains unclear, and affective treatments are currently lacking. However recent studies from three different disciplines, neuropathology, genetics and biophysics, have begun to converge on a novel target for therapeutic attack: ordered protein aggregation. Indeed, neurodegenerative disorders are the result of abnormalities in the transport, degradation and aggregation of particular types of proteins in the brain that take to abnormal protein aggregation in specific neuronal population. These aggregates usually consist of fibers caused by the incorrect folding (*misfolding)* of specific proteins.

The amyloid deposits contain insoluble protein fibrils that share similar morphological features, but comprise many different proteins with no obvious sequence similarity. The deposits physically disrupt tissue architecture, suggesting disruption of function by some bulk process and later the nerve cells death. However, recent investigations demonstrated that the main toxic species are likely the pre-fibrillar, diffusible assemblies of amyloid-forming proteins/peptides.

Currently, intense research activities are focused on the definition of the molecular mechanisms that lead to the formation of neurotoxic species and on the determination of role and properties of potential neuroprotective agents that could prevent the cellular death. In this scenario, the present PhD project has been focused on the study of properties of neuroprotective factors like neurotrophins, and, in parallel, on the definition of structural/dynamical aspect of structure of amyloidogenic peptides. From the methodological point of view these issues will be faced by using molecular dynamics analyses (See Appendix for details).

1.1. Neurotrophins: structure, functions and therapeutic applications

1.1.1. Neurotrophins

Neurotrophins (NTs) are a family of proteins that play a major role in the survival, maintenance, differentiation and other various functions of the neuronal and glial cells of central and peripheral nervous system. The family of NTs includes a number

of structurally and functionally related members, which exhibit a wide and varied repertoire of biological activities, regulating the survival, growth, cell migration, differentiation and synaptic plasticity of specific neuronal populations (Bradshaw et al., 1994) (Petruska and Mendell 2004) (Wiesmann and de Vos, 2001). For these reasons the neurotrophins are the object of enormous studies in neurosciences to understand their physiological role and their involvements in different pathologies of nervous system.
Five distinct neurotrophic factors have been identified: the nerve growth factor (NGF) (Levi-Montalcini, 1964), the brain-derived neurotrophic factor (BDNF) (Barde et al., 1982), neurotrophin 3 (NT3) (Maisonpierre et al., 1990), neurotrophin 4/5 (NT4) (Ip et al., 1992), and neurotrophin 6 (NT6) (Gotz et al., 1994). NTs are synthesized as precursors (proneurotrophins) that are proteolytic cleavaged to generate the mature, biologically active neurotrophins. Since NTs are normally expressed at low levels, their processing and their secretion by neurons and non-neuronal cells in vivo is unclear. In the non-nerve cells, the proneurotrophins are cleaved intracellularly by furins or proconvertases utilizing a highly conserved dibasic amino acid cleavage site to release C-terminal mature protein as stable non-covalent homodimer (Edwards et al., 1988). In physiological conditions, mature NTs are homodimeric proteins, whose polypeptide chains are made of 118-143 residues. The analysis of amino acid composition of these proteins shows the abundance of basic residues (Lys, Arg, His) which are presumably essential for the interaction neurotrophins-receptors. Sequence alignments between the various mature neurotrophins show that the percentage of identity is around 50%. It is important to note that the similarities are not equally distributed along the primary structure. In fact, highly conserved regions are indentified, which presumably coincide with the most important structural and functional regions.

1.1.2. Biological partners of Neurotrophins

The neurotrophins exert their role by interacting with two types of trans-membrane receptors belonging either to the tyrosine kinase (Trk) family (Neet and Campenot, 2001) (Ip and Yancopoulos 1993), or to the tumor-necrosis-factor ($p75^{NTR}$) families. All neurotrophins bind to the common $p75^{NTR}$ receptor with similar affinity, but they show differential affinity toward the Trk receptors. Ligand activation of these two types of receptor can lead to opposite actions, in particular the prevention or activation of programmed cell death.Three forms of Trk receptor (TrkA, TrkB, and TrkC) have been described. TrkA forms a high-affinity binding site for NGF (Wiesmann et al., 1999), TrkB binds to BDNF and NT4/5 (Haniu et al., 1997) (Klein et al., 1992), and TrkC binds to NT3 (Lamballe et al., 1991). NT3 has also been shown to bind TrkA and TrkB but with reduced affinity (Soppet et al., 1991) (Barbacid 1994) (Figure 1A). The binding of NTs to their respective Trk receptor activate the path of cellular survival (Figure 1B).
The Trk receptors, each constituted by ~800 amino acids, have significant sequence identity (≈40-50%). The extracellular portion of Trk receptors, approximately 400 amino acids, is located in their N-terminal region and bears the binding site of neurotrophins (Banfield et al., 2001).

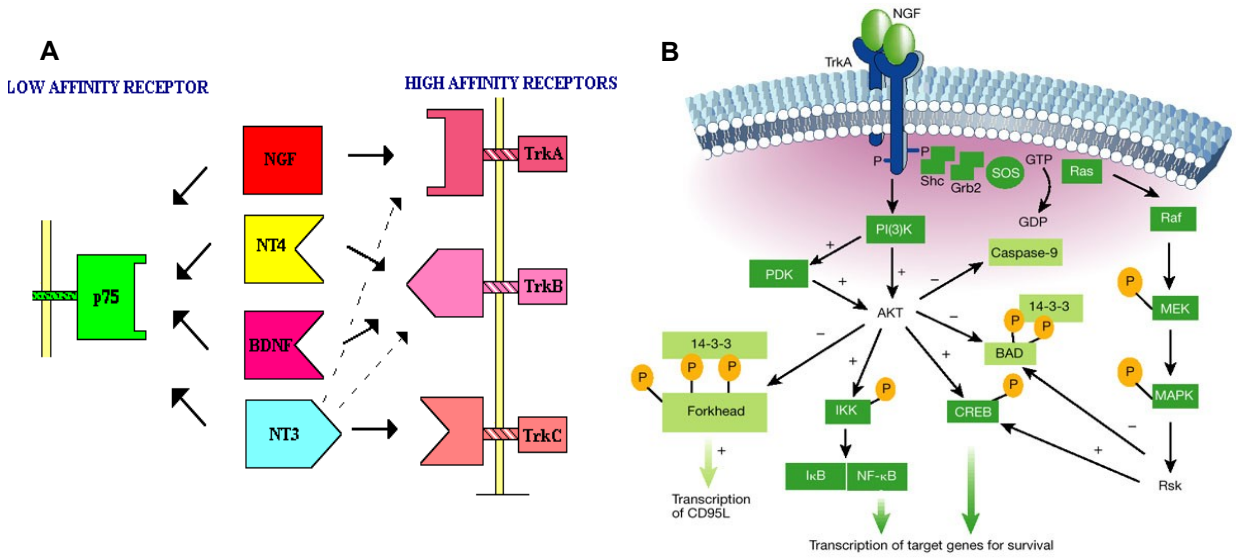

Figure 1
A) Schematic representation of binding NTs-receptors. B) Schematic representation of the mechanism of Trk activation.

The extracellular portion of Trk receptors is constituted by a characteristic domain organization. The first domain consists of a leucine-rich region (domain 2) flanked by two cysteine-rich domains (domains 1 and 3), the fourth and fifth domains (Trk-d4 and Trk-d5) are immunoglobulin (Ig)-like domains. The extracellular portion is linked by a single putative transmembrane helix to the intracellular tyrosine kinase domain (Schneider et al., 1991). NTs bind their TrK receptors to domain 5 of extracellular portion. This event is believed to induce the dimerization of receptors. This dimerization leads, in turn, to the autophosphorylation of several tyrosine residues located in the cytoplasmic domain. Finally, this latter event triggers the intracellular signal transduction cascades essential for cellular survivor (Figure 1B).
NTs activate, with lesser affinity, the receptor $p75^{NTR}$ which belongs to Necrosis Factor Receptors family (TNF) (Zampieri et al., 2004). The $p75^{NTR}$ is a transmembrane glycoprotein with a little cytoplasmic domain containing a death domain constituted by six α-helices in a globular arrangement. The extracellular fragment is constituted by four cysteine-rich domains (CRD) each containing three disulfide bonds. It is generally assumed that the formation of the complex NT-$p75^{NTR}$ induces apoptosis in oligodendrocytes, neurons and in vascular smooth muscle cells (Casaccia-Bonnefil, et al. 1999).

1.1.3. Structural characteristics of Neurotrophins

Over the years, extensive crystallographic investigations have provided a detailed picture of NTs in their unliganded states and in complex with receptors (Trk and $p75^{NTR}$) (Gong et al., 2008) (Wehrman et al., 2007) (Banfield et al., 2001) (He et al., 2004) (Robertson et al., 2001) (Wiesmann et al., 1999) (Bax et al., 1997) (Mc Donald et al., 1991) (Figure2). The analysis of crystallographic structures revealed that NTs are constituted by two polypeptide chains each formed by a variable number of structured amino acids (Wiesmann et al., 2001). All NTs are presents an unusual series of three disulphide bridges (cysteine knot) that give a considerably stability to this factors. The two monomers are been together by non-covalent interactions (hydrogen bonds and van der Waals interactions). Each monomer has an elongated shape with the central region constituted by two pairs of twisted antiparallel β-

strands. Four loop regions are been indentified, three hairpin loops on one end (L1, L3, and L4), and the other end carries a cysteine-knot motif (L2) that stabilizes the fold and locks the molecules in their conformation. In the biologically active form, two monomers are arranged in a parallel manner to form a close-packed structure.

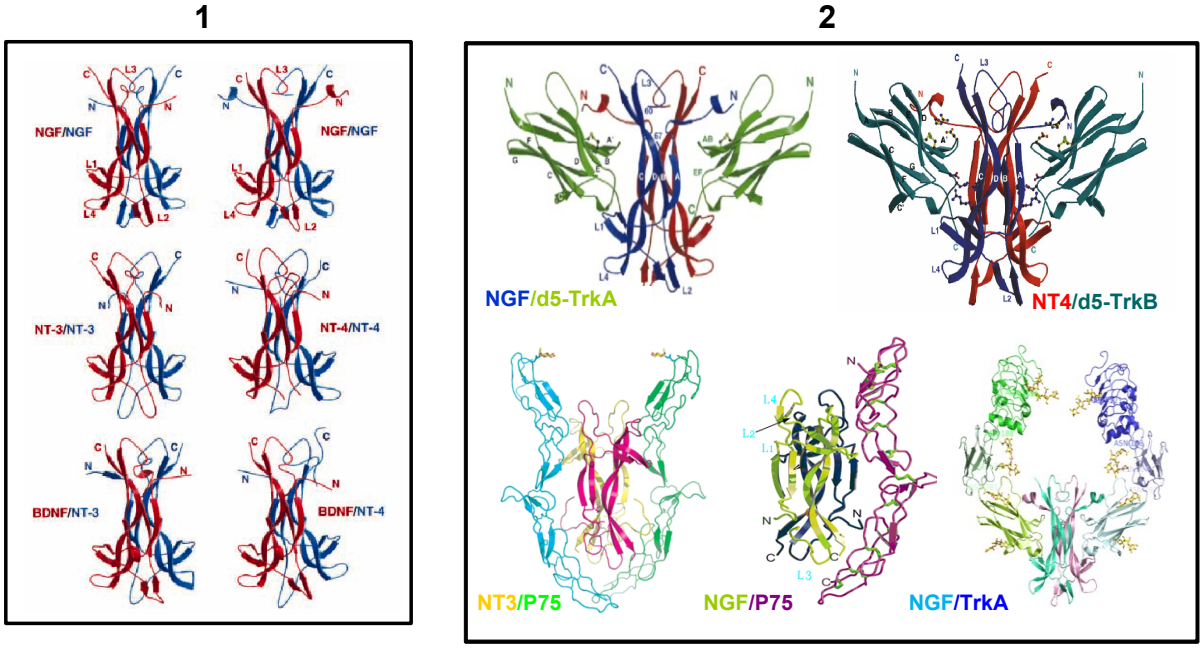

Figure 2
Available crystallographic structures of NTs. Box 1) Crystallographic structures of unliganded neurotrophins. Box 2) Crystallographic structures of NTs in complex with their receptors.

1.1.4. Therapeutic applications of Neurotrophins

NTs appear to play a protective action on neurons affected by neurodegenerative and other neurological and psychological diseases like ischemia, epilepsy, depression and eating disorders. In allergic states high concentration of NTs were found (Dechant and Neumann 2002).
Several studies with cell cultures and animal models have provided strong support to the hypothesis that NTs are able to prevent cellular death. These studies have also demonstrated the involvement of NTs in the ethiopathology of neurodegenerative disorders. Practical applications of NTs are however limited by the difficulties of their transport in the central nervous system caused by the large size of these proteins.
Therefore, current research activities aim at determining the minimum pharmacophoric section of NTs in order to design effective agonists able to overcome the hematoencephalic barrier and to avoid the use of invasive methodologies of application. In the Table 1 is provided a brief overview of possible applications of NTs.

Table1. Biological actions and therapeutic applications of different neurotrophins.

NGF	In recent years, the NGF has become part of clinical trials in peripheral neuropathies induced by diabetes and skin ulcers (Lambiase et al. 1998). Studies carried out in Italian laboratories have tested the applicability of NGF in ophthalmic diseases. NGF extracted from mouse salivary glands, has been successfully used for the treatment of neurotrophic corneal ulcers, ulcers due to several cases in which the cornea due to damage to innervation, are ulcers on the surface can also become opaque and sometimes puncture (Lambiase et al., 1998). NGF has been also used in experimental models of Alzheimer disease (Siegel and Chauhan, 2000). Invasive injections of NGF were shown to prevent the degeneration of cholinergic neurons in rats and primates.
BDNF	One of the most interesting aspects of BDNF is its involvement in the mechanisms of synaptic plasticity. It was assumed that changes in its endogenous levels or its bioavailability, may contribute to the pathogenesis of some neurological diseases. Alterations in the production and secretion of BDNF have been reported for various diseases, including Alzheimer's and Parkinson's disease that are associated with decreased levels of BDNF in the brain (Connor et al., 1997), (Howells et al., 2000); (Levivier et al., 1995), (Michalski and Fahnestock, 2003). In addition, mood disorders like depression are characterized by a lower concentration of BDNF at central (brain) and peripheral (blood) levels (Altar, 1999) (Shimizu et al., 2003). Studies *in vivo* have shown that in Parkinson's patients there is a reduction in the expression of BDNF in the *substantia nigra*. Several studies conducted on rats have shown, however, that BDNF prevents spontaneous death of mesencephalic dopaminergic neurons in rats (Hyman et al., 1994).
NT3	The activities *in vivo* of the neurotrophic factor NT3 are less known than those of other NTs. Recent studies suggest role for NT3 in the prevention of neuronal death of central noradrenergic neurons, and that it is important for the development of many types of mechanoreceptors (Arenas and Persson, 1994).
NT4	NT4 is synthesized by neurons of the pre-and paravertebral sympathetic ganglia (Roosen et al., 2001). All published studies that have investigated the role of NT4 in the development of spinal pain have provided negative results. Recent studies have demonstrated a role for NT4 in ischemia of the retina that is caused by many diseases including glaucoma and diabetic retinopathy.

1.2. Amyloid fiber and amyloidogenic peptides

1.2.1. Neurodegenerative diseases and Amyloid fiber

The onset of neurodegenerative diseases is commonly associated with the accumulation of insoluble amyloid plaques in specific neuronal population. These fibrillar deposits, structurally well-defined, are due to abnormal proteins that acquire the property to accumulate in different tissues and organs. The presence of protein aggregates in the brain suggests that neurodegenerative diseases share dysfunction of the molecular chaperone systems normally responsible for prevention of protein *misfolding*. Over the past decade, data derived from several independent investigations suggest that prefibrillar, diffusible assemblies of amyloid-forming proteins and peptides are the most harmful species (Chiti and Dobson 2006) (Walsh and Selkoe 2007). Neurons are vulnerable to the toxic effects of mutant or misfolded

protein as they are not subject to somatic maintenance and turnover. Dysfunction of the systems involved in detection and elimination of misfolded proteins, such as the HSPs and the ubiquitin-proteosome system (UPS) plays a role in the pathogenesis of neurodegenerative diseases. The UPS itself has also been suggested to be disrupted by toxic proteins in what essentially amounts to a catastrophic feedback mechanism leading to accumulation of ever-increasing amounts of abnormal protein

1.2.1.1. Misfolded protein deposition

A given polypeptide chain typically assumes a single, or a limited number, of 3D conformations; usually only one of these states is the correct 'native' fold. Any other conformations that may form during the course of folding of the nascent polypeptide chain, such as folding intermediates, or as the result of insult (heat/redox/chemical/irradiation *etc*.) may be deleterious to the cell. Protein folding involves transition through folding intermediates stabilized by the HSPs molecular chaperones. Protein misfolding can results in prefibril formations. Normally, the prefibrils are targeted with ubiquitin for destruction by the proteosome, but under pathological conditions they may accumulate and lead to disease through production of amyloid fibrils. Accumulation of excess amounts of misfolded protein due to overproduction, insult, or dysfunction of the chaperone system can lead first to prefibril formation then plaque and consequently to cell death and disease (Figure 3).

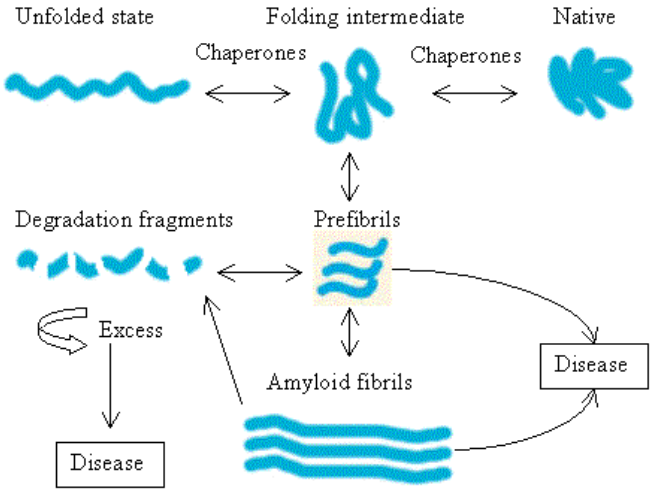

Figure 3
Summary of proposed involvement of protein misfolding in neurodegenerative diseases.

1.2.2. Amyloid fiber: properties and structural characteristics

Amyloidogenic proteins differ in size, three-dimensional structure and biological function but form amyloid aggregates with similar morphologies and properties.
For pathologists to designate a disease as amyloid, the fibril must have determined properties, include, extracellular deposition, an elongated morphology, the binding of Congo red (giving an 'apple-green' birefringence) (Westermark, 2005), formation from their constituent protein molecules with cooperative, nucleation-dependent kinetics, and so-called cross-β X-ray diffraction pattern (Sunde and Blake 1997). This pattern consists of an X-ray reflection at ~4.8 Å resolution along the fibril direction,

and another X-ray reflection at ~8-11 Å resolution perpendicular to the fibril direction (Eanes and Glenner 1968) (Sunde et al., 1997).
The pattern reveals that the fibrils contain β-sheets parallel to the fibril axis, with their extended protein strands perpendicular to the axis (Figure 4). Recent investigations demonstrated that many toxic species are likely the pre-fibrillar, diffusible assemblies of amyloid-forming proteins/peptides. One of the main factors hampering the definition of the molecular bases of these diseases is the structural characterization of the elusive molecular species involved. The detection of structural features for both fibrillar and soluble oligomers is extremely difficult due their intrinsic properties.

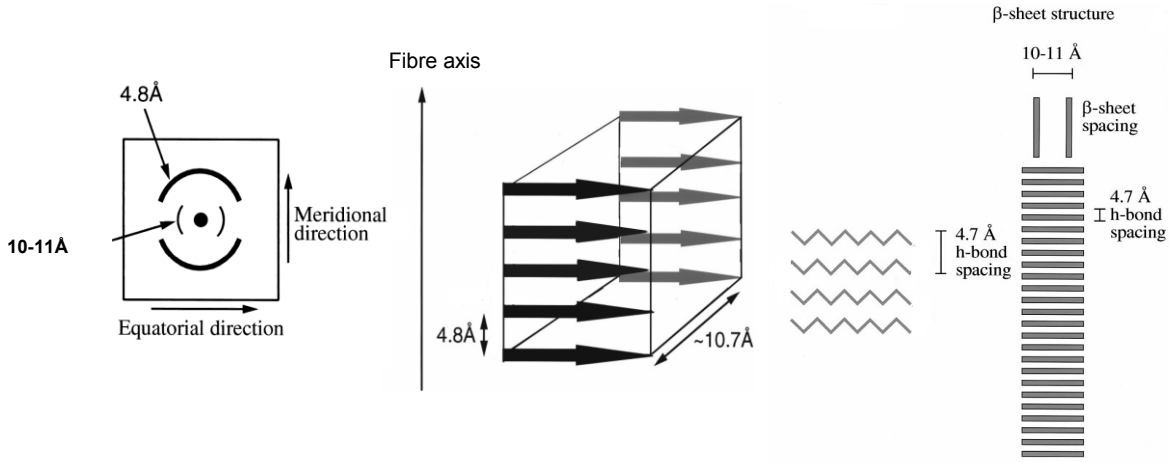

Figure 4
X-ray diffraction pattern: x-ray reflection ~4.8 Å resolution along the fibril direction and X-ray reflection at ~8-11 Å resolution perpendicular to the fibril direction.

Structural models for the amyloid core have been proposed, based on solid-state NMR, EM data, X-ray fiber diffraction. Much of the high-resolution, detailed structural data, has been obtained from amyloid-like fibrils assembled from short peptides (homologous to regions of disease-related proteins or designed) (Petkova et al., 2002) (Makin et al., 2005) (Nelson et al., 2005) (Perutz et al., 2002) (Sikorki and Atkins 2005). The structural characterization of amyloid-like assemblies of the GNNQQNY from yeast prion Sup35 represented a major advance in the field (Nelson et al., 2005). The 7-residues peptide GNNQQNY displays the same amyloid properties of the full-lenght Sup35. This structure revealed how short segments form fibrils; the cross-β-spine consists of a pair of β-sheet, each sheet is formed from extended strands of the segment, hydrogen-bonded up and down the sheet to identical molecules, all perpendicular to the axis of the fibril. Two sheets mate tightly at a completely dry interface. At this interface, the residue side chains are strictly interdigitate forming what is denominated the “steric zipper motif” (Figure 5).

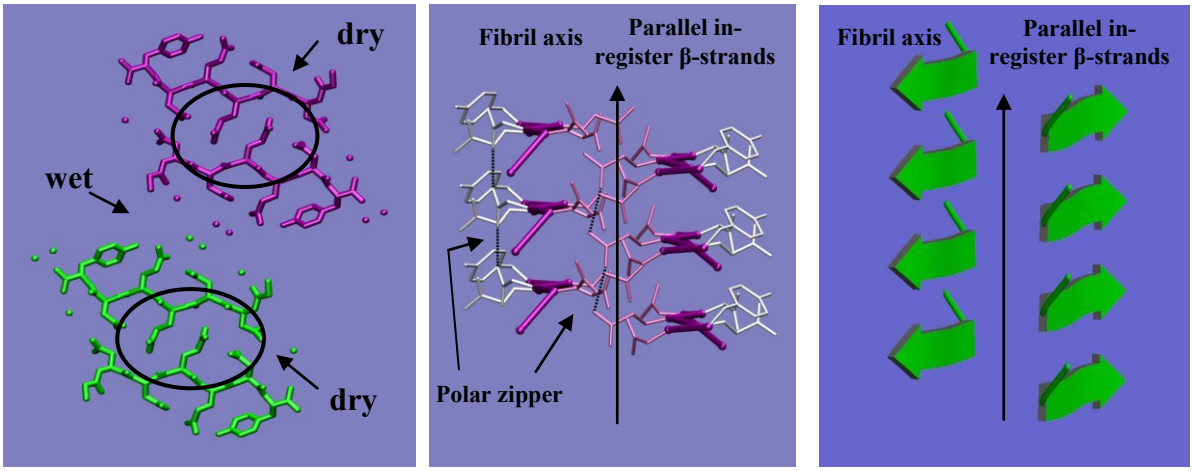

Figure 5
Eisenberg's model

The pair-of-sheets motif, with its dry, steric-zipper interface repeated along the entire length of the needle-shaped crystal, accounts for the elongated shape of the crystal and presumably of the fibril (Balbirnie et al., 2001).
In these years other fibril-forming segments in other disease-related and fibril-forming proteins have been identified (Sawaya et al., 2007) (Wasmer et al., 2008) (Walsh et al., 2009) (Wiltzius et al., 2009).
Despite the wide variety of protein sequences that form fibrils range from highly polar (for example NNQQ) to highly apolar (for example MVGGVV), and from small side chains (SSTSAA) to large (FYLLYY), these sequences have a property in common: their self-complemetary binding. Despite their fundamental similarity, the determined structures display variations of the basic steric-zipper structure and thereby expand our understanding of amyloid structure. The structures can be divided into five classes (Figure 6) distinguished by (1) whether their sheets (that is, the strands in their sheets) are parallel or anti-parallel, (2) whether sheets pack with the same ('face-to-face') or different ('face-to-back') surfaces adjacent to one another, and (3) whether the sheets are oriented parallel ('up-up') or antiparallel ('up-down') with respect another. To distinguish this third type of orientation from the first, the relative sheet orientation is defined in terms to given sheet edge facing 'up' or 'down' (Sawaya et al., 2007). Combinations of these three structural arrangements give eight theoretically possible classes of steric zippers. In several of these crystal structures sheet-to-sheet interactions involve more than just a one zipper, with offer possibilities for polymorphic structures that might be connected to the phenomenon of prion strains.

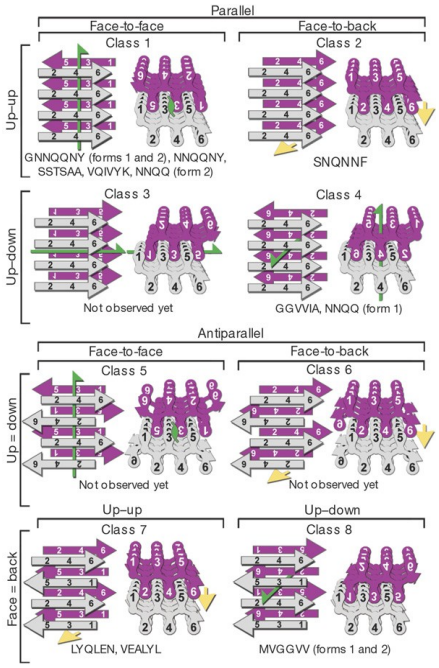

Figure 6
The eight classes of steric

1.2.3. Amyloid fiber: dynamical properties

The use of model peptides whose solid aggregates display most of the features associated with the amyloid fibers has proven to be an important strategy used to overcome the difficulty due to the limited information about the insoluble aggregates. (Rousseau et al., 2006) (Zanuy et al., 2003). Molecular dynamics studies have provided valuable complementary information on different features of the peptide assemblies detected by X-ray crystallography. These investigations have provided insights into (a) the intrinsic propensities of peptide fragments to associate in amyloid-like states, (b) the energetic factors stabilizing these aggregates, and (c) the possible structural states of either oligomeric precursors or larger assemblies. These analyses reveal that the assembly identified in the crystalline state is also stable in solution, but it undergoes a large structural re-organization (β-sheet twisting) (Figure 7) (De Simone et al., 2008) (De Simone et al., 2008) (Esposito et al., 2008) (Vitagliano et al., 2008) (Esposito et al., 2006).

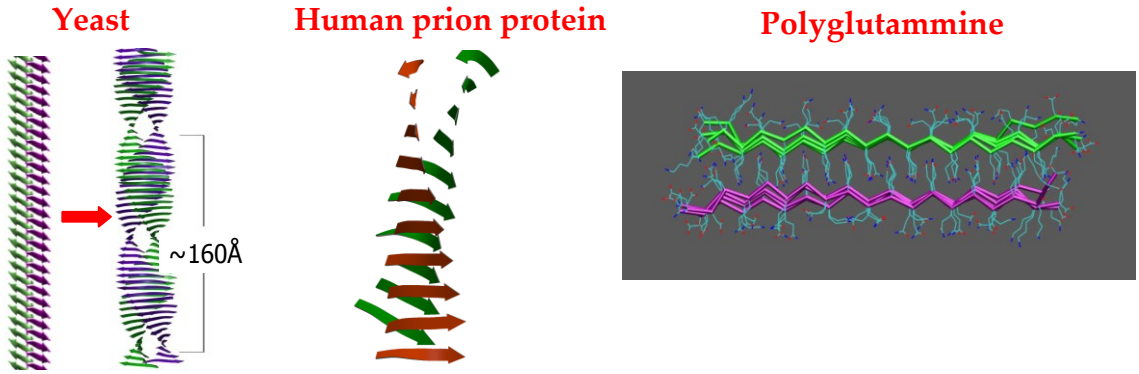

Figure 7
Representative examples of dynamical properties of various amyloid aggregates. In all examples reported an arrangement of the strains is observable.

For the GNNQQNY peptide the twist of the sheet is left-handed around the axis normal to the peptide chain. Stepwise superimpositions of successive strands within each sheet indicate that the average twist is ≈11°. Several MD simulations indicated that a complete 360° twist is achieved by 35 strands, with the pitch of the helical suprastructure of ≈160° Å. These data suggested twisted β-sheet structures as a basic motif of amyloid fibrils.

1.2.4. Amyloid fibers: from diseases to devices

Molecular self-assembly is a powerful approach for fabricating novel supramolecular architectures. The clumps of the insoluble amyloid fibrils generally fall into the realm of biomedical research. But the greater-than-steel strength of amyloid fibrils, combined with their flexibility, versatility, and ability to self-assemble, has also begun to pique growing interest in their potential as advanced nanofiber materials. The researchers have begun to envision useful possibilities for the amyloid fibers, they are now using fibrils to design new types of conducting nanowires, bioactive ligands and biodegradable material, among other potential applications.
A class of natural amyloid-like fibrils, produced by *Escherichia and Salmonella* species, is involved in the colonization of inert surfaces and biofilm formation. A

remarkable aspect of their production is the level of control imposed over fibril localization and assembly. Harnessing or mimicking such mechanisms may enable the controlled deposition of fibrils at defined locations on solid surfaces for the directed assembly of new materials, three-dimensional architectures, or devices. In addition to high-order structures, many *in vitro* β-sheet fibrillar systems form aqueous gels. This raises possibilities for their use as hydrogels, which are integral to the cosmetic and other industries and biotechnologies such as drug delivery and release (Peppas et al., 2000), microfluidics (Beebe et al., 2001), and tissue engineering (Lee and Mooney 2001) (Holmes 2002). For example, Zhang and co-workers demonstrate the utility of self-assembling β-sheet fibrillar scaffolds in promoting cell adhesion and growth for tissue engineering (Holmes et al., 2000). The scaffold designs are based on short peptides with alternating hydrophobic and polar amino acids. In the presence of salt, these form membranes that comprise fibrils with the structural and tinctorial properties of amyloid. The group report a number of chemically different scaffolds synthesized using this design strategy, which promote neuronal cell adhesion and opens possibilities for cartilage repair (Kisiday et al., 2002). The use of β-sheet fibrils is not restricted, however, to mimicking biological materials or promoting a biological function. Different researchers describe templated assembly of metal nanowires using β-sheet fibrils (Sheibel et al., 2003) (Reches and Gazit 2003). Reches and Gazit, for example, used analogs of amyloid fibrils and other bionanostructures to create a conducting biomaterial. The researchers created an hallow, self-assembling diphenylalanine-based synthetic tubular fibrils, with the structural and tinctorial properties of amyloid fibrils. Addiction of ionic silver to solutions of these materials results in the deposition of nanoparticulate silver inside the tubes. Dissolving the diphenylalanine nanotube with proteinase K exposed the silver nanowire within. Such metallic nanowires may be used in next-generation computers, batteries, and light-emitting diodes.
Nevertheless, a desire for amyloid-based nonomaterials is indeed beginning to arise in industry. The cellular telephone company Nokia has begun design on a partly biodegradable and presumably environmentally more benign cell phone dubbed “Morph”. Prototype design began with collaboration between Nokia and the Nanoscience Research Centre at the University of Cambridge, headed by Welland. Welland’s team combined amyloid fibrils with other plastics on the market to create a composite material. They then used this material to construct a cell phone that is sturdy and partially biodegradable.

1.3. Objectives of the present PhD project

As mentioned before, the main scopes of the present PhD project have been the analysis of structural/dynamic determinants of the function of neuroprotective proteins (neurotrophins) and the study of structural properties of amyloid aggregates and their toxic precursors. We the aim of gaining insights for the design of novel compounds with neuroprotective properties, we carried out a detailed analysis of the intrinsic conformational preferences of two of the most important NTs: NGF and NT4. In parallel, we also analyzed the conformational stability of several amyloidogenic peptides to unveil the basis of amyloid-fiber formations. Finally, MD analysis was also conducted for the identification of the nucleus involved in prion fibrillogenesis. The main findings of these activities are delineated in the next chapters of this thesis.

2. ROLE OF THE CONFORMATIONAL VERSATILITY OF THE NEUROTROPHIN N-TERMINAL REGIONS IN THEIR RECOGNITION BY TRK RECEPTORS

2.1. Background

The involvement of NTs in biological processes linked to the emergence of severe and widespread pathologies has suggested their use as promising therapeutic agents. Although several independent investigations have indeed provided support on this idea (Covaceuszach et al., 2009) (Saragovi et al., 2009) (Williams et al., 2006) (O'Leary and Hughes, 2003), a major obstacle to the neurotrophin-based therapies is their poor pharmaceutical properties (Apfel 2002) (Aloe 2004). Indeed, significant doses of proteins must be achieved in the target region to really counteract disease processes and, simultaneously, the delivery of NTs must be hampered in other region to prevent side-effects. Therefore, a particular attention been given to the development of mimetics endowed with NT-like activities. Using different approaches, over the last fifteen years, a number of NT agonists or competitive antagonists have been synthesized and characterized (Colangelo et al., 2008) (Peleshock and Saragovi 2006) (Xie et al., 2000) (Massa et al., 2002) (Beglova et al., 2000). Some of them have also proven to be active *in vivo*. Indeed, experiments conducted with synthetic NGF agonists have shown (i) improvement in memory and cholinergic phenotype in cognitively impaired aged rats (Bruno et al., 2004) or (ii) ability to restore neuronal function and reduce reactive gliosis in a rat model of chronic constriction injury (Colangelo et al., 2008).
The rational design of effective NT mimetics is strongly depending from detailed information about their interaction with receptors.
Comparative analyses of different crystallographic structures have unveiled an intriguing dynamic behavior of NT N-terminal regions. There is clear evidence that these fragments, which are likely unfolded in unliganded NTs and in complex with the $p75^{NTR}$ receptor, become ordered only upon binding to Trk receptors (Wiesmann and de Vos 2001) (Fig.2). Moreover, N-terminal regions of different NTs exhibit different structural properties. Indeed, the N-terminus of NGF mediates the interactions with TrkA by assuming an α-helical structure (Wiesmann and de Vos 2001). On the other hand the N-terminal region of NT4 forms 3_{10} helix upon binding to TrkB (Banfield et al., 2001).
In contrast, computational studies aimed at unveiling the dynamic properties of NTs and their receptors are rather limited (Settanni et al., 2003) (Berrera at al., 2006).
Previous molecular dynamics simulations focused on the analysis of the dynamic properties of the complex NGF-TrkA and on the analysis of the energetic factors involved in the NGF N-terminal recognition by the TrkA receptor (Settanni et al., 2003) (Berrera at al., 2006).
Because the N-terminal regions of NTs have been considered as hot spots for the design of NT agonist/antagonists (Saragovi and Zaccaro 2002), a section of my PhD project is focused on the characterization of this region. In particular, we combined circular dichroism and molecular dynamics investigation aimed at identifying the intrinsic conformational preferences of the N-terminal regions of both NGF and NT4**.**
The results of the present investigation provide insights into the recognition process between NTs and Trk receptors and guidelines for the design of new NT mimetics.

2.2. MATERIALS AND METHODS

2.2.1. Peptide synthesis

Peptides corresponding to the N-terminal region of NT4 and NGF (See Table 1 for the sequence) were purchased from Inbios laboratories (Pozzuoli, Italy), and used without further purification.

2.2.2. CD spectroscopy

CD spectra on the peptides were recorded with a Jasco J-810 spectropolarimeter equipped with a Peltier temperature control system (Model PTC-423-S). Molar ellipticity per mean residue, $[\theta]$ in deg $cm^2 \cdot dmol^{-1}$, was calculated from the equation: $[\theta] = [\theta]_{obs} \cdot mrw \cdot (10 \cdot l \cdot C)^{-1}$, where $[\theta]_{obs}$ is the ellipticity measured in degrees, mrw is the mean residue molecular mass, *C* is the protein concentration in $g \cdot l^{-1}$ and *l* is the optical path length of the cell in cm. Far-UV measurements (190-230 nm) were carried out using a 0.1 cm optical path length cell. The concentration of NGF-Nter and NT4-Nter was 0.030 and 0.027 mM respectively. The CD spectra reported in Figure 1 were signal-averaged over three scans. Other parameters of the CD spectra registration are identical to those adopted in previous studies (Granata et al., 2006).

Table 1

	1 5 10 15
NT4-Nter	GVSETAPASRRGELAV
NGF-Nter	SSSHPIFHRGEFSVCD

Sequences of the peptides characterized in the present study. The highlighted regions in gray represent the α-helical region detected in the structure of the complex NGF-TrkA (PDB code 1WWW) and the 3_{10} helix found in the complex NT4-TrkB (PDB code 1HCF).

2.2.3. MD simulations

The MD simulations were conducted on the N-terminal fragments (residues 1-16) of NGF and NT4 (Table 1). In order to avoid any bias in the MD analysis, the simulations were performed by assuming an extended conformation for both peptides. To emulate the state of the peptides in the corresponding proteins, their N- and C-termini were kept charged and uncharged, respectively. Because the overall charge of NT4-Nter was +1, a Cl^- ion was added to neutralize the simulated system. The AMBER03 force field (Duan et al., 2003) and the TIP3P water model implemented in the program GROMACS (Van der Spoel et al., 2005) were used in the simulations (See Appendix for details). For both systems, in order to relax bond geometries, the potential energy of the system (peptides and water) was minimized by using the steepest-descent method until convergence was reached. The solvent

was then relaxed by 50 ps of MD at 300 K, restraining protein atomic positions with a harmonic potential. The system temperature was brought to 300 K in a step-wise manner: 30 ps MD runs were carried out at 50, 100, 150, 200, 250, and 300 K. It has been checked that, in each step of the heating of the different systems, the potential energy reached a stable value. The timescale of the individual simulations is reported in Table 2. The simulations were run with periodic boundary conditions. Bond lengths were constrained by the LINCS algorithm (Hess et al., 1997). The electrostatic interactions were calculated using Part Mesh Ewald (PME) algorithm with a cutoff of 0.9 nm. The cutoff radius for the Lennard-Jones interactions was set to 0.9 nm. A dielectric constant of 1, and a time step of 2 fs were used. We used the NVT ensemble in all simulations. The temperature was maintained constant using the Berendsen thermostat with a time constant of 0.1 ps (See Appendix for details). Trajectory structures were analyzed by using GROMACS (Van der Spoel et al., 2005) and VMD (Humphrey et al., 1996) routines.

Table 2. Summary of the Simulations Performed

Model	Atom peptide/Atom water/Cl^-	Box dimensions ($Å^3$)	Simulation time (ns)	T (K)
NT4-Nterm	227 / 23991/ 1	62 x 62 x 62	200	300
NGF-Nterm	240 / 23952	62 x 62 x 62	200	300

2.3. RESULTS AND DISCUSSION

In order to characterize the intrinsic conformational preferences of the N-terminal regions of both NT4 and NGF, we adopted an integrated experimental (circular dichroism) and computational (molecular dynamics) approach.

2.3.1. CD spectroscopy

To avoid any bias caused by chain termination, the length of the peptides corresponding to the N-terminus of the two NTs considered here was larger than the regions that become helical upon binding to Trk receptors. As shown in Table 1, the first sixteen residues of the two proteins were considered. The far-UV spectrum of NT4-Nter measured at room temperature shows a minimum at ~200 nm (Figure 1A). A similar trend is exhibited by the spectrum of NGF-Nter (Figure 1B). Although, due to the intrinsic limitations of the technique, these analyses do not preclude the possibility that structured forms of these peptides occur in solution as minor conformational states, these spectra clearly indicate that both peptides show a preference for random coil states.

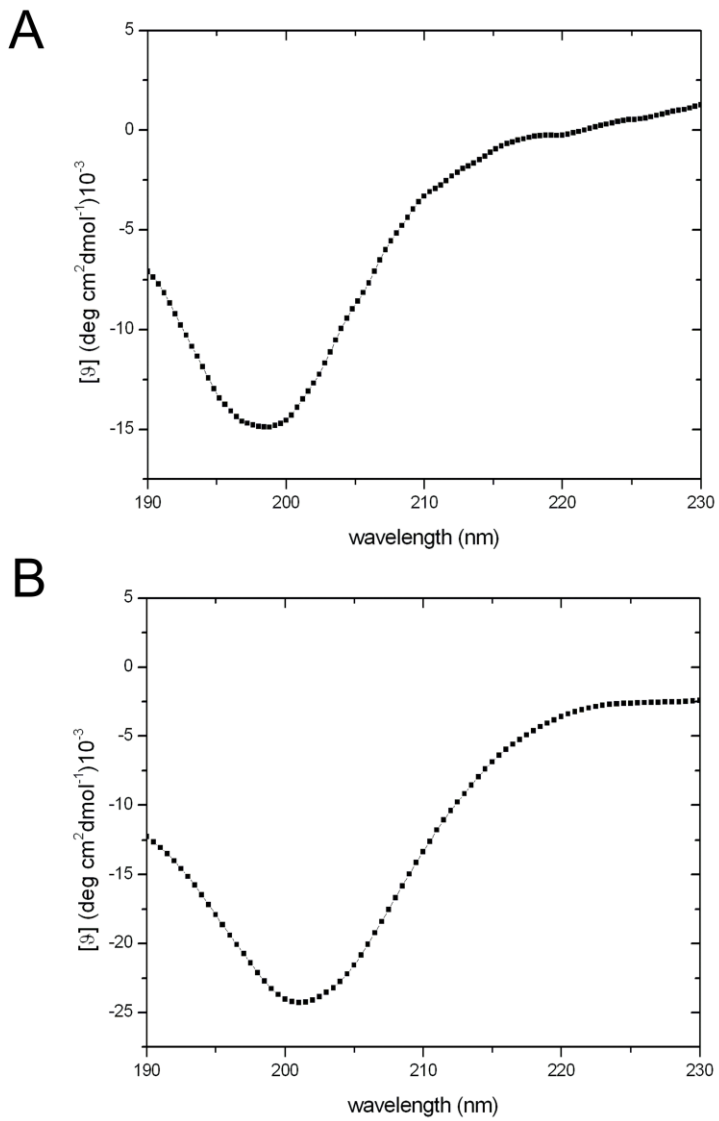

Figure 1
Far-UV CD spectra of NT4-Nter (A) and NGF-Nter (B)

2.3.2. MD simulations

In order to investigate the structural ensemble of these peptide at atomic level and to verify the occurrence of low-populated structured states, we performed rather long molecular dynamics simulations (200 ns) on both NT4-Nter and NGF-Nter by using the AMBER03 force-field (Duan et al., 2003), which has been proven to be well suited for the analysis of the peptide structured states (Best et al., 2008), implemented in the program GROMACS (Van der Spoel et al., 2005).

2.3.2.1. NT4 N-terminal peptide

To minimize the bias caused by specific structural features of the starting model of the peptide used in the MD simulations, it was built in an extended conformation (Figure 2A).

The initial stages of the simulation were characterized by a collapse of the extended conformer. These transitions led to the formation of transient turns and bends within the peptide. The analysis of the MD structures was conducted by excluding the first 50 ns of the trajectory, which could have been influenced by the starting state. As shown in Figure 2, the NT4-Nter displays a remarkable dynamical behavior. The ensemble of the structures detected in the MD trajectory is highly variable. In line with the results of the CD analysis, most of NT4-Nter structures do not exhibit regular secondary structure elements. Nevertheless, in a small, but significant (~20 %), fraction of conformers a 3_{10} helix motif is detected in the central region of the peptide. As shown in Figures 2B-2E, residues spanning from 8 to 10 form a short 3_{10} helix that folds and unwinds many times in the simulation. A deeper inspection of the trajectory shows that the helical structure is more persistent in the 55-70 and 150-170 ns intervals (Figures 2D-2E).

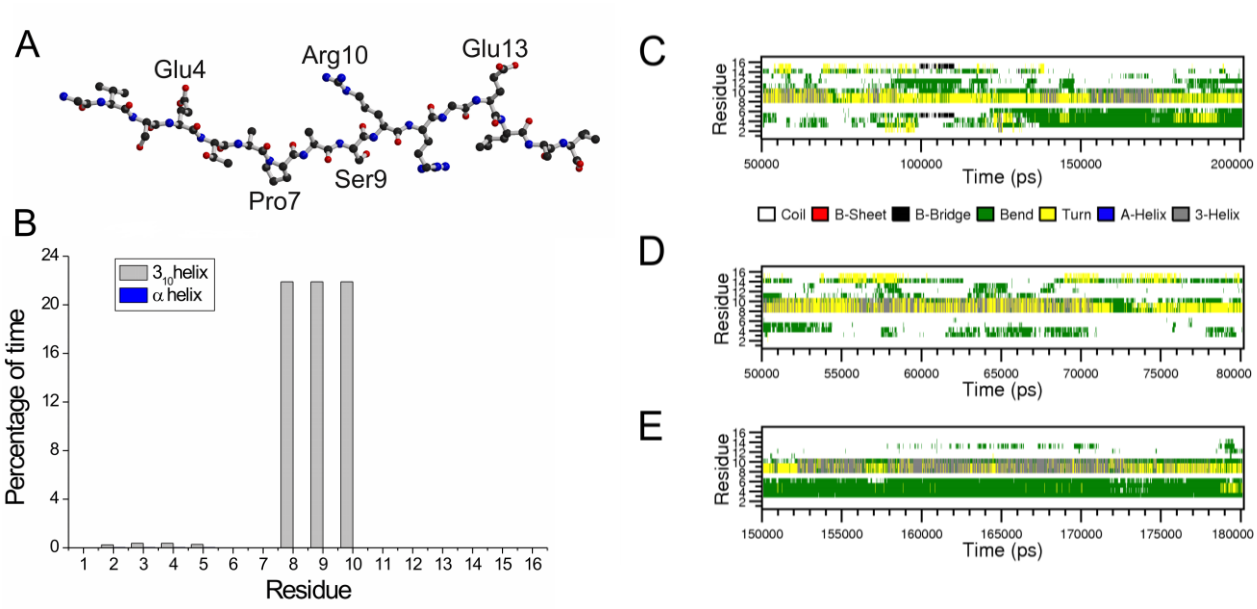

Figure 2
Molecular dynamics of NT4 N-terminal peptide: (A) starting model, (B) percentage of time that each residue spent in helical conformation in the simulation timescale 50-200 ns, (C) secondary structure formation along the trajectory, (D-E) snapshots on the secondary structure formation of specific regions of the trajectory.

As this secondary structure motif relies on the formation of backbone hydrogen bonds, we analyzed the evolution of distances between potentially interacting atoms. We detected the formation of transient hydrogen bonds between (i) the O atom of Pro^{7} and the N atom of Arg^{10}, and (ii) the O atom of Ala^{8} and the N atom of Arg^{11} (Figure 3). Although these atoms were quite distant in the starting extended NT4-Nter model (~15 Å), they frequently come closer than 3.0 Å. It is worth noting that the interaction between O Pro^{7} and N Arg^{10} is more preserved than the one between O Ala^{8} and N Arg^{11}. Notably, these hydrogen bonds are also detected in the structure of NT4 in its complex with TrkB (Banfield et al., 2001). Although NT4-Nter region contains charged groups its helical state is not stabilized by specific electrostatic interactions. The structural similarity of the 3_{10} conformers identified in the MD ensemble with the structure of the NT4 N-terminus in the complex with TrkB is of particular interest. As shown in Figure 4, a representative example of the 3_{10}

conformers detected in the simulation perfectly fits the structure of the protein in the complex. This finding suggests that, although highly flexible, the conformation needed for the binding to the receptor is present in the repertoire of structures intrinsically accessible to NT4-Nter.

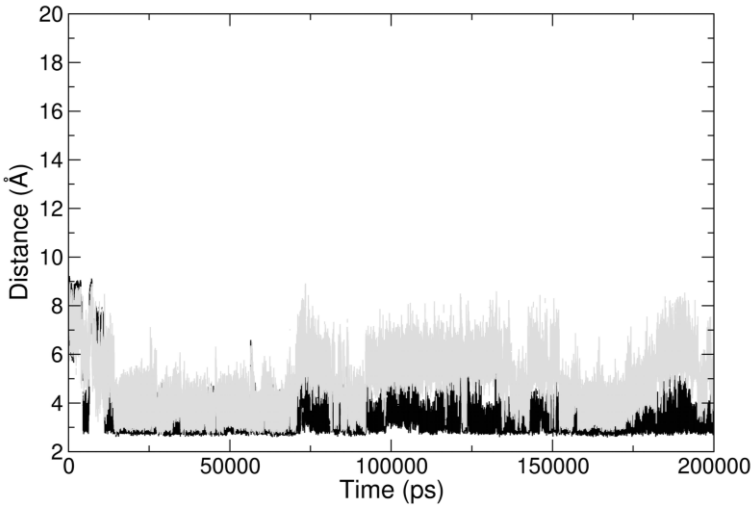

Figure 3
Evolution of the distances between atoms involved in the H-bonds that stabilize the 3_{10} helix in the complex NT4-TrkB: O Pro^{7}-N Arg^{10} (black), and O Ala^{8}-N Arg^{11} (grey).

Figure 4
A representative example of a 3_{10} helical model of NT4-Nter emerged from the simulation (magenta) superimposed to the N-terminal region of the NT4 (light grey) in the NT4-TrkB complex. The TrkB receptor is colored in dark grey. The model of the complex has been generated from the coordinates of the PDB entry 1HCF.

2.3.2.2. MD simulation on the NGF N-terminal peptide

The overall procedure adopted for investigating the intrinsic conformational preferences of NT4-Nter was extended to NGF-Nter, the N-terminal region of NGF (see Table 1 for the sequence). As found for NT4-Nter, the 200 ns MD simulation on NGF-Nter clearly shows that this peptide is intrinsically highly flexible (Figure 5). In line with the CD experiments, most of NGF-Nter conformations do not present regular secondary structure. A helical structure is detected for a limited fraction of conformers present in the ensemble. In contrast to what observed for NT4-Nter, the helical structure is detected for a NGF-Nter region (residues 10-12) that is buried in the native protein. Only an almost negligible portion (~1%) of NGF-Nter simulation structure presents a helical structure in the region that NGF N-terminus uses for TrkA binding (residues 6-8). The analysis of the distances between NGF-Nter atoms that are hydrogen bonded in NGF-TrkA complex shows that these atoms infrequently come close in the simulation. This is particularly evident for the hydrogen bonding partners O Ile^{6}-N Gly^{10}, whose distance is rarely lower than 6 Å in the simulation. In conclusion, the MD simulation carried on NGF-Nter is in line with the CD results. It also highlights significant differences in the conformational behavior of this peptide when compared to NT4-Nter.

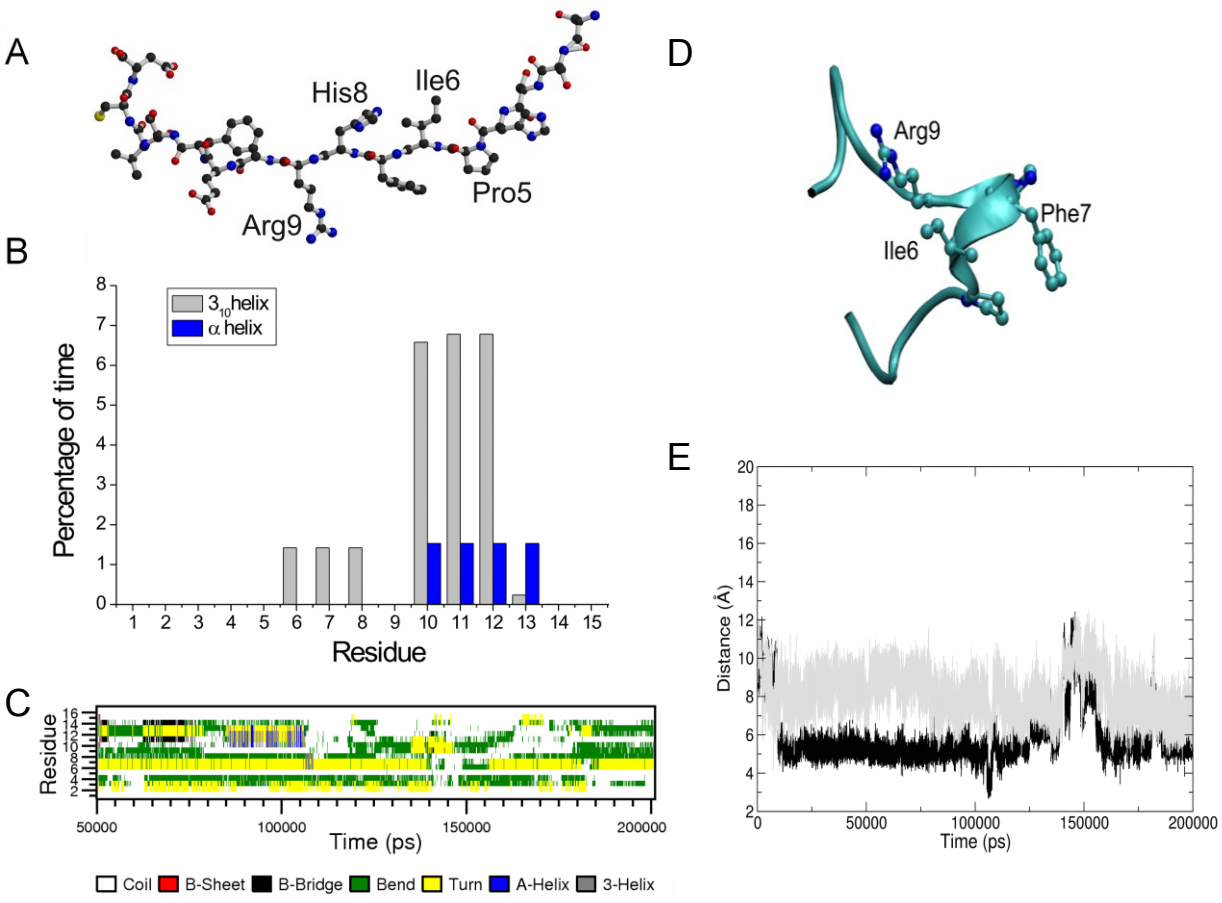

Figure 5
Molecular dynamics of NGF N-terminal peptide: (A) starting model, (B) percentage of time that each residue spent in helical conformation in the simulation timescale 50-200 ns, (C) secondary structure formation along the trajectory, and (D) a representative helical structure selected from the trajectory, (E) Evolution of the distances between atoms involved in the H-bonds that stabilize the α helix in the complex NGF-TrkA: O Pro^{5}-N Arg^{9} (black), and O Ile^{6}-N Gly^{10} (grey).

2.4. Implications for the molecular recognition of neurotrophins by receptors

Because the structural studies have unveiled that the N-terminal regions of NT4 and NGF are not involved in specific interactions with the rest of the protein (Banfield et al.,2001) (Wiesmann and de Vos 2001), the findings reported in the previous section, generated from the analysis of the isolated peptides, are also significant in the framework of the entire proteins. The observation that both peptides display a variety of different states is in line with crystallographic data. Indeed, these previous studies showed that they assume different conformations in the unliganded NTs, or when the NTs are in complex either with Trk or with $p75^{NTR}$ receptors. This conformational versatility is an important structural feature that allows these proteins to interact with diversified receptors. Present data unveil that for NT4-Nter, and to a lesser extent for NGF-Nter, the conformation of the peptide that is prone to the Trk binding is already present among the energetically accessible states. If these considerations are put in a more general context, the findings here described show that the mechanism of Trk recognition by NTs falls in the general mechanism denoted as population shift (Boehr et al., 2009) (Gunasekaran et al., 2004). In other words, rather then re-modeling the structure of the N-terminal region of the NTs (induced fit), the receptor selects states that are already populated.

The MD simulations here reported also suggest that the N-termini of the two NTs have a distinct conformational behavior. This is not surprising as the sequences of the N-termini of these NTs do not display any significant similarity (Table 1), despite an overall 47% sequence identity for the rest of the proteins. The lower tendency of NGF-Nter to intrinsically assume the helical state essential for the binding to TrkA may be related to the presence of a Ile residue in its central region (position 6). Indeed, it is well established that Ile residues have a poor helical propensity. The crystallographic structure of the complex NGF-TrkA shows that this residue makes extensive hydrophobic contacts with the receptor. Evidently, these interactions compensate for the lower helical pre-organization of the peptide due to the presence of this residue. Notably, in forty-eight NGF sequences isolated from different organisms reported in Swiss-Prot database (http://www.expasy.ch/sprot), this residue is either conserved or replaced with a valine. Since valine has a similar low propensity for helical structures and a similar hydrophobic side chain, the considerations reported above hold for all known NGF variants.

It is also important to note that an analysis of secondary structure prediction by using the PSIPRED: Protein Structure Prediction Server (http://www.psipred.net/psiform.html) of peptide fragments analyzed here indicates a general agreement with the MD simulations. Indeed, this analysis suggests that NT4-Nter has a limited intrinsic tendency to form helical structure in the region 8-12 (confidence score of 3 out of 9).

On the other hand, according to the prediction, the peptide NGF-Nter does not display any significant tendency to form helical structure. The preference of NT N-termini for unstructured states also provides insights into the ineffectiveness of peptides designed on the sequence of NGF N-terminus as NTs mimetics. In fact, it has been shown that, when the sequence of the NGF N-terminus is conjugated to sequences of loops of the protein, negligible effects in their agonist activity are observed (Colangelo et al., 2008). The limited population of the helical state, which is required for binding, straightforwardly explains these observations. This consideration also prompts feasible strategies for the design of effective NT agonist/antagonists. Indeed, variants of this peptide with an increased helical

propensity likely better mimic the NT functions. Several literature successful examples on other systems conducted using this strategy provide an indirect support to the proposed approach (Diana et al., 2008) (D'Andrea et al., 2005) (Walensky et al., 2004).

2.5. Conclusions

The combined experimental and theoretical approach here reported has provided a detailed picture of the NT N-terminal regions, which are considered hot spots in the molecular recognition between NT and their Trk receptors. Previous MD analyses have been focused on the evolution of the determinants of NGF-Nter recognition in its helical state by TrkA. We complement those studies by providing information on the intrinsic conformational properties of NT N-terminal regions. Present MD simulations, which are compatible with the experimental CD analysis, have provided insights into the structural features of low populated species. Not only do the present findings provide a structural explanation for the observed activity of synthetic peptides containing these NT regions, but they also suggest strategies for the development of effective peptide-based biologically active molecules. In particular, the design of peptide mimetics of these regions, containing amino acids endowed with enhanced preferences for these structural motifs, is likely to yield high affinity compounds for these receptors. Depending on their monomeric or dimeric state, these peptides may act as NT antagonist or agonist. Moreover, these peptides may be used to create conjugates with bioactive oligonucleotides for the selective targeting of cells over-expressing Trk receptors (Ma et al., 2004).

3. INTRINSIC FLEXIBILITY OF THE NERVE GROWTH FACTOR ANALYZED BY ESSENTIAL MOLECULAR DYNAMICS

3.1. Background

Neurotrophins (NTs) are able to promote neuronal cell survival, or cell death, depending on the context of neuronal environment (Lewin and Barde 1996). As mentioned in the Introduction, mature homodimeric NTs, bind to two type-I cell-surface receptors with different affinities. All NTs bind to $p75^{NTR}$, while each NT preferentially interacts with different Trk receptor subtypes (Chao 1994) (Chao et Hempstead 1995). The interaction of NTs with Trk receptors has been analyzed in detail as described in Chapter 2. Here the attention is focused on NTs-$p75^{NTR}$ recognition. Structural data on this interaction have collected in the last few years. The structural characterization of the complex between NGF and $p75^{NTR}$ have shown the formation of a complex with an unexpected 2:1 (NGF:$p75^{NTR}$) stoichiometry (He and Garcia 2004). The asymmetric receptor binding by the symmetric homodimer of NGF stimulated further investigations in very recent years. The physiological relevance of the asymmetric compound has been questioned by Blundell and co-workers who detected, by using a combination of mass spectrometry, analytical ultracentrifugation, and solution x-ray scattering measurements, the formation of a 2:2 complex (Aurikko et al. 2005). The initial report on the asymmetric assembly has been further undermined by the structural characterization of the complex of NT3-$p75^{NTR}$, which displays a 2:2 stoichiometry (Gong et al., 2008). Very recently, the structural and biochemical characterization of the interaction of proNGF, the NGF precursor, with $p75^{NTR}$ unveiled a 2:2 symmetric binding mode (Feng et al., 2010). It has been suggested that the 2:1 NGF–$p75^{NTR}$ complex may be an intermediate in the path to, or from a 2:2 complex and that a dynamic equilibrium of stoichiometries during receptor activation may exist. This topic has been further complicated by discovery that $p75^{NTR}$ is able to form dimers linked by disulfide bridges even in the absence of NTs (Vilar et al., 2009). In conclusion, the available literature data do not assure a precise role for asymmetric and symmetric NGF–$p75^{NTR}$ complexes. Both of them however, could be relevant to different stages of $p75^{NTR}$ signalling and function.
Regardless of the biological relevance, the ability of a symmetric NGF homodimer to form both symmetric and asymmetric complexes with one of its biological partners is nevertheless an intriguing property of this protein. Although NGF and other NTs have been the subject of several crystallographic investigations, studies on their dynamical properties are very limited. The only molecular dynamics simulation hitherto reported on these proteins are limited to the complex TrkA-NGF (Settanni et al., 2003) and to the analysis of the intrinsic properties of NTs N-terminal fragments (Stanzione et al., 2010) (Berrera et al., 2006). So far, analyses of the intrinsic dynamical properties of unliganded NTs have not been performed. In order to provide further information on receptor recognition by NGF during the PhD is carried out a detailed characterization of its intrinsic dynamical properties. In particular, by performing a rather long MD simulation (200 ns) we analyzed symmetric and asymmetric states in the ensemble of conformations accessible to the ligand-free protein. On the basis of these analyses the NGF–$p75^{NTR}$ recognition process was classified according to current models (population shift or induced fit). The implications of these findings for the design of NT mimetics are also discussed.

3.2. MATERIALS AND METHODS

3.2.1. System

In Protein Data Bank there are several crystallographic structures of NGF which were derived from different organisms or were representative of different binding states. Structures of human NGF include the complex with TrkA domain 5 (PDB code 1WWW, resolution 2.2 Å) (Wiesmann et al., 1999), with the entire extracellular domain of TrkA (PDB code 2IFG, resolution 3.4 Å) (Wehrman et al., 2007), and with the $p75^{NTR}$ (PDB code 1SG1, resolution 2.4 Å) (He and Garcia 2004). Each NGF monomer exhibits a folding characterized by an extended β-structure stabilized by a cysteine knot motif formed by the disulfide bridges Cys15-Cys80, Cys58-Cys108, and Cys68-Cys110. The strands of the protein are connected by loops that play an important role in protein-protein interactions involving NGF. The four main loops are defined as L1 (residues 29-35), L2 (40-49), L3 (67-75), and L4 (91-97). As starting model for the MD simulations, we used the highest resolution structure of human NGF, the PDB entry 1WWW. Homology modelling techniques were used to model the residues of the loop L3 61-66 that were missing in the crystallographic model. The last three residues at the C-terminus that were disordered in the crystalline structure were not considered in the present simulation. Moreover, being the N-terminus (residues 1-9) of NGF typically disordered in ligand-free NGF and in the complex with $p75^{NTR}$, it was not considered in the simulated model. In conclusion the simulation was performed with the NGF dimer corresponding to residues 10-115 (Figure 1). In order to remove the bias of the crystallographic context of the starting model, its energy was minimized by using the steepest-descent method until convergence was reached. Comparative analyses with trajectory structures were performed using this minimized model.

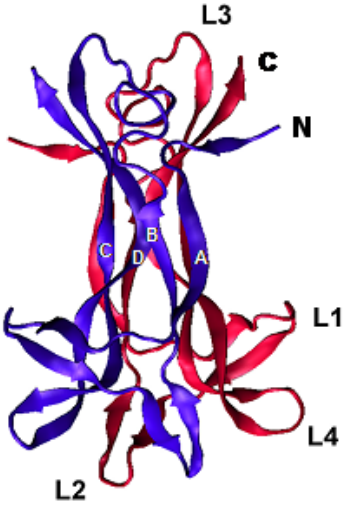

Figure 1
Cartoon representation of NGF model derived by the complex NGF-TrkA (PDB entry 1WWW). For each subunit, only the main body of the structure (residues 10-115) is shown. The two chains are colored in blue and in red. The C- and N-termini and loops and secondary elements are labeled.

3.2.2. Molecular Dynamics parameters

The MD simulation was preformed with GROMACS software package 3.3.3 (Van der Spoel et al., 2005) (See Appendix for details). The NGF model was immersed in a

triclinic box filled with 10475 water molecules. Being both ends of the model truncated (see above), the termini were considered not charged. The overall charge of the model (+4) was neutralized with addition of four chloride counterions. The GROMOS43a1 force field and the SPCE water model were used. In order to relax bond geometries, the potential energy of the system (peptides and water) was doubly minimized by using the steepest-descent method until convergence was reached. The solvent was then relaxed by 100 ps of MD at 300 K, restraining protein atomic positions with a harmonic potential. The system temperature was brought to 300 K in a step-wise manner: 50 ps MD runs were carried out at 50, 100, 150, 200, 250 and 300 K, in the end a step of 50 ps were carried out with the Temperature and Pressure coupled. It has been checked that, in each step of the heating of the different systems, the potential energy reached a stable value. The timescale of simulation is reported in Table 1. The simulations were run with periodic boundary conditions and bond lengths were constrained by the LINCS algorithm (Hess et al., 1997). The electrostatic interactions were calculated using Part Mesh Ewald algorithm with a cutoff of 1.0 nm. The cutoff radius for the Lennard-Jones interactions was set to 1.0 nm. A dielectric constant of 1 was used, and Newton's equation was integrated within a timestep of 2 fs. The temperature was maintained constant using the Berendsen thermostat with a time constant of 0.1 ps (See Appendix for details). Trajectory structures were analyzed by using GROMACS and VMD routines. Pictures were generated using the programs VMD (Humphrey et al., 1996).

Table 1. Summary of the Simulations Performed

Model	Atom peptide	Atom water	Cl-	Box dimensions ($Å^3$)	Simulation time (ns)	T(K)
NGF	2164	31425	4	55 x 68 x 93	200	300

3.2.3. Essential Dynamics

To characterize the global motions of protein segments, essential degrees of freedom were extracted according to the essential dynamics method (ED) (Garcia 1992) (Amadei et al., 1993). The ED method, often referred to as principal component analysis (PCA), is based on the multivariate analysis. PCA rests on the assumption that the major collective modes of fluctuation dominate the functional dynamics. Because these principal modes of motion could, in many cases, be linked to protein function, the dynamics in the low-dimensional subspace spanned by these modes was termed "essential dynamics", to reflect the notion that these are the modes essential for function (Amadei et al., 1993). The subspace spanned by the major modes of collective fluctuations is accordingly often referred to as "essential subspace." Practically, the ED is based on the construction of the covariance matrix C_{ij} of the coordinate fluctuations from the equilibrated portion of the trajectory from which overall translational and rotational motions have been removed:

$$C_{ij} = \langle (X_i - X_{i,0})(X_j - X_{j,0}) \rangle$$

where X are the *x*-, *y*- and *z*-coordinates of the atoms fluctuating around their average positions X_0 and where $\langle \ldots \rangle$ denote an average over time. Here, to construct the protein covariance matrices we have used C^{α} atom trajectories. Indeed, it has been shown that the C^{α} atoms contain all the information for a reasonable description of the protein large concerted motions (Amadei et al., 1993).
Upon diagonalization of the covariance matrix, a set of eigenvectors and eigenvalues is obtained, that provide information about correlated motion throughout the protein. Eigenvectors represent the directions of motion in 3*N* dimensional space (where *N* is the number of C^{α} atoms). Eigenvalues represent the amount of motion along each eingenvector and correspond to concerted fluctuations of atoms. The eigenvectors are then sorted according to their eigenvalues in descending order. Usually, the first 10–20 eigenvectors suffice to describe almost all conformational substates accessible to the protein (Amadei et al., 1999).
In order to demonstrate that a good convergence in the essential space had been reached in our simulation, root mean square inner product (RMSIP) between two halves of the equilibrated trajectory was calculated as described in previous works. (Ceruso et al., 1999) (Arcangeli et al., 2001) (Merlino et al., 2003) (Merlino et al., 2004) (Merlino et al., 2005) (Rueda et al., 2007).
The RMSIP is defined as:

$$RMSIP = \sqrt{\frac{1}{10}\sum_{i=}^{10}\sum_{j=}^{10} \eta_{\cdot} \cdot \eta_{\cdot})^2}$$

Where $\eta_{\cdot}$ and $\eta_{\cdot}$ are the *i*th and *j*th eingenvectors from a first and second half of the equilibrated trajectory, respectively.

3.4. RESULTS

3.4.1. Structural stability of NGF in the simulation

The overall stability of the protein during the simulation has been monitored by using several structural properties (See Appendix for details) (Figure 2-3). The root mean square deviations (RMSD) of the model coordinates during the simulation *versus* the starting structure as function of time are reported in Figure 2A. The analysis of this plot indicates that RMSDs approached values of ~1.5 Å since the very early stage of the simulation. Minimal variations have been observed in the later stages of the trajectory. In the time interval 80–200 ns the RMSD values reached a *plateau* around ~2.0 Å. Similar deviations are exhibited by the two chains within the dimer (Figure 2B). The structural integrity of the model in the simulation is also evidenced by the analysis of the radius of gyration (Figure 2C), the total number of hydrogen bonds (Figure 2D) and the secondary structure content (Figure 3). Trajectory structures were also compared with other NGF crystallographic structures. In particular, MD NGF models were compared with the NGF structure of the NGF-$p75^{NTR}$ complex and with the mouse ligand-free structure (PDB code 1BET) (McDonald et al., 1991). As shown in Figure 2A, the structures generated from the simulation generally show lowest RMSD values when compared to the starting NGF model. The highest RMSDs values are detected for the comparison with the NGF taken from the NGF-$p75^{NTR}$ complex. Intermediate values are detected for the

comparison with the mouse NGF structure. More detailed inspections of these data show that only 38 MD structures out 200,000 are closer to NGF taken from the $p75^{NTR}$ complex. On the other hand, 1897 structures of the MD ensemble are closer the mouse structure 1BET than human starting model. Although the structures of the trajectory show as expected the highest level of similarity with the structure of the unliganded human model, it is important to note that they are closer to the unliganded mouse model rather than to the $p75^{NTR}$ bound form. This suggests that structural alterations induced by the receptor binding are larger than those due to differences in the sequence.

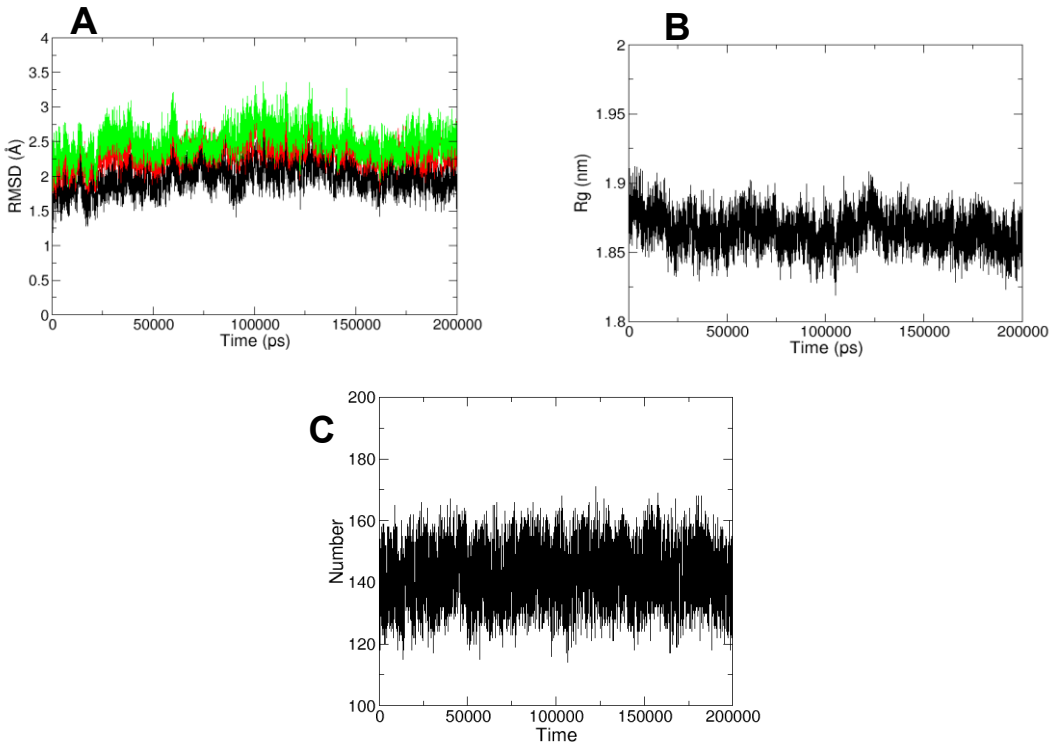

Figure 2
Evolution of structural parameters in the simulation: A) RMSD values computed on C^{α} atoms of trajectory structures versus (i) the starting model (black line) (ii) the ligand-free mouse structure (PDB code 1BET) (red line), and (iii) the NGF structure of the NGF-$p75^{NTR}$ complex (green line); B) the radius of gyration; C) the total number of hydrogen bonds.

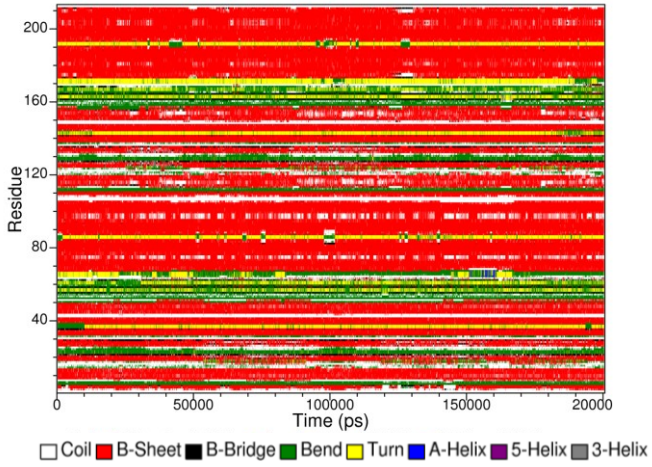

Figure 3
Evolution of the secondary structure elements during the simulation.

3.4.2. NGF fluctuation in the MD simulation

The analyses of NGF motions were conducted by considering structures in the *plateau* region of the trajectory. As shown in the Figure 2, RMSD values are rather constant in the time interval 80–200 ns. Quantitative evaluations of the convergence of the trajectory in this time interval were performed by comparing average structures and the trace of the covariance matrix (see methods) in the two halves of the *plateau* region (80–140 ns and 140–200 ns). In particular, the RMSD between the two average structures is as low as 0.28 Å. Moreover, the trace of the covariance matrix (see methods for the definition), which provides an estimate of the overall motion of the protein during the simulation, is also rather similar in the two halves, being 3.43 nm^2 and 2.85 nm^2 in the 80–140 ns and 140–200 ns intervals, respectively. Collectively, these findings demonstrate that a good convergence of the system has been achieved in the *plateau* region of the trajectory. This observation is corroborated by the RMSIP calculations performed in the framework of the essential dynamics study (see below). It is worth noticing that the trace of covariance (3.26 nm^2) matrix in the plateau region 80–200 ns is indicative of a protein endowed with a significant structural mobility. The ensemble of the structures present in the plateau region was used to generate the average MD NGF model for the subsequent analysis. In this average structure, the two chains present an RMSD value of 0.96 Å.
The root mean square fluctuations (RMSF) (See Appendix for details) around the average structures per residue computed for trajectory structure present in the rime interval 80-200 ns are reported in Figure 4.
The analysis of the plot clearly indicates that the mobility of equivalent residues in the two subunits is very similar motilities. As expected, terminal ends and loop regions L1-L4 (29-35, 40-49, 67-75, 91-97) exhibit pronounced fluctuations. Equivalent loops of the two regions also display similar RMSF values. A very large flexibility is also displayed by NGF regions that are involved in receptor binding. In particular, L4 which is contributes to the binding of both TrkA and $p75^{NTR}$ exhibits the largest RMSF values (~2.5 Å). High values are also displayed by L1 residues that is also involved in the binding of both receptors and by the L3 residues which is implicated in the binding of $p75^{NTR}$. The residues comprising the β-structure regions of the protein show lower RMSF values compared to loop regions. Nevertheless, some of the residues in β-structure are endowed with a significant flexibility. Interestingly, the most rigid amino acids in the protein structure correspond to cysteine residues involved in the three disulfide bridges (Cys68-Cys110, Cys15-Cy80, and Cys58-Cys108) that constitute the cysteine knots motif. These findings show that cysteine residues of the knot represent fundamental anchoring of the protein scaffold.

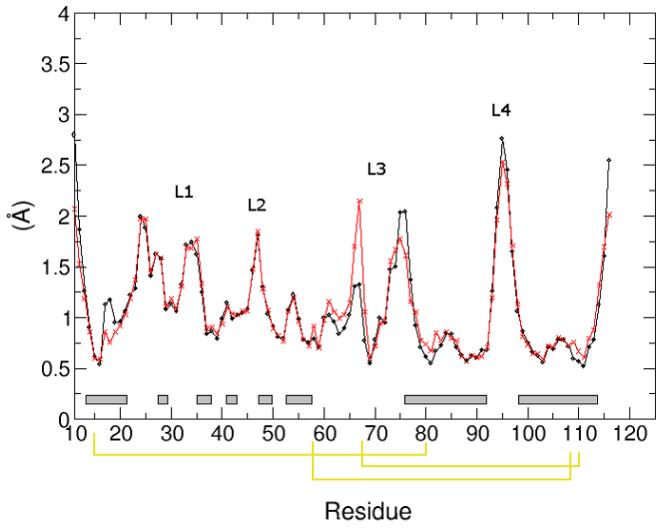

Figure 4
Root mean square fluctuations (RMSF) of C^{α} atoms in the equilibrated region of the trajectory. The two values corresponding to the two subunits are superimposed (black and red lines). Loop and β-sheet regions are highlighted. Yellow lines represent the three disulfide bridges of the cysteine knot.

3.4.3. Essential dynamics and concerned motion

To characterize collective global and local motions of the protein, we analyzed the MD trajectory by using essential dynamics techniques (see methods for details) (Amadei et al., 1993). This approach is based on the assumption that major collective modes of fluctuation dominate the functional dynamics. This method is based on a preliminary generation of the covariance matrix of the C^{α} atom whose diagonalization leads to a set of eigenvectors and eigenvalues that provide information about correlated motion in the protein. Eigenvectors represent the directions of motion in 3*N* dimensional space whereas eigenvalues represent the amount of motion along each eingenvector. The configurational space of C^{α} coordinates of the present NGF model consists consist of 636 dimensions ($3NC^{\alpha}$, *N*= 212 residues*).*
The covariance matrix for the NGF dimer is shown Figure 5. Atoms that move concertedly give rise to positive peaks in this symmetric matrix. Negative peaks are observed for anti-correlated motions. The analysis of the matrix obtained for NGF shows close similarities in the relative motions observed within monomer 1 and monomer 2. Indeed, peaks observed in the lower left quadrant and in the upper right quadrant have very similar distributions and intensities. Similarly, inter-subunit motions are also heavily correlated. Indeed, relative motions between residues of subunit 1 and subunit 2 and those detected between residues of subunit 2 and subunit 1 are also strikingly similar. This observation indicates an elevated degree of symmetry in the motility of NGF dimer. As stated above, this matrix was used to generate eigenvectors and eigenvalues. The total positional fluctuation of the protein as function of the 636 eigenvectors is shown in Figure 6A. Notably, the first 10 eigenvectors account for the 65% of the total motions of the protein. This means that most of the NGF intrinsic flexibility can be represented by a subspace whose dimension is much smaller than the original 3*N* configurational space. The generation of the covariance matrix and the related eigenvectors/eigenvalues for the two halves of the trajectory (80–140 ns and 140-200 ns) provides a further indication of the

convergence of the trajectory. The RMSIP (see methods), computed considering the first 10 eigenvectors for each half, was as high as 0.64. This indicates that the essential subspace obtained from one half of the equilibrated trajectory is similar to that calculated from the other, thus ensuring that a good convergence was reached in the simulation. The analysis of Figure 6B indicates that the first eigenvector provides a significant description of the overall motion of the protein. Indeed, it accounts for 36% of the essential subspace and for 23% of the overall motion.

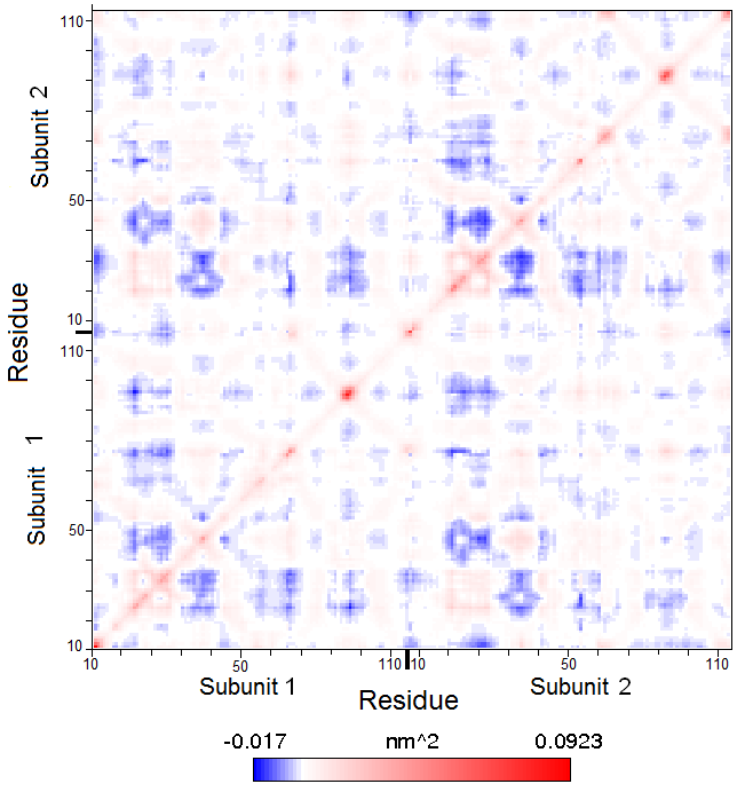

Figure5
Covariance Matrix derived from the plateau region of the trajectory. Residues are numbered from 10 to 115 following the NGF sequence. Atoms that move concertedly give rise to positive peaks (red colour) in this symmetric matrix. Negative peaks (blue colour) are observed for anti-correlated motions.

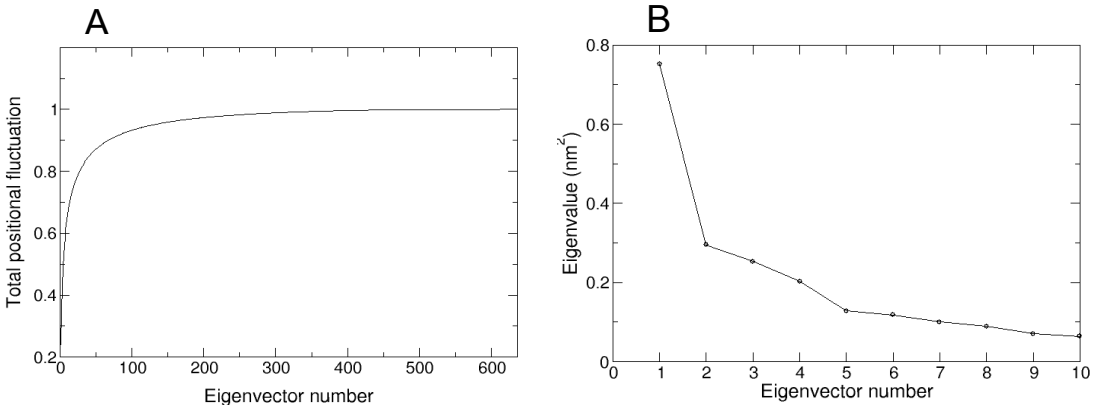

Figure 6
A) Total positional fluctuations as a function of eigenvectors computed from the Cα covariance matrices. B) Eigenvalues against their corresponding eigenvector numbers, calculated from the MD ensemble. The first eigenvectors correspond to large eigenvalues. The steepness of the curve indicates that the first eigenvectors describe a large fraction of the total motion in the system.

The inspection of the film-like representation of this eigenvector indicates that several regions of the proteins are endowed with a significant flexibility. Indeed, even β-strands present significant fluctuations (Figure 7). A comparative analysis of the motions of the two subunits within the dimer is indicative of symmetrical overall motions. Indeed, corresponding loops of the two subunits move in the same directions. L2 and L4 loops show an anti-correlated motion with respect to the main β-structure of the molecule. Similarly the movements of L3, which is located on the other side the molecule, are also anti-correlated with respect to the central sheet. On the other hand, L1 moves in the same direction of the β-sheet. Intriguingly, L1 and L4 (Figure 7B), having anti-correlated motions, collectively undergoes a breathing motion. Indeed, in different conformational states of the protein they show very different relative distances. The overall flexibility of these loop regions are in line with the experimental observation that they undergo significant transition upon $p75^{NTR}$ binding.

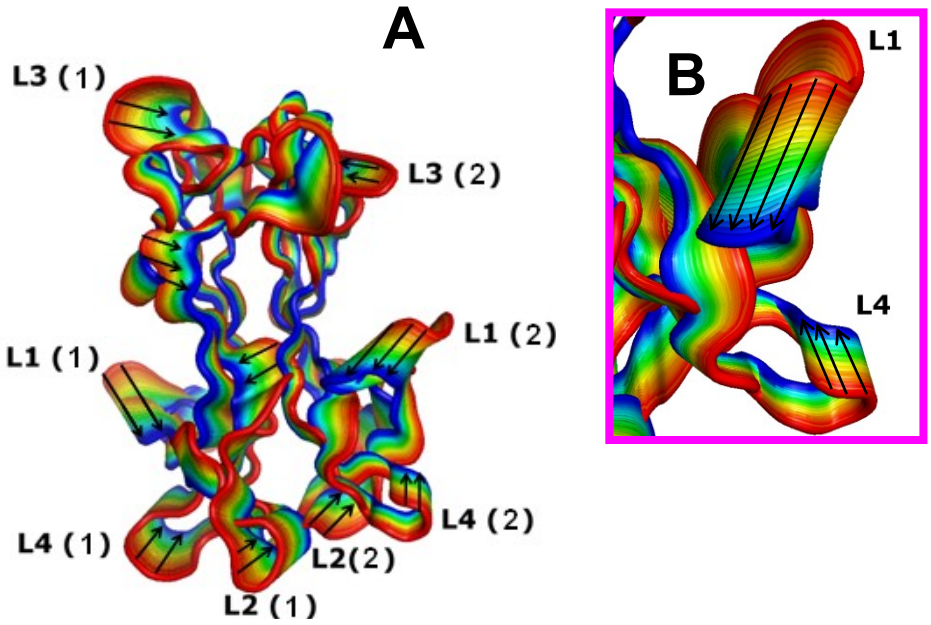

Figure 7
Protein motions along the first eigenvector. The colour scale is used to represent motions in a film-like fashion. Vectors are qualitative indicators of the direction of C^{α} atom motions. A) Representation of the correlated motes of loop regions and β structure. In the panel B a snapshot on the region embedding L1 and L4 is shown.

3.5. DISCUSSION

NGF and other neurotrophins are key factors in many processes of the nervous system. Their potential as candidates for therapeutical treatment of different types of neurological disorders has been proven. However, their concrete use is limited by their poor pharmacological properties. As reported in other sections of the present thesis, many efforts are devoted to the search of small molecules with NT agonist/antagonists activities. A profound knowledge of the intrinsic structural and dynamical properties of these proteins is an important requisite for the design of

peptide-based NT mimetics. Over the last two decades several fundamental studies have provided information on the structural properties of different NTs and on their complexes with receptors. Although these studies have fully elucidated many features of these proteins, some controversial aspects still remain. Despite the extensive crystallographic investigations on these proteins, studies aimed at unveiling their dynamic properties are very limited. Contributions hitherto reported are related to the complex between NGF and TrkA and to small fragments of the N-termini of NGF and NT4. One of the most striking features of these proteins emerged from both comparative analysis of different crystallographic studies and from independent MD simulations is the high intrinsic flexibility of NTs regions directly involved in partner recognition. Indeed, receptor binding by NTs is frequently mediated by high flexible regions such as the N-termini and the loop regions. In this scenario, it is evident that a detailed characterization of the intrinsic dynamic properties of the protein represents an important step for understanding the structural basis of partner recognition by NTs. In chapter 2 the intrinsic conformational properties of NT4/NGF N-termini have been characterized. In the present chapter the attention has been focused on the intrinsic dynamic properties of the main body of the protein (residues 10-115). The present MD analysis confirms the high motility of the loop regions. Notably, a significant flexibility is also displayed by some of the β-strands of NGF core β-structure. The most rigid parts of the protein correspond to the cysteine residues involved in the disulfide bridges that constitute the characteristic knot motif of the structure. The presence of this anchoring motif may allow significant motions also for the typically rigid secondary structure elements. Several distinct indicators (RMSF and RMSD values, eigenvectors of principal component analysis, etc) demonstrate that NGF motions are highly symmetrical. Indeed, even high flexible loop regions of the two monomers within the dimer display concerted motions. These findings hold implications on the particularly puzzling is the topic of the stoichiometry of the complex between NGF and $p75^{NTR}$. The marginality of asymmetric states in the simulation ensemble indicates that the protein is not intrinsically prone to form asymmetric complexes. The formation of asymmetric complexes between NGF and $p75^{NTR}$, which have detected both in solution and in the crystalline state, likely relies on significant alterations of the protein structure induced by the receptor binding. In more general terms, the generation of the 2:1 NGF-$p75^{NTR}$ complex falls in the general “induced fit” rather than “population shift” mechanism. This indicates that different regions of the same protein may establish interactions with different biological partners by adopting distinct structural pathways. The high motility of L1 and L4 regions in the protein may account for the ability of flexible peptides based on these regions to mimic NGF activity both *in vivo* and *in vitro* (Colangelo et al., 2008). It has been shown that these peptides are endowed with an enhanced NGF-like activity when compared with more structurally constrained peptides, derived from the same protein regions.

In conclusion, present data provide information on the dynamics of regions that, despite their intrinsic flexibility, play a major role in receptor binding. These considerations suggest that flexibility may be an important feature to be considered in the design of NGF agonist molecules. Finally, the structural analogy between NGF and other NTs indirectly suggests that the results here reported can be extended to the other members of this protein family.

4. DYNAMICS AND STABILITY OF AMYLOID-LIKE STERIC ZIPPER ASSEMBLIES WITH HYDROPHOBIC DRY INTERFACES

4.1. Background

In the last years enormous efforts have been made to obtain insights into the structure of the amyloid-like forms of proteins and peptides involved in the insurgence of neurodegenerative diseases. The intrinsic difficulties of these investigations have been overcome by adopting innovative structural methodologies (solid state NMR) or by using X-ray crystallography on model systems. (Nelson et al., 2005) (Sawaya et al., 2007) (Wasmer et al., 2008) (Heise 2008) (Tycko 2006).
In this framework, MD simulations on the steric zipper models have shown that these assemblies are endowed with a remarkable stability also in a crystal-free context. However, MD simulations were limited to peptides with polar and/or aromatic dry interfaces. A section of my PhD project is focused on MD simulations to steric zipper assemblies whose dry interface involves exclusively aliphatic residues. We characterized a variety of assemblies formed by the peptides SSTSAA and VQIVYK, whose structures have been recently solved at high resolution (Sawaya et al., 2007). In particular, SSTSAA is a fragment of the hinge region of ribonuclease, whereas VQIVYK is a fragment of the tau protein, which is involved in the pathogenesis of Alzheimer's disease. Although the crystalline assemblies of these peptides present interface areas comparable to those exhibited by the peptides endowed with a polar interface, data presented here indicate that aliphatic apolar residues at the interface provide them with a loose association. In order to further investigate the role of hydrophobic surfaces in the stabilization of other amyloid-like systems, MD analysis were also extended to the HET-s(218-289) prion model recently proposed on the basis of solid state NMR data (Wasmer et al., 2008).

4.2. MATERIALS AND METHODS

4.2.1. Systems

Starting models for the two peptides SSTSAA and VQIVYK were generated by using the coordinates of the Protein Data Bank files 2ONW and 2ON9, respectively (Sawaya et al., 2007). The assemblies were generated by applying the symmetries of the crystalline structures. For the SSTSAA the first ten-stranded sheet was generated by applying the translation operation symmetry along the y axis to the coordinates of the molecule present in the asymmetric unit. To generate the second opposing sheet, the 2_1 symmetry operation along an axis parallel to y was applied to the coordinates of each strand of the first sheet. For VQIVYK, depending on the dry interface characterized, two different pair-of-sheet models were generated. In the first model, endowed with the apolar interface (VQIVYK-dA), each ten-stranded sheet was generated by applying the translation operation symmetry along the x axis to the coordinates of the two chains present in the asymmetric unit. In the second model, endowed with the polar interface (VQIVYK-dP), the first sheet was generated by applying the translational operation symmetry along the x-axis to the coordinates of chain B of the asymmetric unit. The second sheet of this model was built by applying

the translational operation symmetry along the z-axis to the coordinates of the first sheet. To generate the models made of three sheets, we added a third sheet to the two-sheeted model VQIVYK-dA. The third sheet was generated by applying to one of the two sheets a translation operation symmetry along the z-axis; the translation applied in opposite directions resulted in the different VQIVYK-T1 and VQIVYK-T2 models. Residues of SSTSAA or VQIVYK systems were numbered from 1 to 6 in the first strand, from 7 to 12 in the second strand, and so on. Taking into account the crystallization conditions of these systems, in both cases simulations were carried out on peptides with charged ends. For HET protein, the coordinates of the PDB entry 2RNM (model 1) were used as starting model for the MD simulation. The C-terminal polyHis tag of the PDB model was deleted and the region corresponding to residues 218-287 was used.

4.2.2. Molecular dynamics parameters and protocols

MD simulations were performed with the GROMACS software package.3.3 (Van der Spoel et al., 2005) (See Appendix for details). The models were immersed in rectangular or cubic boxes filled with water molecules. When required, Cl^- ions were added to neutralize the simulated system. The GROMOS43a1 force field and the SPCE water model were used in the simulations. For all systems, in order to relax bond geometries, the potential energy of the system (peptides and water) was minimized by using the steepest-descent method until convergence was reached. The solvent was then relaxed by 100 ps of MD at 300 K, restraining protein atomic positions with a harmonic potential. The system temperature was brought to 300 K in a step-wise manner: 30 ps MD runs were carried out at 50, 100, 150, 200, 250, and 300 K. It has been checked that, in each step of the heating of the different systems, the potential energy reached a stable value. The timescale of the individual simulations is reported in Table 1. The simulations were run with periodic boundary conditions. Bond lengths were constrained by the LINCS algorithm (Hess et al., 1997). The electrostatic interactions were calculated using Part Mesh Ewald algorithm with a cutoff of 1.0 nm. The cutoff radius for the Lennard-Jones interactions was set to 1.0 nm. A dielectric constant of 1, and a time step of 2fs were used. We used the NVT ensemble in all simulations. The temperature was maintained constant using the Berendsen thermostat with a time constant of 0.1 ps (See Appendix for details). Trajectory structures were analyzed by using GROMACS and VMD routines (Humphrey et al., 1996).

Table 1: A summary of the simulations performed. The notation of the models is reported in the Materials and Methods section.

Model	atoms peptide / atoms waters / Cl^-	Box dimensions ($Å^3$)	Simulation time (ns)	T(K)
SSTSAA	960 / 22107 / -	62.6 x 80.9 x 46.0	60	300
VQIVYK-dA	1420 / 24240 / 20	81.7 x 64.4 x 50.1	40	300
VQIVYK-dP	1420 / 22881 / 20	82.6 x 48.4 x 62.7	40	300
VQIVYK-T1	2130 / 30168 / 30	82.6 x 64.3 x 62.7	40	300
VQIVYK-T2	2130 / 31989 / 30	83.3 x 64.5 x 65.4	40	300
HET-s(218-289)	3490 / 67194 / 5	89.8 x 89.8 x 89.8	40	300

4.3. RESULTS AND DISCUSSION

4.3.1. Model peptides with apolar aliphatic interfaces: the case of SSTSAA

The analysis of the SSTSAA steric zipper motif detected in the crystal state indicates that the two facing sheets are well packed, with an average inter-sheet distance of 5.9 Å.[7] Indeed, the overall dry interface area and the surface complementarity are 122 Å and 0.82, respectively (Sawaya et al., 2007). The inspection of the crystalline structure also shows that apolar aliphatic groups constitute the dry interface. As shown in Figure 1A, the groups of each sheet involved in the dry interface are the side chain of A5 and the methyl group of T3 side chain. On analogy with previous investigations, MD simulations were carried out on a pair of ten-stranded β-sheets (Figure 1A). The evolution of the root mean square deviations (RMSD) (See Appendix for details) between starting and trajectory structures clearly indicates that the system undergoes remarkable transitions (Figure 1B). The analysis of secondary structure evolution suggests that a significant decrease of total β-sheet content occurs (Figure 1C).

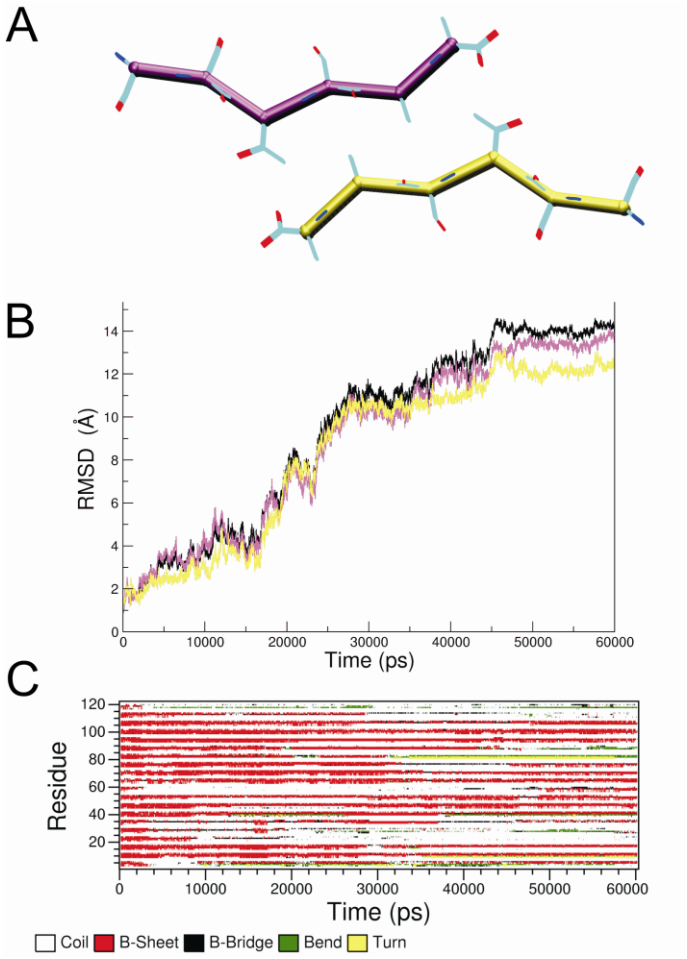

Figure 1
MD simulation of the pair-of-sheet model of SSTSAA. (A) starting model, (B) RMSD values of trajectory structure versus the starting X-ray model computed on the C^{α} atoms of the entire assembly (black line) or of the individual sheets (yellow and magenta), and (C) evolution of the secondary structure.

However, even at the end of the simulation (60 ns) regions with a significant amount of β-structure can be identified. The visual inspection of the structures along the trajectory shows that the steric zipper motif, although highly fluctuating, is preserved in the first 15 ns of the trajectory. At this stage, a significant rearrangement of the assembly overall structure begins. Indeed, in the central part of the model, the β-sheet structure and, consequently, the intersheet association is broken (Figure 2A). This event originates two mini SSTSAA steric zipper aggregates, each made of 6-8 strands. The large RMSD values observed in the 15-25 ns time period of the simulation correspond to the relative re-orientation of these rather stable fragments. In the 25-60 ns interval, the two fragments keep their steric zipper structure and also maintain a stable relative orientation (see Figure 2A-B for a representative structure along the trajectory). The small increase of the RMSD occurring at 40-45 ns can be ascribed to the mobility of external strands of the two fragments. The picture is corroborated by the analysis of several parameters of trajectory structures. The secondary structure elements preserved throughout the entire trajectory correspond to residues of these two fragments. In addition, evaluation of the inter-sheet distance confirms that these two portions of the model still preserve a steric zipper association (Figure 2C-D). Finally, the overall structural organization leads to the formation of new interactions between the external residues of the two fragments that are rather stable once formed (Figure 2E). In conclusion, the analysis of steric zipper assemblies formed by the SSTSAA appears to be rather unstable. Surprisingly, this structural motif is stabilized by lateral interactions established during the simulation by two fragments generated as a consequence of the break of the starting model.

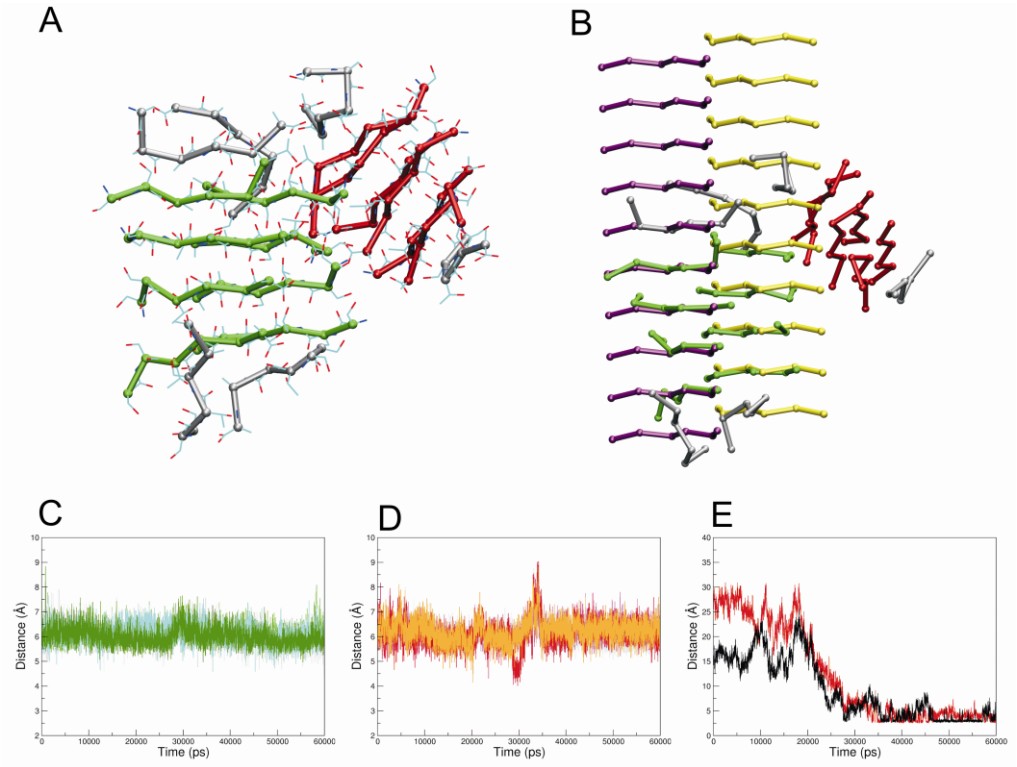

Figure 2
Evolution of SSTSAA during the simulation. (A) A representative structural model of the simulation where the two conserved mini steric zipper aggregates are highlighted in red (residues 7–24 and 61–78) and green (residues 31–54 and 91–114), (B) superimposition of this model to the starting X-ray model, (C) intersheet C^{α}-C^{α} distances: A47–S100 (green), A41–S100 (grey), A101–S40 (dark green), A101–S46 (cyan), (D) intersheet C^{α}-C^{α} distances: A11–S70 (orange), A17– S70 (magenta), A71–S10 (grey), A71–S16 (red), and (E) H-bonded interactions established by the external surface of the two fragments (S38–A72 in red, and S19–S34 in black).

4.3.2. Model peptides with apolar aliphatic interfaces: the case of VQIVYK

The analysis of the VQIVYK packing of the peptide crystalline structure indicates that two different pair-of-sheets with significant interface area and surface complementarity may be identified (Sawaya et al., 2007). One is characterized by an apolar dry interface made essentially by the side chains of V1 and I3 of the two sheets (Figure 3A, Figure 5A), while the other is rather polar as it involves Tyr and Gln side chains (Figure 5A). It should be noted that the pair with the apolar interface exhibits larger vales of the surface area (113 *versus* 89 Å) although coupled with a slightly lower surface complementarity (0.76 versus 0.82) (Sawaya et al., 2007). MD simulations were carried out on assemblies made of ten-stranded pair-of-sheets with the apolar interface (model VQIVYK-dA) (Figure 3A). MD tests were also conducted on assemblies with the polar interface (VQIVYK-dP).
The evolution of the RMSD values between the trajectory structures and the starting model of VQIVYK-dA shows that there is a rapid transition of the system (within the first 1000 ps) (Figure 3B). This rearrangement, mostly due to the twisting of the initially flat β-sheets, is followed by the appearance of less variable states in the rest of the trajectory. The significant variation of the RMSD values in the 1000-40000 ps interval is, however, still indicative of a fluctuating system. This observation is corroborated by the analysis of the root mean square fluctuation (RMSF) values computed in the 5000-40000 region of the trajectory (See Appendix for details) (Figure 3C).

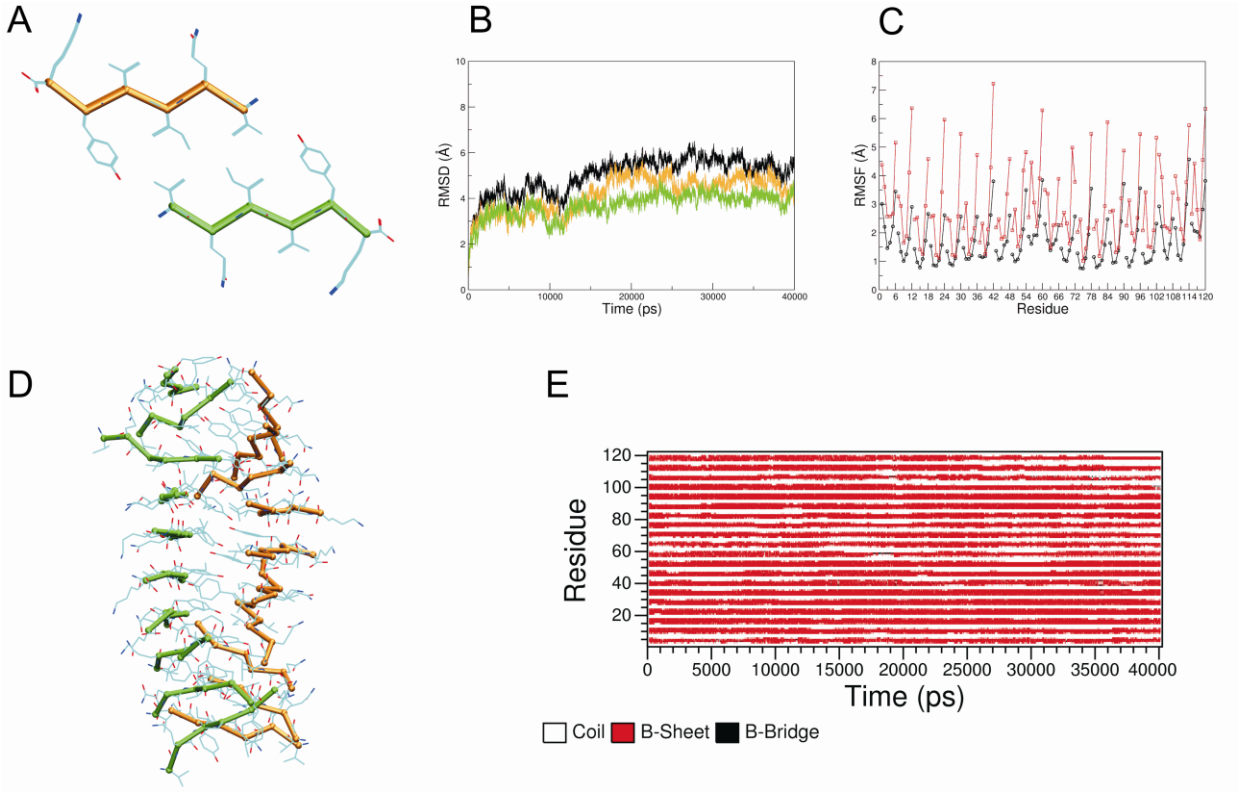

Figure 3
MD simulation of the pair-of-sheet model of VQIVYK. (A) Packing of the peptide in the crystalline structures, (B) RMSD values of trajectory structure versus the starting X-ray model computed on the C^{α} atoms of the entire assembly (black line) or of the individual sheets (gold and green), (C) RMSF values computed on backbone atoms (black) and on side chain atoms (red) of each residue in the trajectory region 5000–40,000 ps, (D) a representative structural example of the trajectory, and (E) evolution of the secondary structure.

In particular, a comparison of these values with those reported for the residues of the dry interface of the peptide GNNQQNY clearly indicates that the dry interface of VQIVYK-dA is significantly more mobile. Furthermore, in contrast to GNNQQNY, RMSF values of VQIVYK-dA residues of the dry interface are not markedly smaller those exhibited by the external ones. This suggests that these motions are not limited to the side chains. The analysis of the secondary structure evolution throughout the simulation indicates that the β-structure of the peptide is rather well conserved. The inspection of the trajectory structures suggests that frequent breaks in the β-structure of the two sheets occur (see Figure 3D for a representative example).
Collectively, these data indicate that there are frequent and temporary displacements of few strands from the rest of the sheet. These displaced strands, however, keep their local β-sheet structure (Figure 3E).
MD analysis carried out on the assembly VQIVYK-dP which is endowed with the polar interface displays even larger fluctuations (data not shown). This is likely due to the very limited surface area of this dry interface (<100 Å) (Sawaya et al., 2007).
In order to verify whether interactions arising from lateral association could have stabilizing effects on the steric zipper motif of VQIVYK-dA, additional MD simulations were carried out by considering systems made of three different β-sheets. These assemblies were built by taking into account the symmetry mates found in the crystal structure of the peptide (Figure 4).

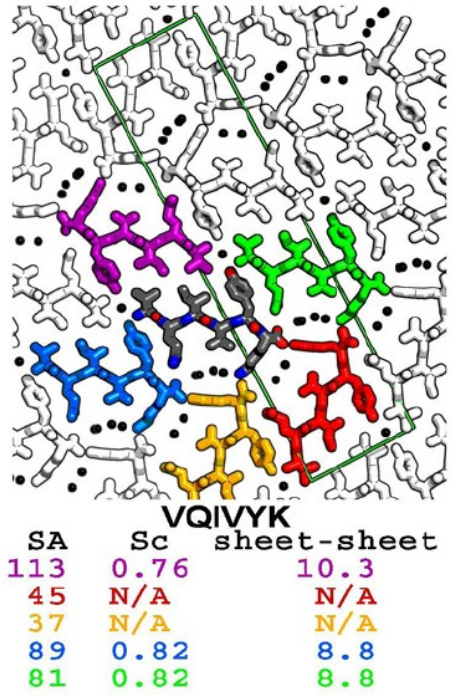

Figure 4
The microcrystal structure of steric zipper formed by the VQIVYK segment. A reference pair of sheets is coloured with the silver sheet extended towards the right and the purple sheet being the sheet that covers the greatest area on the silver sheet. Water molecules are shown as black spheres. Sheets of other colours cover smaller areas on the silver sheet. Shown below each diagram are the solvent accessible surface areas (SA) in $Å^2$ covered on the silver sheet by the sheet of the corresponding colour, as well as the shape complementarity parameter (Sc), giving the tightness of fit for the interactions, and the average backbone-to-backbone distances between sheets in Å. Crystallographic unit cells are shown in green.Water molecules are shown as aqua spheres.

In particular, two different three-sheeted models were considered. In both cases, one sheet interacts with the other two by forming both the polar and the apolar dry interface. In the first one (VQIVYK-T1) there is a central sheet with the other two located at the opposite sides of the central one (Figure 5). In the second one (VQIVYK-T2), it is the same side of one sheet that forms the two types of interfaces with the other sheets (Figure 6).

The analysis of both VQIVYK-T1 and VQIVYK-T2 models suggests that both systems undergo large transitions while preserving the local secondary structure (see Figure 5B and Figure 6B). The analysis of VQIVYK-T1 trajectory structures indicates that the extra sheet, which interacts with the central one through the polar interface, completely displaces from its starting position. Indeed, this β-sheet quickly (within the first 2000 ps of the trajectory) rotates with respect to the other two strands and, eventually, its orientation becomes almost perpendicular to the other two (Figure 5C-D). Notably, this sheet preserves its β-structure in the remaining interval of the trajectory (2000-40000 ps) (Figure 5B), despite the fact that a substantial part of it does not make any intersheet contact. Although the timescale of this event prevents definitive conclusions, this finding suggests that, as found for the GNNQQNY peptide, the VQIVYK fragment may have an intrinsic tendency to form β-sheet structures, independently of intersheet association. Moreover, the observation that in this three-sheeted system the most dramatic structural transition is observed for the sheet that is linked to the central one through the polar interface provides further support to the indication that this interface is less stable than the apolar one.

The structural changes observed for VQIVYK-T2 during the simulation are also remarkable. Although the three sheets are rather stable (Figure 6C) and remain in contact, both polar and apolar dry interfaces are strongly altered (Figure 6D). This overall rearrangement is likely dictated by electrostatic interactions between the terminal ends of the strands of the three sheets. As shown in Figure 6A, in the starting model the positively charged N-terminus of the strands of the extra sheet protrudes toward the positively charged end of an adjacent sheet. This perturbation leads to the disruption of both starting interfaces within the first 2000 ps of the simulation. Charged ends also play a role in the stabilization of the final aggregate (Figure 6D). These considerations are corroborated by a MD test carried out by treating the termini of the strands as uncharged (data not shown). This finding further suggests that the apolar interface of the VQIVYK system is rather unstable since it can be easily destroyed by a limited perturbation.

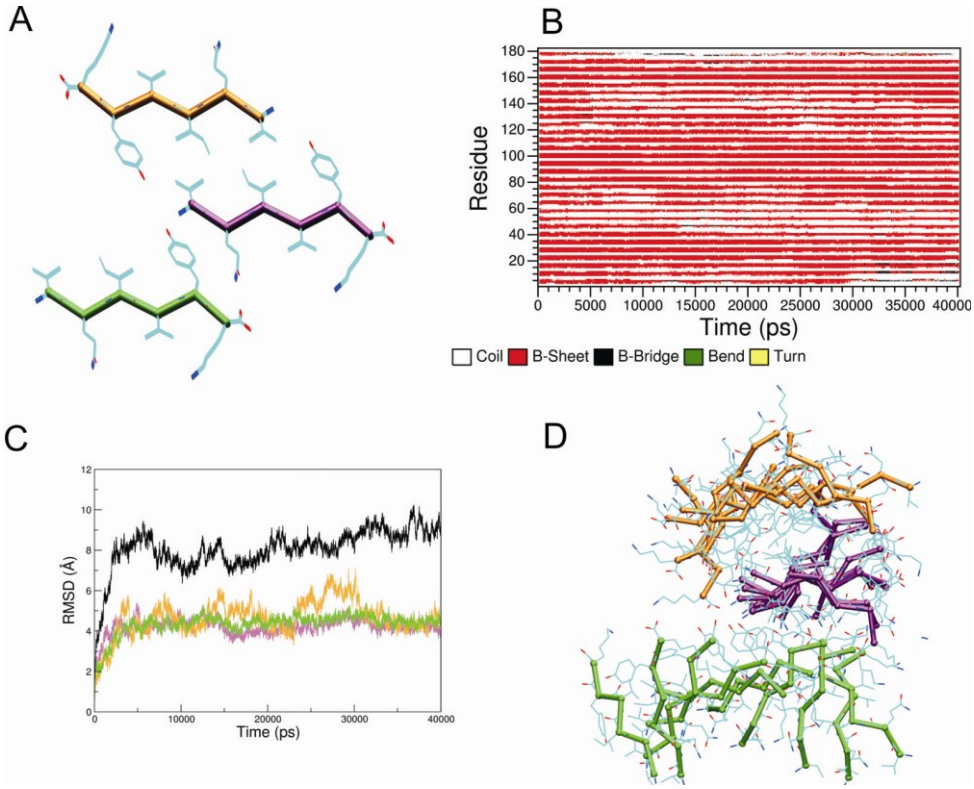

Figure 5
MD simulation of the three sheet model VQIVYK-T1. (A) Starting model, (B) evolution of the secondary structure, (C) RMSD values of trajectory structure versus the starting X-ray model computed on the C^{α} atoms of the entire assembly (black line) or of the individual sheets (orange, green, and magenta), (D) a representative structural example of the trajectory.

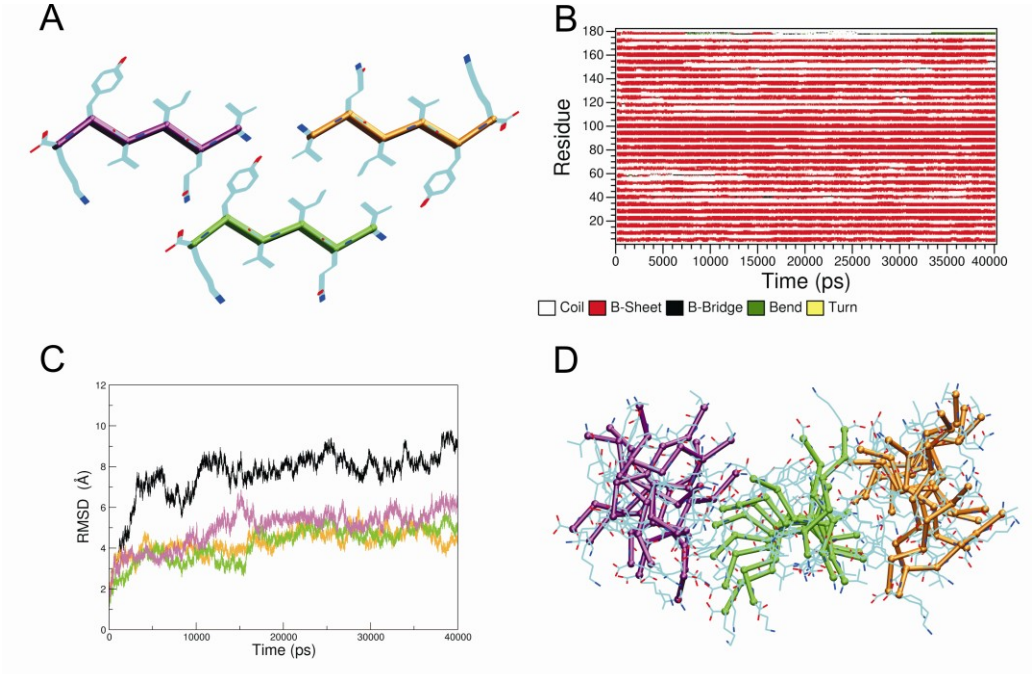

Figure 6
MD simulation of three sheet model VQIVYK-T2. (A) Starting model, (B) evolution of the secondary structure, (C) RMSD values of trajectory structure versus the starting X-ray model computed on the C^{α} atoms of the entire assemblies (black line) or of the individual sheets (orange, green, and magenta), and (D) a representative structural examples of the trajectory.

4.3.3. Structural stability of the HET-s (218-289) pentamer evaluated by MD simulations

In order to obtain further insights into amyloid-like association dictated by apolar aliphatic residues we performed a MD analysis on the pentameric form (hereafter referred to as HET5) of the β-helix structure recently proposed, on the basis of solid state NMR data, for the prion protein HET-s (218-289) (Wasmer et al., 2008). The solenoid structure of this aggregate is stabilized by an internal dry surface made of apolar residues (Figure 7A-B). Since each monomer within this molecule contributes with two turns of the β-helix, ten turns are present in the pentamer.

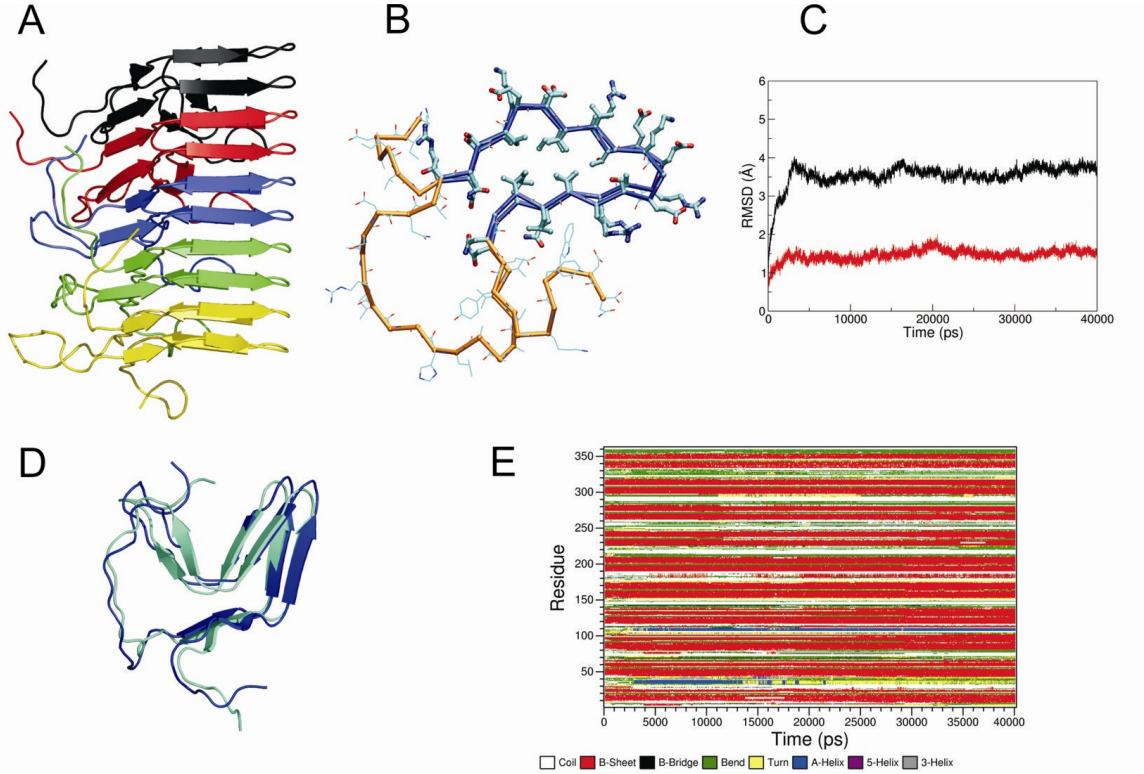

Figure 7
MD simulation of HET-s (218–289). (A) Overall view of the pentameric starting model, (B) dry interface in the central monomer of the X-ray structure, (C) RMSD values of trajectory structure versus the starting X-ray model computed on all C^{α} atoms (black line) and on C^{α} atoms of the core β-sheets (red line), (D) superimposition of the central monomer of a representative structure (cyan) of the trajectory with the correspondent portion of the starting model (blue), and (E) evolution of the secondary structure (the 72 residues of each monomer are numbered sequentially from 1 to 360).

In contrast to the findings obtained for SSTSAA and VQIVYK aggregates, the MD simulations carried out on HET shows that this model is endowed with a remarkable stability. Indeed, all of the parameters typically used for checking the stability of structural models in MD simulations (secondary structure content, gyration radius, RMSD values) (See Appendix for details) clearly indicate that the system is stable, with minimal overall variations from the starting NMR model (Figure 7).
The trends of the RMSF values (See Appendix for details) show that the residues embedded in the β-structure are rather rigid (Figure 8), while those located in the linkers are highly flexible. Interactions between polar or charged side chains of solvent-exposed residues of the β-structure region contribute to the reduction of their mobility. Interestingly, the hydrophobic patch of the structure is surrounded by two

hydrated regions. One is located in the flexible part of the molecule and the other in the corner formed by the linkers between the β-strands β1b-β2a and β3b-β5a. The unexpected location of these latter water molecules in this tight region is in line with a very recent analysis of HET-s (218-289) structure carried out by using the three-dimensional molecular theory of salvation (Yamazaki et al., 2008).

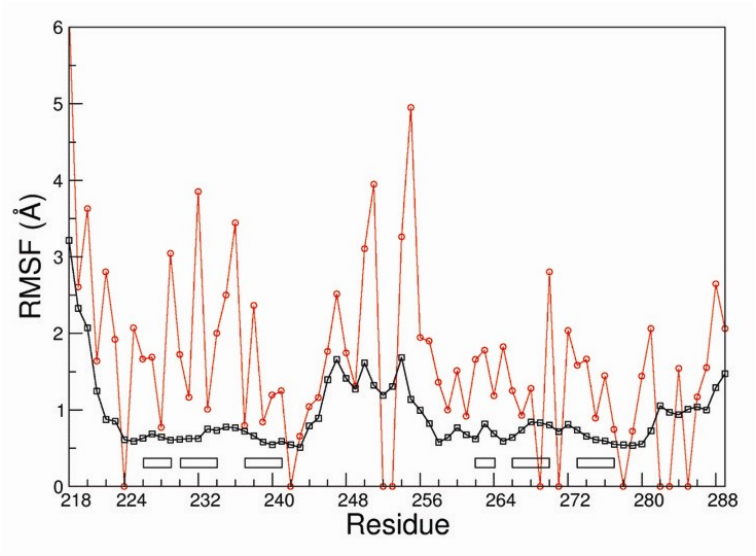

Figure 8
RMSF values of HET-s (218–289) residues computed on backbone atoms (black) and on side chain atoms (red) of each residue in the trajectory region 5000–40,000 ps. The bars denote core β strands of the structure.

The present MD analysis also highlights that, as suggested in the NMR study, electrostatic interactions established by charged residues protruding toward the solvent contribute to the stability of the assembly. As shown in Figure 9, the electrostatic interactions formed by the pairs Lys229-Glu265, Glu234-Lys270, and Arg236-Glu272 are well preserved in the simulations. The frequent swap of the interacting atoms of these residues unveils the dynamic nature of these contacts. The inspection of other side chain–side chain interactions also show that stable hydrogen bonds are also formed by Asn residues (Figure 9D). These interactions resemble the polar zipper motifs proposed by Perutz in his pioneering investigations on the amyloid-like fiber structure (Perutz 1995).

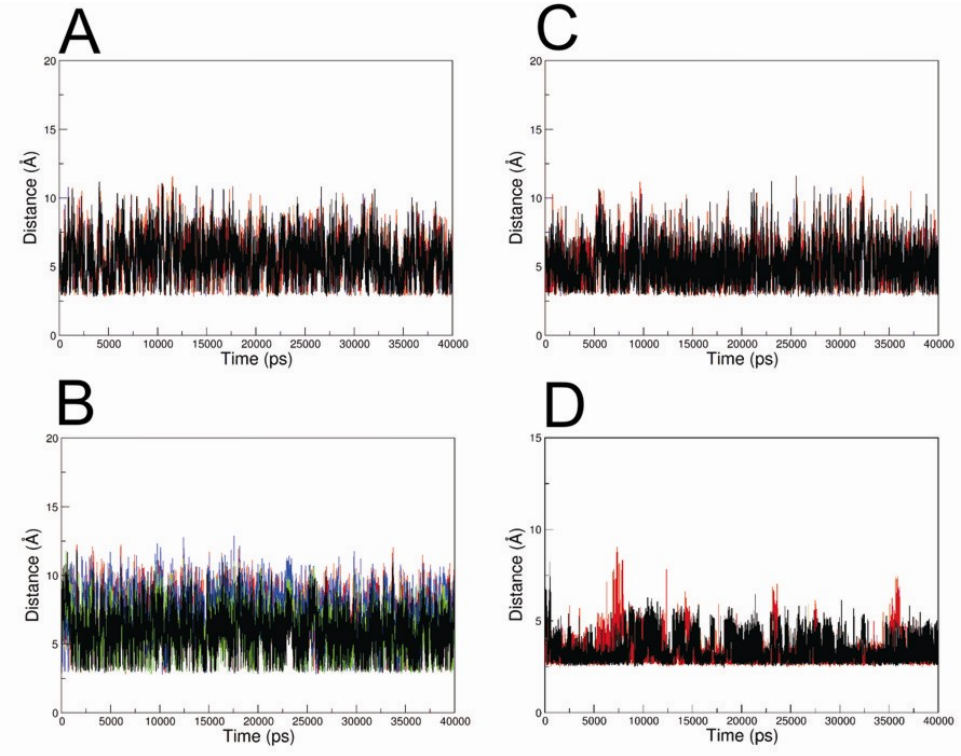

Figure 9
Stability of electrostatic and H-bond interactions in HET-s (218–289) MD simulation. (A) Lys229-Glu265 (interacting pairs: $N^{\zeta}229$-$O^{\varepsilon 1}265$ shown in black, and $N^{\zeta}229$-$O^{\varepsilon 2}265$ in red), (B) Arg236-Glu272 (interacting pairs: $N^{\eta 1}236$-$O^{\varepsilon 1}272$ shown in green, $N^{\eta 1}236$-$O^{\varepsilon 2}272$ in black, $N^{\eta 2}236$-$O^{\varepsilon 1}272$ in blue, and $N^{\eta 2}236$-$O^{\varepsilon 2}272$ in red), (C) Glu234-Lys270 (interacting pairs: $N^{\zeta}270$-$O^{\varepsilon 1}234$ shown in black, and $N^{\zeta}270$-$O^{\varepsilon 2}234$ in red), (D) Asn226-Asn262 between adjacent monomers (interacting pairs: $O^{\delta 1}262B$-$N^{\delta 2}226C$ shown in black, and $O^{\delta 1}262C$-$N^{\delta 2}226D$ in red).

4.4. Conclusions

The steric zipper assemblies composed of a pair of ten-stranded β-sheets for SSTSAA and VQIVYK peptides, show high fluctuations and significant distortions in the simulation timescale. Taking into account the crystal packing, for VQIVYK the effect of the addition of an extra sheet to the assemblies was also evaluated. In the two cases tested, the addition of the additional sheet did not increase the stability of the assemblies. Indeed, the inclusion of the extra-sheet had strong destabilizing effects on the basic steric zipper motif. These findings have been rationalized by taking into account the overall distribution of the charged ends in the three-sheeted models. This observation represents a further evidence of the loose dry interface in these models since limited external perturbations have profound effects on the steric zipper association. These results also suggest that the packing of these peptides in the crystal state is determined by a delicate balance of different factors (pair-of-sheet association, electrostatic contacts between symmetry mates, presence of solvent and counterions, etc.).
It is worth mentioning that present data do not preclude that the basic motif of SSTSAA and VQIVYK fibrils may resemble the one identified in the crystallographic analysis. Indeed, in the process of the fibril growth the pair-of-sheet motif may be stabilized by additional sheets that, once laterally packed, may contribute to the

stabilization of the steric zipper. Nevertheless, the striking different behavior of these peptides with those previously characterized highlights the importance of the nature of residues directly involved in the steric zipper motif. Indeed, aliphatic residues are unable to form the intra-sheet and inter-sheet interactions established by polar and aromatic residues that likely provide a strong contribution to the steric zipper motif stability. Along this line, amyoid-like assemblies endowed with hydrophobic residues presumably require larger interfaces. In line with this suggestion, MD analysis of the HET-s (218-289) prion models composed of a similar number of strands shows that the assembly is endowed with a remarkable stability.

In conclusion, present data indicate that MD simulations represent a valuable tool to gain insights into the relevance of structural motifs identified in X-ray structure analyses of small model peptides. Indeed, considerations based on the extent of the dry interface or on the values of the interface surface complementarity may lead to an oversimplified view of these complicated systems.

5. DYNAMICAL PROPERTIES OF STERIC ZIPPER POLYMORPHS FORMED BY AN IAPP-DERIVED PEPTIDE

5.1. Background

Understanding the molecular basis of neurodegenerative diseases have enormous implications for the development of effective therapeutic strategies. One of the most puzzling features of these pathologies is the occurrence of distinct strains, which are believed to be generated by alternative conformational transitions of the same protein/peptide. Very recently, it has been discovered that small model peptides are able to form alternative tightly packed assemblies (polymorphs) in the crystalline state. Intriguingly, it has been postulated that the different polymorphs of the same polypeptide sequence may be representative of distinct strains.
However, due to the limited size of the investigated peptides, the relevance of these findings for the amyloid fibers of proteins/peptides directly involved in neurodegenerative diseases still requires further validation.
Theoretical approaches such as molecular dynamics simulations have proven to be helpful tools in this field (Zheng et al., 2006) (Vitagliano et al., 2009) (Colombo et al., 2008) (Periole et al., 2009) (Strodel et al., 2007) (Gsponer et al., 2003) (Zheng et al., 2006). These studies, by analyzing peptides assemblies in a crystalline-free context, have provided information on the intrinsic propensities of peptide fragments to associate in amyloid-like states. In this framework, here we report an analysis of the dynamic properties of a model peptide which is able to form two different steric zipper assemblies in the crystalline state (Wiltzius et al., 2009)
In particular, we carried out a detailed MD analysis to evaluate the stability of the two polymorphic structures formed by a segment (SSTNVG) of the islet amyloid polypeptide (IAPP), that have been recently reported by Eisenberg and co-workers. IAPP is a 37-residue hormone that forms fibrillar amyloid-like deposits in pancreatic β-islet cells and that has been implicated in the pathogenic process associated with type II diabetes (Hoppener et al., 2000).

5.2. MATERIALS AND METHODS

5.2.1. Models

MD simulations were carried out by considering two distinct assemblies of the IAPP-derived peptide SSTNVG (residues 28-33 of the parent polypeptide). One is characterized by the presence of a pair of serine residues in the central zone of dry interface (Protein Data Bank entry 3DG1) (Wiltzius et al., 2008), whereas the other presents a pair of interdigited asparagine residues at this interface (PDB code 3FTR) (Wiltzius et al., 2009). Assemblies made of a pair of 10-stranded β-sheets used as starting models in the simulations were generated by applying the symmetries of the corresponding crystalline structures. Throughout the text the two assemblies have been denoted using the PDB code of the starting coordinates (3DG1 and 3FTR). Throughout the text, residues will be denoted as S1, S2, T3, N4, V5, and G6.

5.2.2. MD parameters and protocols

MD simulations were performed with the GROMACS software package.3.3.3 (Van der Spoel et al., 2005) (See Appendix for details). The models were immersed in a triclinic box. Taking into account the crystallization conditions of these systems, in both cases simulations were carried out on peptides with charged ends. Initial analyses were carried out by using GROMOS43a1 force field and the SPCE water model. Alternative simulations, performed to check to impact of the force-field on the results, were conducted by using all-atom OPLS-AA force field and the TIP3P water model. In order to relax bond geometries, for all models, the potential energy of the entire system (peptides and water) was doubly minimized by using the steepest-descent method until convergence was reached. The solvent was then relaxed by 100 ps of MD at 300 K, restraining protein atomic positions with a harmonic potential. The system temperature was brought to 300 K in a step-wise manner: 50 ps MD runs were carried out at 50, 100, 150, 200, 250 and 300 K, in the end a step of 70 ps were carried out with the Temperature and Pressure coupled. It has been checked that, in each step of the heating of the different systems, the potential energy reached a stable value. The timescale of the individual simulations is reported in Table 1. The simulations were run with periodic boundary conditions. Bond lengths were constrained by the LINCS algorithm (Hess et al., 1997). The electrostatic interactions were calculated using PME algorithm with a cutoff of 1.0 nm. The cutoff radius for the Lennard-Jones interactions was set to 1.0 nm. A dielectric constant of 1, and a time step of 2 fs were used. We used the NVT ensemble in all simulations. The temperature was maintained constant using the Berendsen thermostat with a time constant of 0.1 ps (See Appendix for details). Trajectory structures were analyzed by using GROMACS (Van der Spoel et al., 2005) and VMD (Humphrey et al., 1996) routines. Pictures were generated using the program VMD.

Table 1. Summary of the Simulations Performed

Model	Atoms peptide / atoms water	Box dimensions ($Å^3$)	Simulation time (ns)	T (K)
3DG1-gromos	1040 / 19851	57 x 81 x 49	100	300
3FTR-gromos	1040 / 20757	49 x 81 x 57	100	300
3DG1-OPLS	1520 / 20742	57 x 81 x 49	100	300
3FTR-OPLS	1520 / 20766	49 x 81 x 57	100	300

5.3. RESULTS AND DISCUSSION

5.3.1. Description of the two SSTNVG polymorphs

The two polymorphs of the IAPP-protein SSTNVG fragment here investigated present different organizations of the dry interface of the steric zipper motif (Wiltzius et al., 2009) (Wiltzius et al., 2008). In both models the individual sheets are made of parallel β-strands. In one of the polymorphs, the dry interface is characterized by the juxtaposition of two serine residues (S2) belonging to the two facing sheets (model 3DG1) (Figure 1A). The other (model 3FTR) is characterized by a dry interface, in

which an important role is played by two facing asparagines residues (N4) (Figure 1B).

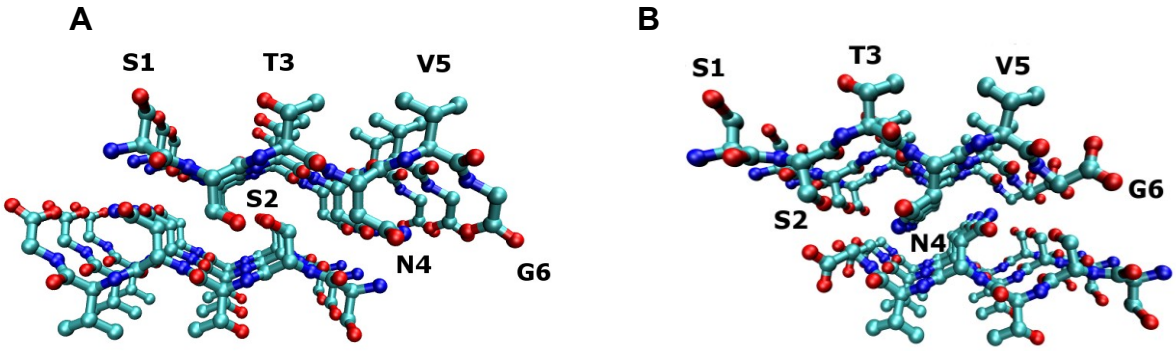

Figure 1
Crystalline structure of the steric zippers polymorphs of SSTNVG from IAPP. The fibril axes of the two models are perpendicular to the plane. Each strand forms backbone hydrogen bonds to strands above and below it. The polymorph 3DG1 (A) can be transformed into 3FTR one (B), by moving the top sheet to the left and flipping side chains S2 and N4.

Both steric zipper interfaces are stabilized by van der Waals interactions. An extra-stabilization to the 3DG1 model is provided by H-bonds established by the hydroxyl groups of S2 side chains (Figure 1A). The two assemblies show similar inter-sheet distances (~5.7-5.8 Å), buried areas and surface complementarities at the dry interface. Indeed, the buried areas and surface complementarities are 474 $Å^2$ and 0.86, and 444 $Å^2$ and 0.80 for 3DG1 and 3FTR, respectively.

5.3.2. Molecular dynamics simulations on the 3DG1 model

On analogy with previous investigations, MD simulations were carried out on model made of a pair of 10-stranded β-sheets. The initial simulation was performed by using the GROMOS43a1 force field. The stability of the system in the timescale of the simulation (100 ns) was checked by evaluating the evolution of the geometrical parameters of trajectory structures (Figure 2). The analysis of root mean square deviations (RMSD) of the trajectory (See Appendix for details) indicates that the system reaches a rather stable state after the early stages of the simulation. The RMSD values computed on the entire system oscillate in the range of 2-3 Å (Figure 2A). Lower values are observed for the ten strands that constitute the central core of the assembly. The overall stability of the system is confirmed by the analysis of the secondary structure content (Figure 2B). The average structure, computed from the trajectory models detected in the 50-100 ns (Figure 2C) displays a marginal level of twisting. As expected on the basis of the secondary structure preservation throughout the trajectory, the intra-sheet H-bonds formed by consecutive strands are well preserved (data not shown).

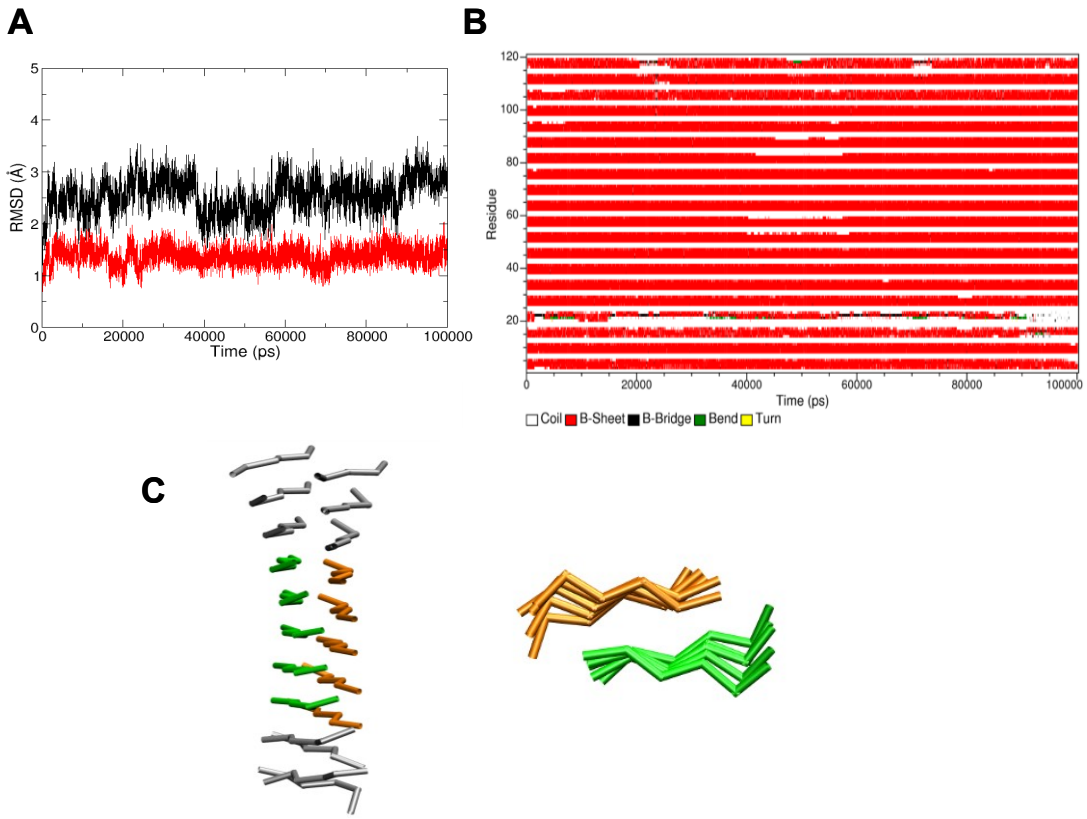

Figure 2
Molecular dynamics of the assembly 3DG1 carried out by using the GROMOS43a1 force field. (A) RMSD values, computed on the C^{α} atoms, of the trajectory structures versus the starting X-ray model. Values calculated on the entire assembly and on the ten strands of its central core are reported in black and red, respectively; (B) Evolution of the secondary structure elements along the trajectory; (C) Two alternative views of the average structure of the assembly computed in the 50-100 ns interval. The flexible external strands are colored in grey, while peptides of the central core of the two sheets are colored in orange and green.

It is important to note that the individual sheets are also stabilized by H-bond interactions formed by asparagines side chains belonging to adjacent strands. These interactions are well preserved throughout the simulations (Figure 3).

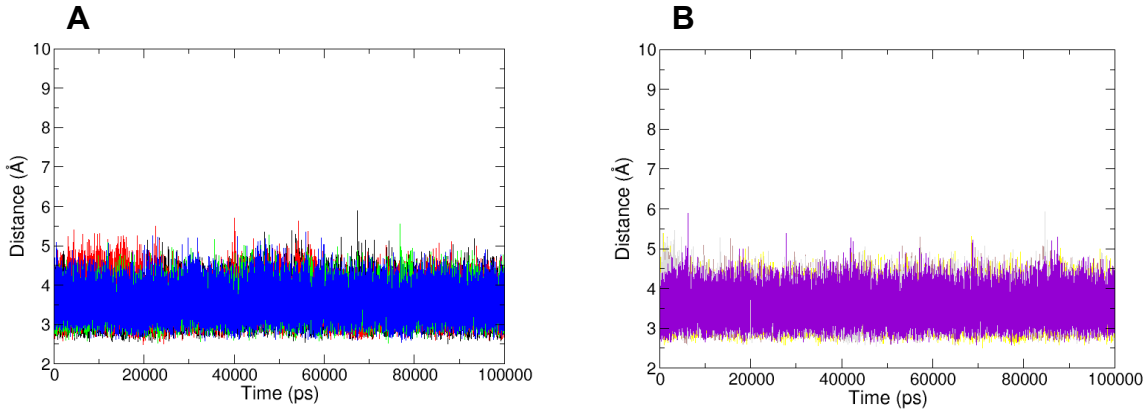

Figure 3
Evolution in the 3DG1 MD simulation of the intra-sheet H-bonds formed by $O^{\delta 1}$ and $N^{\delta 2}$ of N4 belonging to consecutive strands located in the first (A) or in the second (B) sheet.

In the crystalline structure, inter-sheet H-bonds are also formed by S2 residues belonging to facing strands. Although S2 side chains display some degree of mobility in the trajectory structures, also these bonds are dynamically preserved in the simulation (Figure 4).

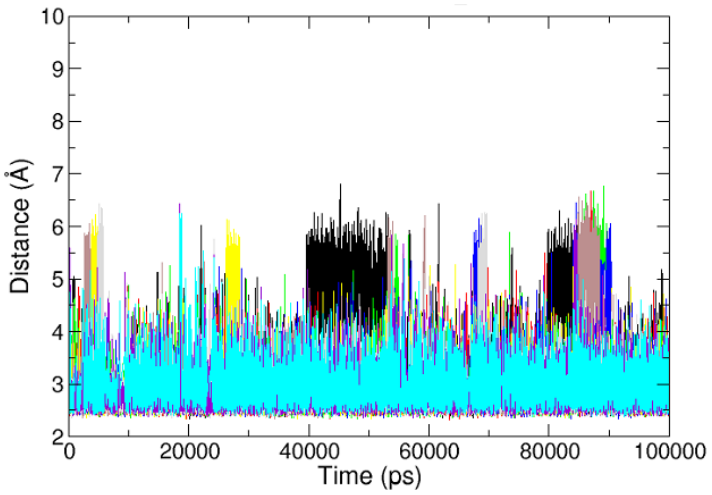

Figure 4
Evolution in the 3DG1 MD simulation of the inter-sheet H-bonds formed by O^{γ} of S2 belonging to the two facing sheets.

To check the impact of the force field on the results described in the previous paragraph, the simulation was repeated by using the all-atom OPLS-AA force field. As shown in Figure 5A, the RMSD values of the trajectory structures versus the starting X-ray model displays larger values compared to the GROMOS43a1. However, a closer inspection to the trajectory structures indicates that the main displacements occur for the terminal strands of the assembly. Indeed, when the RMSD values are calculated on the central 10 strands of the 3DG1 model are in the range of 1.0–2.0 Å.
The analysis of the secondary structure content confirms the overall stability of the assembly. It is worth mentioning that, despite the general agreement of the simulations performed with the two force fields, the model displays a larger rigidity in the simulation carried out using the GROMOS43a1 potential.

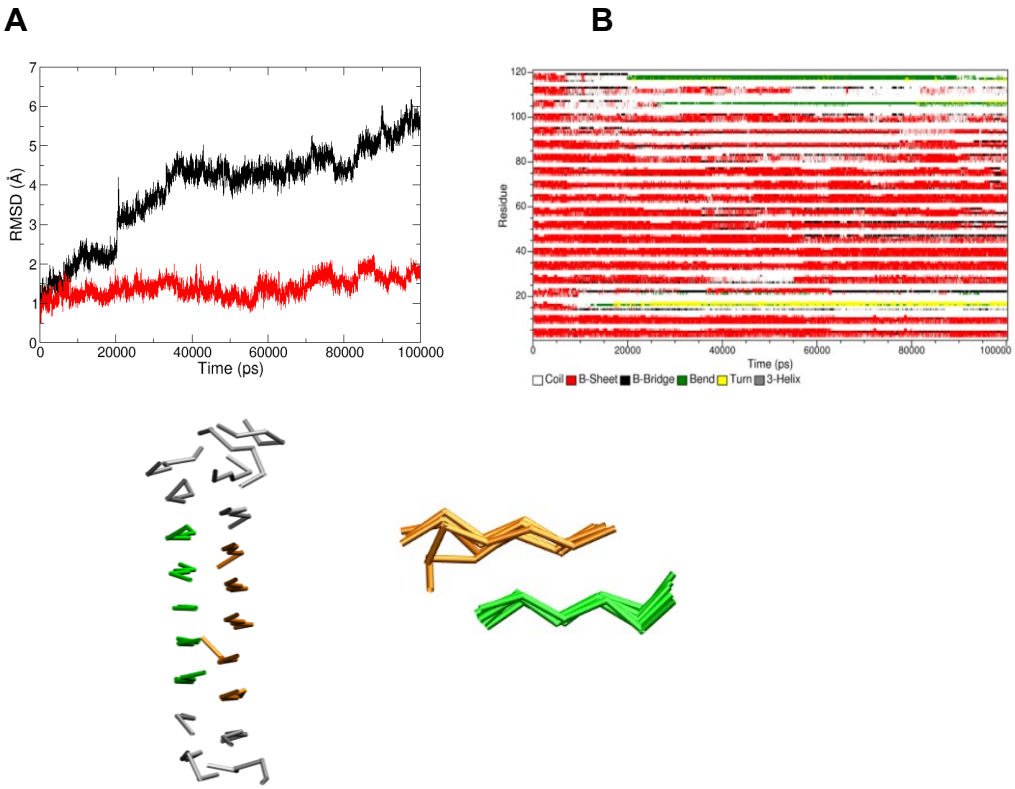

Figure 5
Molecular dynamics of the assembly 3DG1 carried out by using the OPLS-AA force field. (A) RMSD values, computed on the C^{α} atoms, of the trajectory structures versus the starting X-ray model. Values calculated on the entire assembly and on the ten strands of its central core are reported in black and red, respectively; (B) Evolution of the secondary structure elements along the trajectory; (C) Two alternative vies of the average structure of the assembly computed in the 50-100 ns interval. The flexible external strands are colored in grey, while peptides of the central core of the two sheets are colored in orange and green

5.3.3. Molecular dynamics simulations on the 3FTR model

MD simulations conducted on the polymorph 3FTR show similarities and analogies when compared to those conducted on 3DG1 (Figure 6-7). The analysis of representative structures sampled from 3FTR simulations carried out by using either GROMOS43a1 or OPLS-AA force fields indicates that the central core of the assembly retain the steric zipper structure, whereas the terminal strands are highly mobile (Figure 6C-7C). This observation is confirmed by the analysis of the secondary structure content, which is well preserved only for the central core of the assembly. Indeed, even in the simulation carried out using the GROMOS43a1, the terminal ends lose their β-structure. In both simulations, a significant twist of the central core strands is observed. A comparative analysis of the simulations carried out on 3DG1 and 3FTR polymorphs clearly indicate that the former is more stable.

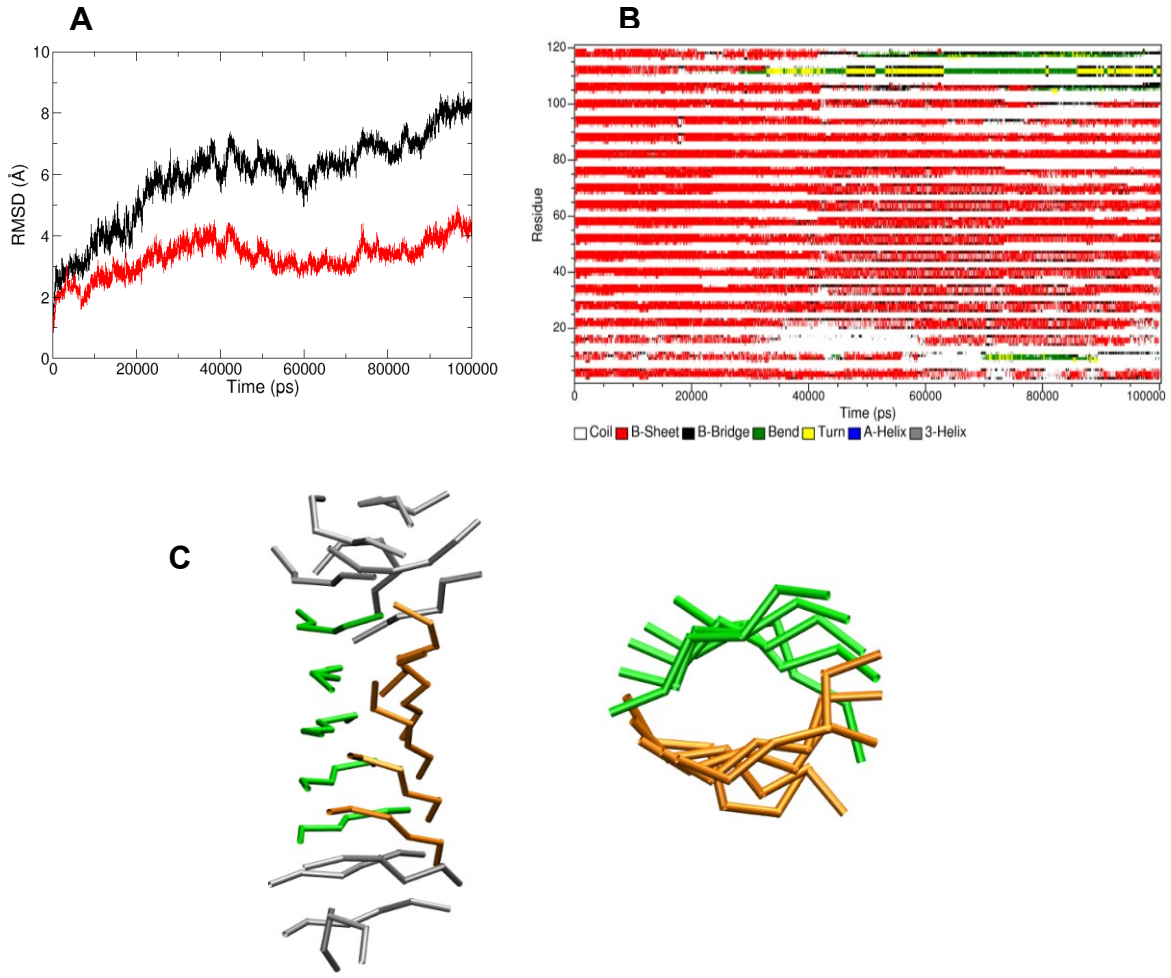

Figure 6
Molecular dynamics of the assembly 3FTR carried out by using the GROMOS43a1 force field. (A) RMSD values, computed on the C^{α} atoms, of the trajectory structures versus the starting X-ray model. Values calculated on the entire assembly and on the ten strands of its central core are reported in black and red, respectively; (B) Evolution of the secondary structure elements along the trajectory; (C) Two alternative vies of the average structure of the assembly computed in the 50-100 ns interval. The flexible external strands are colored in grey, while peptides of the central core of the two sheets are colored in orange and green

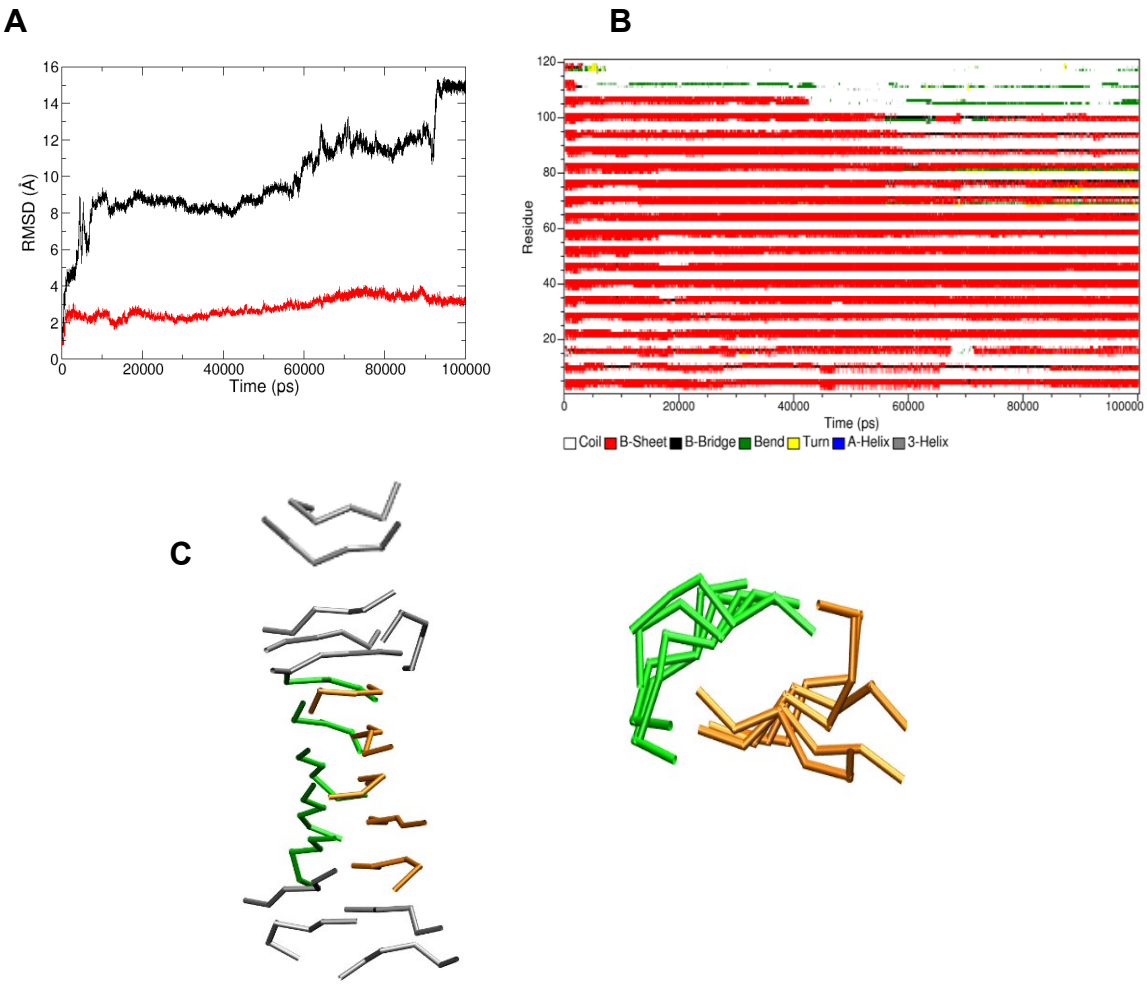

Figure 7
Molecular dynamics of the assembly 3FTR carried out by using the OPLS-AA force field. (A) RMSD values, computed on the C^{α} atoms, of the trajectory structures versus the starting X-ray model. Values calculated on the entire assembly and on the ten strands of its central core are reported in black and red, respectively; (B) Evolution of the secondary structure elements along the trajectory; (C) Two alternative vies of the average structure of the assembly computed in the 50-100 ns interval. The flexible external strands are colored in grey, while peptides of the central core of the two sheets are colored in orange and green

5.3.4. Molecular dynamics simulations on single ten-stranded sheet of SSTNVG

In order to gain further insights into the determinants that drive the formation of steric zipper polymorphs, MD simulations were also conducted on a single ten-stranded β-sheet of SSTNVG. Two independent 50 ns simulations carried out using the GROMOS43a1 force field clearly indicated that the individual sheet is highly unstable. Indeed, since the early stages of the simulations large deviations from the starting X-ray models are detected. As shown Figures 8-9, RMSD values approach 10 Å in the first 10 ns of the simulation. Accordingly, representative structures selected from the trajectory do not retain the features of the starting β-sheet structure (Figure 8-9). The presence of residual β structure in the trajectory is essentially due to small β-sheet fragments of the starting model.

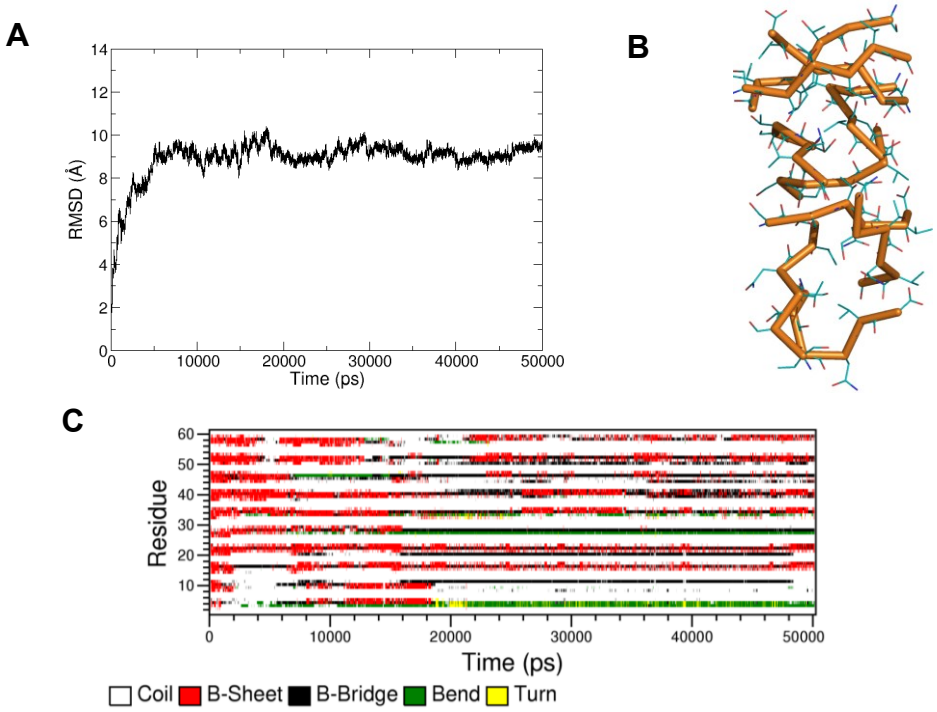

Figure 8
MD simulation conducted on a single ten-stranded β-sheet of SSTNVG carried out by using the GROMOS43a1 force field. (A) RMSD values, computed on the C^{α} atoms, of the trajectory structures versus the starting X-ray model, (B) A representative structure in the trajectory, (C) Evolution of the secondary structure elements along the trajectory.

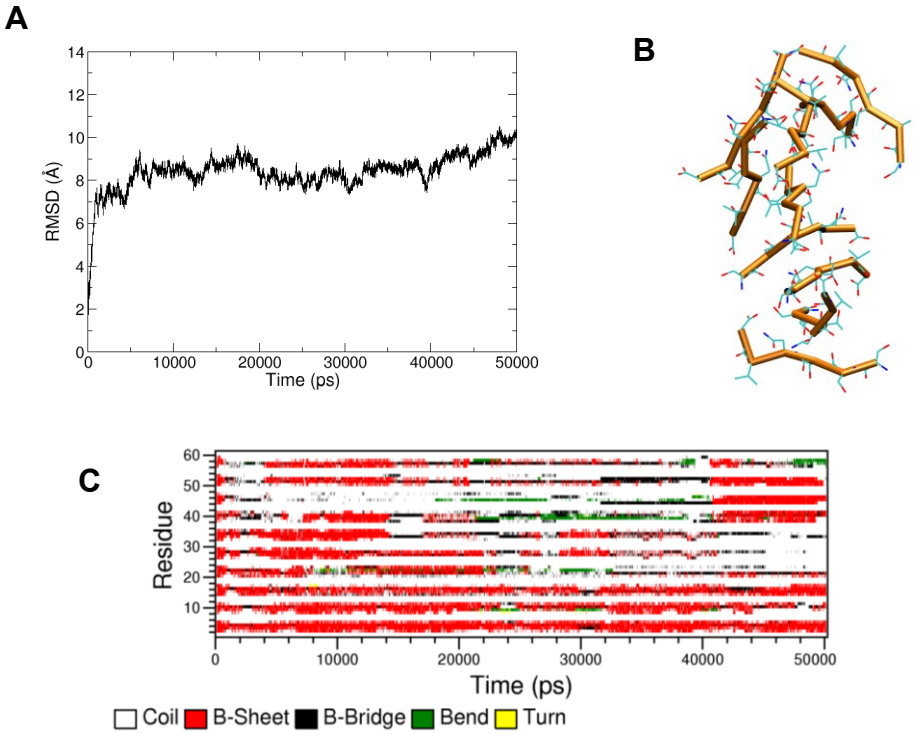

Figure 9
Second independent MD simulation conducted on a single ten-stranded β-sheet of SSTNVG carried out by using the GROMOS43a1 force field. (A) RMSD values, computed on the C^{α} atoms, of the trajectory structures versus the starting X-ray model, (B) A representative structure in the trajectory, (C) Evolution of the secondary structure elements along the trajectory.

5.4. Conclusions

The recent structural characterization of small amyloidogenic peptides has provided fundamental clues toward the comprehension of the structural basis of protein/peptide aggregation associated with neurodegenerative diseases (Nelson eta al., 2005) (Eisenberg et al., 2006). However the organization of crystalline aggregates of small peptides may be heavily biased by crystal packing. Therefore, additional characterizations of these assemblies in non-crystalline contexts may provide valuable information. We here show, by performing MD simulations, that the two steric zipper polymorphs of the IAPP-derived fragment SSTNVG are rather stable even in a crystalline-free environment. This finding supports the hypothesis that the occurrence of strains in neurodegenerative diseases may be related to the possibility that a single peptide/protein chain may self-associate in alternative steric zipper-based assemblies (Wiltzius et al., 2009). The tight association of the steric zipper motif makes the conversion of one polymorph to the other highly unlikely.

Although polymorphs are rather stable in the simulation timescale, the β-structure of the 3DG1 model is significantly more rigid than that of 3FTR model. This is not trivial since the two polymorphs presents similar buried areas and surface complementarities at the dry interface. Since the two assemblies present identical structures for the individual sheets, these observation suggests that inter-sheet interactions provide extra-stabilization to the 3DG1 model. The preservation in the simulation of the H-bond between the side chains of S2 residues of facing sheet indicates that this interaction may play a role in the stabilization of the adduct. In principle, the formation of alternative polymorphic structures may be favoured by particularly stable individual sheets. In this scenario, the formation of polymorphs simply requires the alternative pairings of this intrinsically stable sheet. Present data, however, show that the individual β-sheet formed by SSTNVG strands is somewhat unstable. This indicate that the stability of both polymorphs here investigated deeply rely on inter-sheet interactions.

In conclusion, present data corroborate the hypothesis that steric zipper assemblies are good candidates to account for the phenomenon of strain in neurodegenerative diseases. As already pointed out (De Simone et al., 2008), the tight association observed in steric zipper assemblies may be sensitive to subtle sequence variations. This may explain the species barrier observed in prion transmission. Collectively, these considerations support the idea that models derived from small peptides do represent reliable models for toxic/infective species in neurodegenerative diseases.

More detailed studies of stability of polymorphic structures, extended also to other system, by using more sophisticated techniques of metadynamics are still in progress.

6. INSIGHTS INTO STABILITY OF SYMMETRY-RELATED HPRP MOLECULES BY REPLICA EXCHANGE MOLECULAR DYNAMICS ANALYSES.

6.1. Background

An aberrant protein folding, or “misfolding”, gives rise to a growing number of pathologies classified as “protein conformation disorders” (Buxbaum, 2003). As mentioned in the previous chapters, they include neurodegenerative diseases such as Alzheimer’s disease, Parkinson’s or Huntington’s disease and the prion disorders. The latter diseases include the Creutzfeldt-Jacob disease, the Gerstmann-Straussler-Scheinker syndrome, fatal familial insomnia, and kuru. The critical event in these diseases is a significant change in secondary and/or tertiary structure of a native protein or its fragment, which occurs without any modification of the primary structure. The conformational change leads to the aggregation of aberrantly folded proteins, which first form pre-fibrillar oligomers and then the mature amyloid fibers.
The human prion diseases are associated to the misfolding of the prion protein (HPrP) which contains a globular domain that extends approximately from residues 125–228 and an N-terminal flexibly disordered ‘‘tail’’. The globular domain contains a two-stranded antiparallel β-sheet (residues 129-131 and 161-163) and three α-helices (residues 144-154, 172-194 and 200-223).
Crystallographic studies have revealed that the globular domain frequently associates in the crystal context by forming non-covalent dimeric structures. These associations are invariably mediated by the β-sheet of each monomer (Antonyuk et al., 2009) (Lee et al., 2010) (Haire et al., 2004). Indeed, these intermolecular interactions lead to the formation of a 4-stranded antiparallel β-sheet that involves the two short β-strands of different HPrP monomers.
Although the intermolecular interaction can be slightly different in the various crystal structures, the frequent β-sheet association suggests that it is not an artefact of crystal packing but it might have an important biological significance (Figure 1).

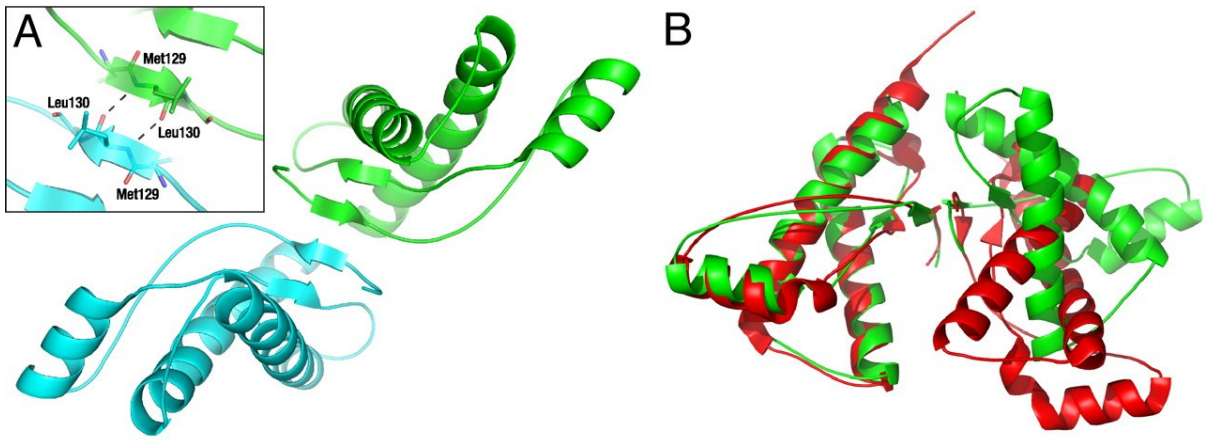

Figure 1
The interaction of PrP chains in the crystal. A) Illustration of the intermolecular 4-stranded antiparallel β-sheet formed between neighboring PrP chains (in cyan and green). B) Superimposition of the sheep (red) and human (green) PrP dimers from the respective crystal structures (Antonyuk et al., 2009).

Indeed, the exposed β-strand of the original two-stranded antiparallel β-sheet has been proposed as a nucleation site for the conformational transition of monomeric HPrP into the aggregated pathogenic state (Riek et al., 1996).
We have therefore undertaken a molecular dynamic study of the HPrP β-sheet to evaluate its intrinsic stability outside the protein context, hence mimicking destabilizing conditions associated with the unfolding of the globular domain. To study the stability of the intermolecular β-sheet interactions we have also investigated the four-stranded β-sheet assembly and the new two-stranded β-sheet intermolecular assembly found in the crystal packing of the wt HPrP bound to the antibody ICSM 18-Fab (Antonyuk et al., 2009). Moreover, the effect of point mutations associated to prion pathogenesis on the β-sheet assemblies has also been analyzed. In particular, we have studied structural models containing Met129Val and Gly131Val substitutions. Interestingly, the common human methionine-valine polymorphism at residue 129 has a profound influence on prion pathogenesis, and also plays a key role in conformational selection of prion strains.
It is notable that the stability and physical properties of the host cellular prion protein ($PrP^{c)}$ are not influenced by the residue 129 variation, so its effect must be realized in the physical properties and propagation of the disease-related conformers (PrP^{Sc}). (Hosszu et al., 2004) The mutation G131V, instead, leads to Gerstmann-Straussler-Scheinker (GSS) (Santini et al., 2003).
All the simulations have been carried out by using Replica Exchange Molecular Dynamics methods (REMD) (Sugita and Okamoto 1999), which guarantee an enhanced and significant sampling of conformations.

6.2. MATERIALS AND METHODS

6.2.1. System setup

Replica exchange molecular dynamics simulations have been performed on different β-sheet models built from the crystal structure of wt HPrP bound to the ICSM 18-Fab (PDB code 2W9E) (Antonyuk et al., 2009) (Table 1). We considered extended protein regions, which contain the wild type short β-strands. Each filament is made up of 12 residues (A: 125-136 and B: 158-169).
In particular, we considered (i) the double-stranded antiparallel β-sheet from a single HPrP molecule (AB assembly), (ii) the intermolecular four-stranded antiparallel β-sheet formed by two HPrP monomers related by crystallographic symmetry (ABB'A'), and (iii) the double-stranded antiparallel β-sheet formed at the dimer symmetric interface (BB') (Table 1). For each of the three assemblies both mutations G131V and M129V were modeled, so that 9 models were built (Table 1-2). The M129V and G131V mutants were generated by PyMol software (De Lano, 2002).
The models thus generated were immersed in a cubic box filled with TIP3P water model. Periodic boundary conditions were applied. We used the OPLS-AA force field (see Appendix for details). The N- and C-termini were kept both uncharged, because these regions are internal fragments of HPrP molecule. When necessary, Cl^- ions were added to neutralize the system. After the initial energy minimization, the systems have been equilibrated for 50 ps in order to equilibrate waters and initial thermodynamics properties of each replica.

Table 1

(A)	158	PNQVYYRPMDEY	169	→
(B)	136	RSMASGLMYGGL	125	←
(B′)	125	LGGYMLGSAMSR	136	→
(A′)	169	YEDMPRYYVQNP	158	←

B/B′ 125 LGGY**M**L**G**SAMSR 136

Sequences of the peptides characterized in the present study. The fragments B and B' are directly involved in the intermolecular interaction. The regions in β-structure are highlighted in grey. The residues involved in point mutations are shown in bold and underlined.

6.2.2. Replica exchange molecular dynamics

The simulations were carried out with the GROMACS software package.4.0 (Van der Spoel 2005) by using OPLS-AA force field (Jorgensen et al., 1996) (see Appendix for details) with an integration time step of 2 fs, following the procedure adopted for REMD simulations on prion proteins (De Simone et al., 2007). Bond lengths were constrained by the LINCS algorithm (Hess et al., 1997). The non-bonded interactions were accounted by using the particle mesh Ewald method (grid spacing 0.12 nm) (Darden et al., 1993) for the electrostatic contribution and cut-off distances of 0.9 nm for van der Waals terms.
REMD protocol includes several replicas of the system evolving independently at different temperatures (*T*). Replicas at adjacent temperatures undergo a partial exchange of configuration information.
Therefore, the general idea of replica exchange is to simulate different copies (replicas) of the system at the same time but at different temperatures values. The high temperature systems are generally able to sample large volumes of phase space, whereas low temperature systems, may become trapped in local energy minima during the timescale of a typical computer simulation. Replica exchange achieves good sampling by allowing the system at different temperatures to exchange complete configurations. Thus, the inclusion of higher temperature systems ensures that the lower temperature systems can jump across the energy barriers so that it can be obtained a representative set of low-temperature regions of the phase space that is not accessible by a single-temperature simulation. Exchanges between neighboring temperatures are attempted every t_{swap} on the basis of the Metropolis criterion (Eq. 1):

$$P(1 \leftrightarrow 2) = \min\left\{1, \exp\left[\left(\frac{1}{K_B T_1} - \frac{1}{K_B T_2}\right)(U_1 - U_2)\right]\right\}$$

Where $P(1\leftrightarrow2)$ is the exchange probability, K_B is Boltzmann's constant, U_1 and U_2 are the instantaneous potential energies and T_1 and T_2 are the reference temperatures. Because Eq. 1 is suited in the NVT ensemble, an additional term for

the isobaric-isothermal (NPT) ensemble, adopted here, should be introduced (Sugita el al., 1999). This term is, however, negligible when the volumetric fluctuations are small (Seibert et al., 2005), as in the case of an all-atom simulation.
Both number of replicas, employed in a replica exchange dynamics simulation, and the temperatures of the replicas are issues of great importance. One wishes to achieve the best possible sampling with the minimum amount of computational effort. The highest temperature must be sufficiently high so as to ensure that no replicas become trapped in local energy minima, while the number of replicas used must be large enough to ensure that swapping occurs between all adjacent replicas.
Temperatures are spaced exponentially with $Ti = T0\ e^{|ki|}$, where *i* is the number of replicas, *k* and *T0* can be tuned to obtain reasonable temperature intervals to allow exchanges. In our simulations, the REMD samplings for all systems were composed of 32 replicas ranging from 296.5 to 435 K. The temperatures have been selected to ensuring homogeneous exchange frequencies between replicas. These are: 296.5, 300.5, 304.5, 308.5, 312.5, 316.5, 320.6, 324.7, 328.8, 332.9, 337.1, 341.3, 345.5, 349.8, 354.1, 358.4, 362.7, 367, 371.4, 375.8, 380.3, 385, 398.8, 394.6, 399.5, 404.4, 409.4, 414.4, 419.5, 424.6, 429.8 and 435 K. To achieve consistent exchange frequencies among the various samplings carried out, the same temperature pattern and comparable systems dimensions (Table 2) have been adopted. A t_{swap} of 1000 MD steps (2 ps) was chosen in order to allow the kinetic and potential energy of the system to relax. For all the systems analyzed, the simulation time was 100ns per each replica. As result, for each replica system a total sampling of 3.2 μs (100ns x 32) was carried out.

Table 2. Sampling statistics

System	Average exchange frequency (%)	Atoms (*n*)	Water molecules	Cl^-	Strands	Simulated time
wt ABB'A'	9.5	764	3396	-	4	100 ns
G131V ABB'A'	10.0	782	3393	-	4	100 ns
M129V ABB'A'	10.1	762	3400	-	4	100 ns
wt AB	13.4	382	2869	-	2	100 ns
G131V AB	14.0	391	2867	-	2	100 ns
M129V AB	13.7	381	2871	-	2	100 ns
wt BB'	13.4	346	2876	2	2	100 ns
G131V BB'	14.2	364	2868	2	2	100 ns
M129V BB'	13.5	344	2878	2	2	100 ns

6.3. RESULTS AND DISCUSSION

6.3.1. Systems and overall REMD features

Replica exchange molecular dynamics simulations have been performed on 2-stranded as well as 4-stranded β-sheets of HPrP derived from the crystallographic structure of the protein complexed to the ICSM 18-Fab (Antonyuk et al., 2009).
REMD technique allows for significantly enhanced sampling of conformations, due to frequent switching of simulation temperatures. During one simulation, the high temperature simulation segments facilitate the crossing of the energy barriers while the low temperature ones explore in detail energy minima (see Methods).
We performed REMD runs on 9 different model assemblies (Table 2). Each trajectory comprises the simulation of 32 thermal baths and has a length of 100 ns. All runs have reported significant random walks in the temperature space consistent with fairly good exchange frequencies among replicas (Table 2). These frequencies are essential for the evaluation of the simulation convergence. Each replica explored the whole temperature space by passing repeatedly throughout all thermal baths.

6.3.1.1. AB 2-stranded β-sheet

The globular C-terminal domain of HPrP contains a double-stranded antiparallel β-sheet formed by two short segments: 129-131 (MLG) and 161-163 (VYY). We have investigated the stability of 12-residue regions encompassing the β-strands outside the protein context. In the crystal state this β-strand pairing is formed by three H-bonds connecting residue 129 with residue 163, and residue 131 with residue 161 (namely: N Met^{129}-O Tyr^{163}, O Met^{129} - N Tyr^{163}, O Val^{161}- N Gly^{131}). The β-strand 129-131 is the most surface exposed one.
We analyzed the room-temperature bath (bath1= 300.5 K) of sampling. The secondary structure composition in this selected bath shows the persistence of the β-strand pairings indicating the remarkable stability of the starting β-sheet model (Figure 2).

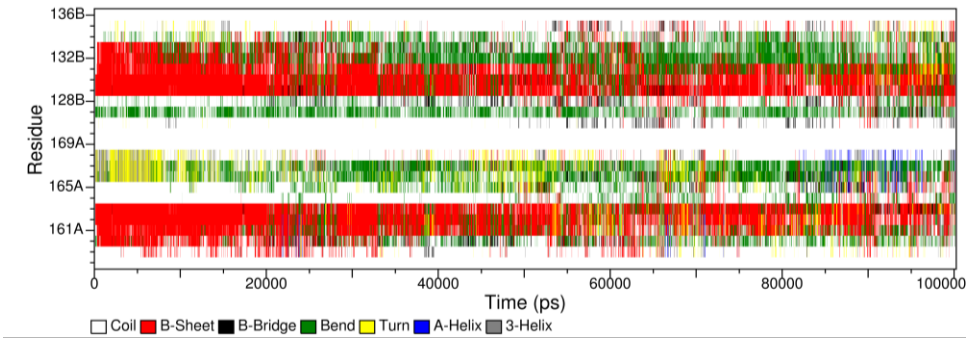

Figure 2
Evolution of secondary structure elements.

In the crystal structure, Val^{161} displays only one H-bond to Gly^{131} (O Val^{161}–N Gly^{131}), whereas in the simulation also the H-bond between N Val^{161} and O Gly^{131} is frequently formed. In particular, in the bath1 sampling the distance between N Val^{161} and O Gly^{131} is smaller than 3.3 Å for the 45% of collected structures. On the other

hand, the distance between O Val^{161} and N Gly^{131} is smaller than 3.3 Å for the 68% of collected structures. Similar percentages (about 70%) are found for the two original backbone hydrogen bonds connecting Met^{129} and Tyr^{163}. Furthermore, in the sampling it can be observed the elongation of the β-sheet in the direction of Asn^{159} residue. Indeed, as expected for a regular pattern of hydrogen bonds in antiparallel sheets (Figure 3), Asn^{159} and Ala^{133} can form two mutual backbone hydrogen bonds to each other's flanking peptide group.

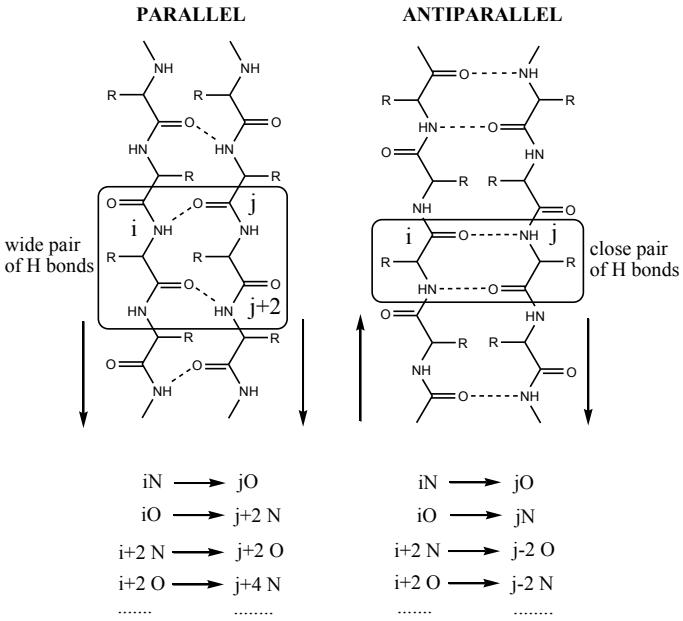

Figure 3
Illustration of the hydrogen bonding patterns, represented by dotted lines, in a parallel and antiparallel β-sheet. The arrows indicate the direction of numeration. In parallel β-sheet structure, a residue "i" may form hydrogen bonds to residues j−1and j+1; this is known as a *wide pair* of hydrogen bonds. In antiparallel β-structure two adjacent i, j residues form two mutual backbone hydrogen bonds to each other's flanking peptide groups; this is known as a *close pair* of hydrogen bonds.

In the simulation, the most persisting contact involves N Asn^{159} and O Ala^{133}, which is observed in 13.5% of collected structures. In Figure 4 a representative structure of elongated β-sheet is shown.

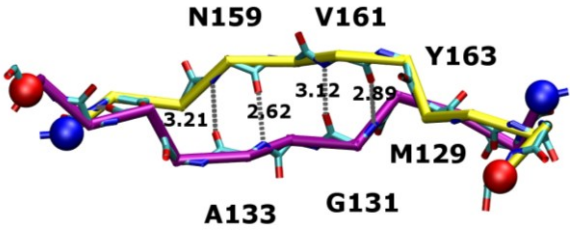

Figure 4
Representative structure of elongated β-sheet of AB 2-stranded β-sheet model. Only the backbone is represented. The N- and C-termini are indicated as blue and red spheres respectively. In this structure the fragment A is colored in yellow and the fragment B in violet. The residues and H-bonds involved in an elongated β-sheet are shown.

Interestingly, the conformational fluctuation of the two 12-residue segments sometimes results in the formation of a parallel arrangement of β-strands (Figure 3). In particular, the H-bond pattern involves Ala^{133} bonded to both Met^{166} and Glu^{168} (Figure 5). The latter acidic residue is also sporadically H-bonded to Ser^{135}.
In order to evaluate the relative abundance of the observed antiparallel and parallel arrangements, two representative H-bonds for each arrangement have been considered. For the antiparallel β-sheet the average value of the two distances, N Met^{129}-O Tyr^{163} and O Val^{161}-N Gly^{131}, has been calculated; for the parallel β-sheet the average value of the two distances, N Ala^{133}-O Met^{166} and O Ala^{133}-N Glu^{168}, has been calculated. The β-sheet is considered to be formed when this average value is smaller than 3.3 Å. The analysis of bath1 sampling reveals that 70.4% and 4.8% of collected structures forms antiparallel and parallel sheet, respectively. These data indicate that an extensive sampling of conformations was achieved.

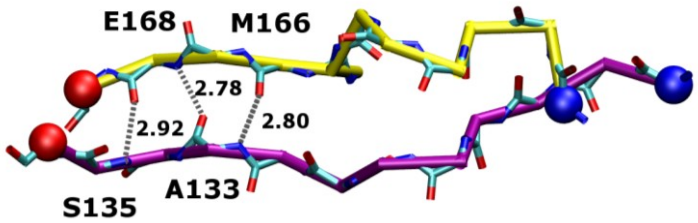

Figure 5
Representative structure of parallel β-sheet of AB 2-stranded β-sheet model. Only the backbone is represented. The N- and C-termini are indicated as blue and red spheres respectively. In this structure the fragment A is colored in yellow and the fragment B in violet. The residues and H-bonds involved in parallel β-sheet are shown.

6.3.1.2. BB' 2-stranded β-sheet

In the crystal structure of HPrP bound to the ICSM Fab fragment, two symmetry-related molecules interact by forming a 4-stranded antiparallel β-sheet made up of the 2-stranded β-sheets originally present in each PrP molecule. Here, we consider the model made up of the two central identical β-strands (residues 125-136; sheet BB') (Table 1). In the starting model, derived from this crystal structure, two H-bonds connect the β-strands in the intermolecular β-sheet, i.e. O Leu^{130}-N Leu'^{130} and N Leu^{130}-O Leu'^{130}.
The analysis of the room-temperature bath (bath1= 300.5 K) of sampling indicates that the two segments widely vary in their conformation (Figure 6).

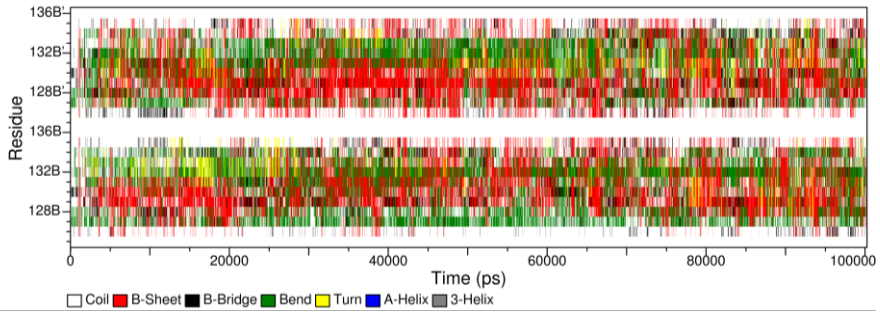

Figure 2
Evolution of secondary structure elements.

Nevertheless, a limited, but significant, intrinsic tendency to form a β-sheet is evident. Indeed, the average value of the H-bond distances, defined above, is smaller than 3.3 Å for the 5.4% of the collected structures at that temperature. Moreover, the persistence of the pairing of β-strands is doubled (10.2% of the collected structures) if we consider the two new H-bonds formed by main chain atoms of residues Ser^{132} and Tyr'^{128} in adjacent strands. In several structures (3.7% of the collected structures) it is also present the close pair of H-bonds involving residues Ser'^{132} and Tyr^{128}. This means that the sampling contains conformations with an elongated β-sheet, which involves Tyr^{128}-Leu^{130}-Ser^{132} residues from adjacent strands. For a representative structure of the elongated β-sheet see Figure 7.
It is worth noting that an intermolecular 4-stranded β-sheet at the crystal interface is also observed in a different crystal form in which three pathogenic mutants of human PrP crystallize (PDB codes: 3HEQ, 3HES, 3HER) (Lee et al., 2010). These mutants contain the M/V129 polymorphism and in fact the above codes refer to isomorphous crystals from D178N/M129, F198S/M129, and F198S/V129 proteins. In all the three structures the intermolecular β-sheets are similar, with the main chain H-bond contacts established between Tyr^{128} and Leu'^{130}. The other two "symmetric" H-bonds between Tyr$^{128'}$ and Leu^{130} are instead lacking. In this conformation the C^{α}-C^{α} distance between residues 129 on facing strands ranges from 4.7 to 5.4 Å, whereas in the starting structure of our BB' model this distance is 7.6 Å. We have searched for a distance lower than 5 Å in the bath1 sampled structures. It comes out that about 120 structures exhibit a short C^{α}-C^{α} distance with β-strand H-bond pairs just involving Tyr^{128} and Leu^{130}. This indicates that, even if sporadically, the 125-136 segment explores extended conformations which arrange in β-sheet interfaces like those observed in the crystal packing of mutant structures.

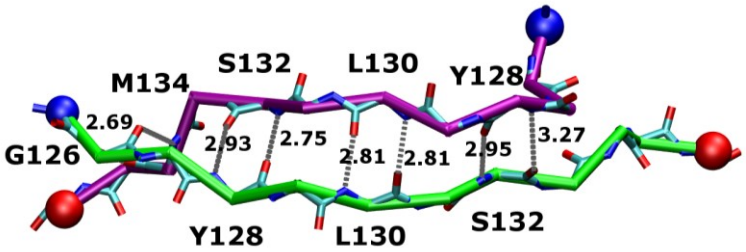

Figure 7
Representative structure of elongated β-sheet of BB' 2-stranded β-sheet model. Only the backbone is represented. The N- and C-termini are indicated as blue and red spheres respectively. In this structure the fragment B is colored in green and the fragment B' in violet. The residues and H-bonds involved in an elongated β-sheet are shown.

6.3.1.3. ABB'A' 4-stranded β-sheet

The starting structure for the four-stranded β-sheet simulation has been derived by applying crystallographic symmetry operations to the AB pair of strands in order to obtain the ABB'A' sheet (Figure 8). The hydrogen bonding features of the starting model are the ones already described for the AB and BB' sheets.

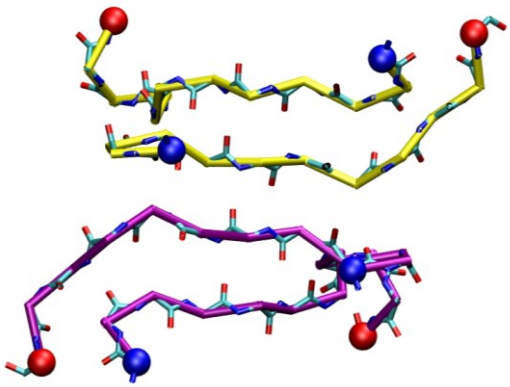

Figure 8
Starting model of ABB'A' 4-stranded β-sheet. The AB and B'A' fragments are colored in yellow and violet respectively. The N- and C-termini are represented by blue and red spheres respectively.

The analysis of the secondary structure present in bath1 sampling clearly shows that both A and B segments maintain their β-strand conformation (Figure 9). The individual β-strand pairings, AB and B'A', are rather stable. The regularity and persistence of the hydrogen bonding pattern is even higher than that observed in the 2-stranded AB simulation. Indeed, the three main chain H-bonds, originally present in the starting structure, are kept quite conserved along the sampling. On average, they are present in 92% of structures in AB sheet and in 86% in A'B' sheet. The fourth H-bond between N Val^{161} and O Gly^{131}, which is frequently formed in the 2-stranded AB simulation, is also observed in the present simulation (60% of structures in AB and 54% of structures in A'B'). Moreover, in the AB pairing, the sheet is elongated to form the H-bond between O Gln^{159} and N Ala^{133} (42% of structures) expected for a regular pattern of antiparallel β-sheet (Figure 3). In the A'B' pairing, the population of this H-bond is halved (21%) and the H-bond of the original β-bulge between O Gln^{159} and N Met^{134} is still present (24%).

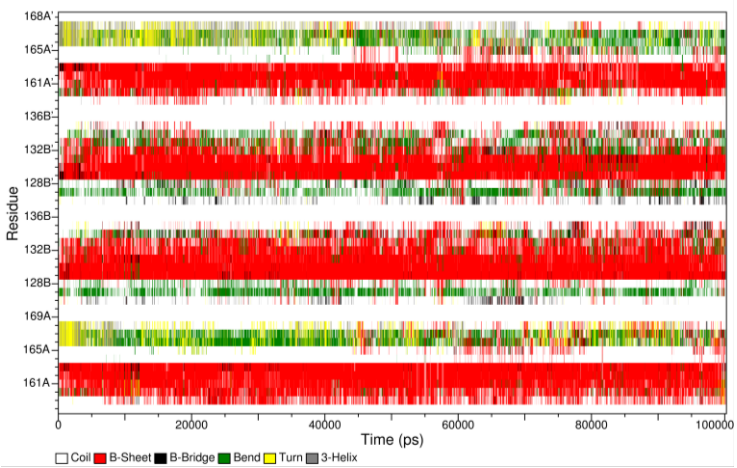

Figure 9
Evolution of secondary structure elements.

Altogether, the results indicate that the β-strand AB pairing is stable and even more than that in isolated 2-stranded AB β-sheet.
When analysing the BB' interface, the picture emerged is very similar to that of the isolated 2-stranded BB' β-sheet. The average value of the original H-bond distances between Leu^{130} residues is smaller than 3.3 Å for the 5.9% of the collected structures at 300.5 K. The persistence of the pairing does not change if we also consider the two new H-bonds formed by main chain atoms of residues Ser^{132} and Tyr'^{128} in adjacent strands (8.2%) or even those formed by Ser'^{132} and Tyr^{128} (less that 1%).
These data indicate that there is no extra stabilization introduced by the initial presence of an extended 4-stranded sheet: the A and B segments have an intrinsic tendency to form a β-sheet pairing so that the 4-stranded sheet breaks into two AB and A'B' sheets (Figure 10).

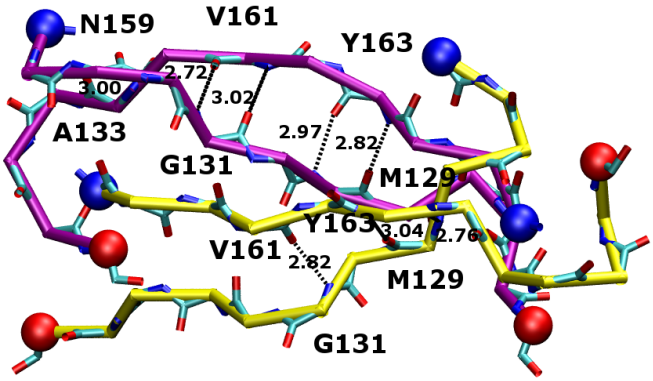

Figure 10
Representative structure of broken ABB'A' 4-stranded β-sheet. In this structure the single AB (yellow) and B'A' (violet) antiparallel β-sheets are stabilized by H-bonds.

6.3.1.4. M129V and G131V mutants

We have carried out preliminary analysis of the simulations on 2-stranded and 4-stranded sheets formed by segments containing M129V and G131V substitutions. The residue replacements are located in the B/B' segment (Table 1).
Our results indicate that the introduction of a valine residue at position 131 leads to a stabilization of the BB' β-sheet pairing. On the other hand, no significant change has been observed when the replacement occurs at position 129 (data not shown).
As an example, we can consider the G131V ABB'A' β-sheet and focus our attention on the close pair of hydrogen bonds displayed by the main chain atoms of residue Leu^{130} on adjacent strands (O Leu^{130}-N Leu'^{130} and N Leu^{130}-O Leu'^{130}). By calculating the average value of the two distances, we found that this value is lower than 3.3 Å for 28% of structures sampled in the bath1 collection at room temperature. This value has to be compared with the correspondent 5.9% value calculated for the wild type ABB'A' simulation. Even if we consider that the formation of BB' β-sheet occurs when H-bonds are formed between Ser^{132} and Tyr'^{128}, in wild type simulation this is observed for only 8.2% of sampled structures. These data clearly show that in the G131V ABB'A' β-sheet the BB' interface is more stable (Figure 11) than in the wt ABB'A' β-sheet.
The reinforcement of the BB' β-sheet pairing, due to the G131V substitution, is also evident in the 2-stranded G131V BB' simulation (Figure 12). The characteristic H-bonds between Leu^{130} residues are present in about 30% of structures (by

considering average value of the two distances lower than 3.3 Å). The same holds for the hydrogen bonding close pair between Ser'[132] and Tyr[128]. Moreover, the two main chain H-bonds connecting Ser[132] and Tyr'[128] occur in 16% of collected structures. Again, collectively these results indicate a greater stability of the G131V BB' interface.
In this intermolecular interface the residues Met[129] and Gly[131] belonging to adjacent strands face each other. This means that, when Gly[131] is replaced by a Val residue, there is a possible van der Waals interaction formed by Met and Val side chains. This effect, together with the advantage of reducing the mobility of the B segment by replacing a flexible Gly residue with a branched Val residue, can be suggested as a stabilizing factor for the formation of a β-sheet intermolecular association.

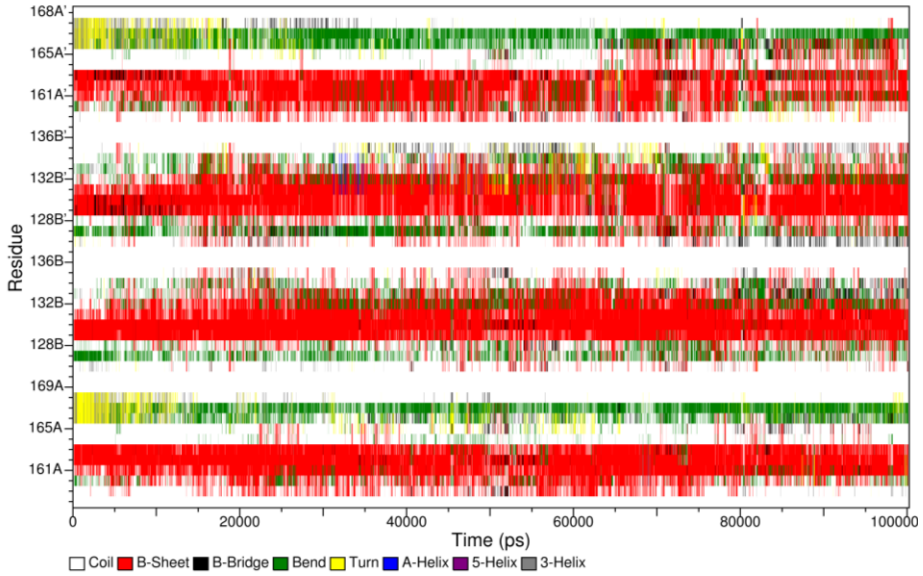

Figure 11
Evolution of secondary structure elements of G131V ABB'A' β-sheet.

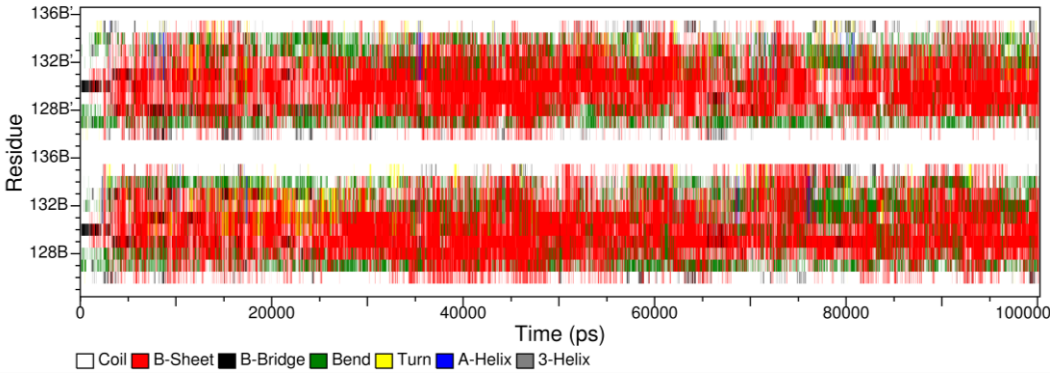

Figure 12
Evolution of secondary structure elements of 2-stranded G131V BB'.

6.4. Conclusions

MD simulations here reported reveal an unsuspected intrinsic stability of the two-stranded β-sheet present in the globular human prion protein. This fragment is stable even when the rest of the protein is removed. This finding holds important implications for the prion transition from the globular to fibrillar state. Indeed, any structural alteration induced by mutations that lead to a major destabilization of the protein, will not perturb this β-structure element. The preservation of this motif even in partially/totally unfolded states may be an important event in the fibrillogenesis process. Indeed, the β-structure of the globular protein may represent the nucleus for the fibril formation process. On this basis, it may be surmised that small peptides mimicking the protein β-structure regions can potentially interfere with the aggregation process of human prion protein. The stability of larger aggregates formed by the juxtaposition of two of these sheets as detected in the crystalline state is very limited. Interestingly, preliminary simulations indicate that the stability of these aggregates may be influenced by mutations linked to the insurgence of pathological states.

7. CONCLUSIONS AND FUTURE PERSPECTIVES

The investigations carried out in this PhD project have provided insightful information into the conformational preferences of potential neuroprotective factors and into the structure of amyloid-like peptides. These studies have been conducted by using either standard molecular dynamics protocols or more sophisticated approaches (essential dynamics, replica exchange molecular dynamics and metadynamics). Computations carried out on neurotrophins have not only provided clues on the intrinsic dynamic features of these protein but they have also suggested strategies for the design and the development of new compounds of potential therapeutic interest. In particular these studies have indicated that the efficiency of peptide designed on the basis of the N-terminal sequence of the protein may be improved by increasing the intrinsic helical propensity of these fragments. Moreover, in line with previous observations (Colangelo et al., 2008), new compounds based on NGF loop region should be endowed with some flexibility as these regions are very mobile even in the native protein. The close structural topology of NGF with the other NTs also suggests that these considerations may also be applied for the structure-based design of agonists/antagonists of the other members of this protein family. Experiments in this direction are currently in progress. From a more basic point of view, these investigations have also provided interesting clues on the structural mechanisms that regulate the binding of NGF to different receptors. Intriguingly, the binding of the N-terminus to TrkA can be interpreted in terms of a “population shift” mechanism, since the conformation assumed by this region in the complex is already present in its intrinsic conformational repertoire. On the other hand, the asymmetric 2:1 complex between NGF and $p75^{NTR}$ is better described in terms of an “induced fit” mechanism.

The simulations focused on amyloid aggregates have highlighted the importance of the chemical nature of the residues involved in the steric zipper interface. Indeed, our results indicate that the aliphatic residues are less prone to form stabilizing intra-sheet and inter-sheet interactions when compared with polar and aromatic residues (De Simone et al., 2008) (Zheng et al., 2006) (Esposito et al., 2006). Along this line, amyloid-like assemblies endowed with aliphatic hydrophobic residues presumably require larger interfaces, as it is observed in the HET structure which presents a remarkable stability in our MD simulations. The results here presented also demonstrate that assemblies derived from crystalline structure are not necessarily stable in non-crystalline environments. Therefore, MD simulations are valuable tools to verify the check the relevance of assemblies detected in crystallographic states for non crystalline states. MD simulations were then applied to gain further data on an intriguing phenomenon that characterized neurodegenerative diseases: the occurrence of distinct strains. It has been recently proposed that distinct steric zipper assemblies observed in the crystal state may represent the structural entities involved in the strain occurrence (Wiltzius et al., 2009). In this context, MD simulations were carried out to check the stability of alternative steric zipper models in non-crystalline environments. Analyses carried out with different force field provide evidence on the stability of these assemblies. These findings support the proposal that distinct steric zipper aggregates formed by the same polypeptide chain may be involved in distinct strains. Moreover, these analyses also provided clues on the energetic involved in the steric zipper formation and on the role played by intra-sheet and inter-sheet interactions. Ongoing investigations carried out by using very

sophisticated MD approaches (metadynamics) will likely provide better insights into the energetic factors underlying the occurrence of these polymorphs.
MD simulations provided interesting information on the structural basis of the transition of the human prion protein from the globular state to the fiber-like state. The analysis of the stability of the β-sheet present in the globular state of the protein indicates that it is endowed with a remarkable intrinsic stability, even when the rest of the protein is removed. Interestingly, independent crystallographic studies have shown the involvement of the β-sheet of the HPrP in intermolecular interactions that lead to the association of two different molecules HPrP in the crystalline state (Antonyuk et al., 2009) (Lee et al., 2010) (Haire et al., 2004). These observations suggest that this association may be representative of the early stages of aggregation of HPrP. The stability of the aggregates formed by the juxtaposition of two of these sheets as detected in the crystalline state is very limited. Interestingly, additional simulations indicate that these aggregates are stabilized by mutations linked to the insurgence of pathological states (Hosszu et al., 2004) (Santini et al., 2003). The observation that the two stranded β-sheet of the prion monomer is intrinsically stable holds important implications for prion polymerization process and for the design of synthetic peptides that potentially can inhibit the aggregation process of human prion protein. Based on these considerations, peptides that can potentially inhibit the aggregation process of human prion protein have been designed and synthesized. Their characterization will be the object of future investigations.

APPENDIX

MOLECULAR DYNAMICS

Molecular Dynamics simulation is one of the principal methods of the computational chemistry that can be applied to biological macromolecules. This computational method calculates the time dependent behaviour of a molecular system.
Using MD it is possible to simulate the time evolution of a molecular system, which is represented classically considering a set of particles defined by their positions and momenta. Starting from a coordinate set taken for example from a crystal structure and assigning velocities to each atom typically from a Boltzmann distribution at a given temperature, successive coordinates and velocities are obtained by integrating the Newton's equation for the motion in each coordinate direction. In one dimension, the equation can be written as:

$$\frac{d^2 x_i}{dt^2} = \frac{F_{x_i}}{m_i}$$

where m_i and x_i are the mass and position of each atom, respectively and F_{xi} is the derivative of the potential according to a force field equation that is described in the next section. The result is a trajectory that shows how atomic positions and velocities evolve with time according to the influence of the remaining atoms in the system. Due to the large number of particles interacting with each other, the integration is performed numerically most commonly using the leap-frog algorithm. The integration step is limited to the fastest motion in the system. Therefore, for atomistic simulations the step size is usually 1 fs, or 2 fs if restraining bond lengths, generally done using SHAKE (Van Gunsteren and Berendsen 1977) and LINCS (Hess et al., 1997) algorithms.
The calculation of the interaction energy within a classical description of a molecular system requires a force field. A force field is built up from two distinct components, a set of equations used to generate the potential energies (and their derivatives, the forces) and the parameters used in these equations. Nowadays, there are four main force fields in common use for simulating biological macromolecules: AMBER, CHARMM, GROMOS and OPLS. The intra-molecular potential energy is typically represented by harmonic oscillators for bond stretching and angle bending, a Fourier series for each torsional angle, and Coulomb and Lennard–Jones (LJ) accounting for the interactions between atoms separated by three or more bonds. The latter two terms referred together as non-bonded terms are evaluated between all atom pairs in the system to yield the intermolecular energy.
Such force fields compute the energy as a sum of terms representing bond elongation, angle and dihedral deformation, and non-bonded interactions with the following general form:

$$E = \sum_{bonds} V^{str} + \sum_{angles} V^{bend} + \sum_{torsions} V^{tors} + \sum_{LJ} V^{LJ} + \sum_{Coulomb} V^{Coul}$$

where the three first summations correspond the bonded terms (that include atoms connected up to three consecutive bonds) and the last two refer to the non-bonded ones. All summations can be easily calculated from the coordinates of the system at a given time. For each pair of bonded atoms (i and j), the stretching term is computed as:

$$V_{ij}^{str}(r_{ij}) = k_{ij}^{r}(r_{ij} - r_{ij}^{0})^{2}$$

where k^{r}_{ij} is the stretching force constant and r_{ij} and r^{o}_{ij} are the distance between atoms and its equilibrium bond length, respectively. For every group of three bonded atoms (i, j and k), the angle term is described as:

$$V_{ijk}^{bend}(\theta_{ijk}) = k_{ijk}^{\theta}(\theta_{ijk} - \theta_{ijk}^{0})^{2}$$

where k^{θ}_{ijk} is the bending force constant, θ_{ijk} and θ^{o}_{ijk} are the angle between atoms and its equilibrium value, respectively. For every group of four bonded atoms (i, j, j, l), the dihedral term is often represented as a cosine expansion:

$$V_{ijkl}^{tors}(\phi_{ijkl}) = k_{ijkl}^{\phi}[1 + \cos(n\phi_{ijkl} - \phi_{ijkl}^{0})]$$

where k^{Φ}_{ijkl} is a dihedral constant affecting the barrier height, n is number of minima in a 360º rotation, and ϕ_{ijkl} and ϕ^{0}_{ijkl} are the dihedral angle and the equilibrium value according the biochemical convention (*trans* ϕ=180º, *cis* ϕ=0º and *gauche* ϕ =60º/300º), respectively. The first non-bonded term is often represented by a 6-12 LJ potential, a simple mathematical model that accounts for two distinct forces (an attractive and a repulsive) that neutral atoms and molecules are subject to:

$$V_{ij}^{LJ}(r_{ij}) = \left[\left(\frac{A_{ij}}{r_{ij}}\right)^{12} - \left(\frac{B_{ij}}{r_{ij}}\right)^{6}\right]$$

where A_{ij} and B_{ij} are parameters that depend from on each pair of atoms. The first term accounts for the attractive forces at long range (van der Waals or dispersion) and the other for the repulsive forces at short range, resulting from the overlap between electron orbitals. Finally, the last term in the force field equation is a Coulombic potential describing the electrostatic interactions:

$$V_{ij}^{Coul}(r_{ij}) = \frac{q_i q_j}{4\pi\varepsilon_0 r_{ij}}$$

where q_i and q_j are the charges of atoms i and j, r_{ij} the relative distance between them and ε the vacuum permittivity.

The constants and parameters of the preceding equations need to be fed from biophysical experiments and/or quantum mechanics calculations which differ from one force field to another. The specific force fields parameters of the different components present in the systems studied proteins and water molecules are discussed in the following sections. The simulations presented with this thesis have been performed using a microscopic description that combines the AMBER03 (Duan et al., 2003), all-atom OPLS (Jorgensen et al., 1996) or GROMOS (Daura et al., 1998) force fields, water molecules and ions.

GROMOS, AMBER and all-atom OPLS force fields

In the context of molecular mechanics, a force field refers to the functional form and parameter sets used to describe the potential energy of a system of particles. Force field functions and parameter sets are derived from both experimental work and high-level quantum mechanical calculations. In "united-atom" force fields as GROMOS the aliphatic and aromatic hydrogen atoms were included implicitly by representing the carbon atom and attached hydrogen atoms as a single group centered on the carbon atom. Whereas, the AMBER and OPLS-AA (all atoms) force field, include every atom explicitly. In AMBER03 the charges and main-chain torsion potentials have been rederived based on quantum mechanical calculations with solvent effects included by means of continuum models and each amino acid is allowed unique main-chain charges. As AMBER, OPLS-AA force field includes explicit representation of all atoms, including nonpolar hydrogens. Later publications include parameters for other specific functional groups and types of molecules such as carbohydrates. A distinctive feature of the OPLS parameters is that they were optimized to fit experimental properties of liquids, such as density and heat of vaporization, in addition to fitting gas-phase torsional profiles.

The water molecules

Many water models are available in the literature for an accurate representation of the liquid water. The most common ones are often distributed together with the force fields described above. These models have been parametrized to reproduce physical and thermodynamical properties such as the density, enthalpy of vaporization, radial distribution functions, energies of hydration or dipole moment. They can be classified by the number of points used to define the model (atoms plus dummy sites), whether the structure is rigid or flexible, and whether the model includes polarization effects or not. The simplest and most popular models for MD are TIP3P (Jorgensen et al.,1983) and SPC (Berendsen et al., 1987) series, which have three interaction sites, corresponding to the three atoms of the water molecule with rigid geometry. These water models can be described as effective rigid pair potentials composed of Lennard-Jones (LJ) and Coulombic terms. All of these water models have three interaction sites and are similar in nature, but the Lennard-Jones (LJ) and Coulombic terms differ. Each atom has a point charge assigned and the oxygen atom also gets Lennard-Jones parameters. The more complex 4-site or 5-site models such as TIP4P and TIP5P, respectively, place the negative charge on either a dummy atom placed near the oxygen along the bisector of the HOH angle or on two dummy atoms representing the lone pairs of the oxygen atom. These models improve the electrostatic distribution around the water molecule, though to a larger computational cost because of the larger number of electrostatic interactions to compute.

Because the SPCE and TIP3P have been shown to provide a good compromise between quality and computational cost they have been chosen as the water models for simulations of this thesis. In particular for the simulations conducted with OPLS-AA or AMBER03 force fields, the TIP3P water model was used. Instead, for simulations with GROMOS43a1 force field a variant of SPCE water model was used, the SPCE. The SPCE water model is a slight reparameterization of the SPC model, with a modified value for the charge. The SPCE model results in a better density and diffusion constant than the SPC model.

Long-range interactions

The computation of the pair-wise non-bonded interactions is the most time consuming part of a MD simulation as the evaluation of the forces scales quadratically with the number of atoms in the system. Accordingly, several approximations have been used the last 20 years in order to reduce the computational effort needed. One of the simplest approximations is to use of a cutoff that defines the maximum distance between pairs of atoms before computing their energy of interaction, under the assumption that the force between atoms can be neglected when they are largely separated. Typical cutoffs used are about 1-2 nm. However, dealing with the Coulombic term, the use of a cutoff is much more critical for the reliability of the simulations. Accordingly, the treatment of long range interactions has been an active field of research in the last years and is still a topic of considerable interest. The most common alternative to truncation is to use Particle Mesh Ewald or PME (Darden 1993), where the long-ranged electrostatic interactions are calculated with fast Fourier transforms. These methods provide an exact solution for the electrostatic interactions for an infinite periodic system. The easiest way of simulating a periodic system is to treat it enclosed in a box and consider replicated boxes (to infinity) by rigid translation in all the three Cartesian directions, completely filling the space. This approximation is called periodic boundary conditions or PBC.

Statistical ensemble

In order to relate the microscopic features of individual atoms and molecules to the macroscopic or bulk thermodynamic properties of materials one needs to use statistical mechanics methods. In this context, an ensemble formalizes the notion that, repeating an experiment again and again, a physicist may expect to observe a range of different outcomes under the same macroscopic conditions, but unable to control the microscopic details. Different macroscopic environmental constraints lead to different types of ensembles, with particular statistical characteristics. The most important ensembles used in MD simulations of biological systems are described below and impose several restrictions. The microcanonical ensemble (NVE) requires keeping the total energy of the system constant (i.e. a system thermally isolated). In contrast, in the canonical ensemble (NVT) a system shares its energy with a large heat reservoir or heat bath (Nose 1984), allowing the system to exchange energy assuming that the heat capacity of the reservoir is so large as to maintain a fixed temperature for the coupled system. In both cases (NVE and NVT) the initials N and V account for a constant number of atoms and volume (i.e. a fixed box shape). The NPT ensemble is analogous to the NVT one, but imposes a barostat
in the same spirit as the temperature coupling that maintains a fixed pressure instead of considering a constant volume (Nose 1983).

GROMACS Protocol for molecular dynamics simulations

For the molecular dynamics simulations discussed in this thesis, the package GROMACS were used (Van der Spoel et al., 2005). GROMACS is versatile software to simulate molecular dynamics mimicking the Newtonian equations of motion for systems with millions of particles. It is a high performance tool developed to study the dynamics of proteins using the classical theory of molecular dynamics. In simulating the time evolution of a protein in solution are usually used the periodic boundary conditions. According to the procedure, the system, the protein molecule with a large number of molecules of solvent, usually water, is placed in a box (of the form of a

parallelepiped or a cube) and is surrounded by an infinite number of identical copies. In this way it is produced and then simulated an infinite periodic system.
The starting models used were obtained from the PDB database. Before performing the simulations was performed stereochemical control on select models. The force field, the characteristics of the box, the solvent used, temperature and pressure of the simulation are discussed in materials and methods section of each chapter of thesis.
At the end of the simulation, the structures of the trajectory were analyzed using a series of programs that can monitor various structural parameters. It is possible to calculate the radius of gyration (Rg) of the molecule to verify the compactness of the structure; it provides a measure of the mass of the atoms in relation to the center of mass of the molecule. The radius of gyration is defined as:

$$Rg = \frac{\sqrt{\sum_i \|r_i\|^2 m_i}}{\sum_i m_i}$$

Where r_i represents the position of *i* atom respect to the center of mass of the molecule and m_i represent the mass of *i* atom.
The mean square deviation of the structure (RMSD) is another parameter that can be calculated easily by GROMACS. The RMSD represents the deviation of the structure from the original starting structure during the simulation, thus providing information on the conformational consistency.

$$RMSD_{(t_1,t_2)} = \frac{1}{N}\sqrt{\sum_i \|r_i(t_1) - r_i(t_2)\|}$$

Where $r_i(t)$ is the position of *i* atom at the time *t.*
Instead, the root mean square fluctuations (RMSF) represents the fluctuation of the relative position of atoms respect to the equilibrium configurations of the molecule (average), calculated exactly in the range of time when RMSD values are rather stable.

$$RMSF = \frac{1}{N}\sqrt{\sum_i (r_i - \langle r \rangle)}$$

The calculation of hydrogen bonds favors a further indication of the properties of the system. It allows to know the number of bonds, the distances and the angles between molecules or groups involved in the simulation. The program provides the distances between charged residues, dividing them into three groups (bonds - / -, + / -, +/+).The program analyzes the hydrogen bonds among the potential donor D and acceptor A. To determine whether the hydrogen bond exists, it is used a geometric criterion:

D-A distances ≤ 3.5 Å

D-H·····A angles > 110°

ACKNOWLEDGEMENTS

I thank Dr. Luciana Esposito and Dr. Luigi Vitagliano for the help and support during these years. Moreover I would thank all my colleagues and friends that lived this experience with me.

REFERENCES

Aloe L. 2004. Nerve growth factor, human skin ulcers and vascularization. Our experience. *Prog Brain Res.*146:515-22.

Altar, C. A. 1999. Neurotrophins and depression. *Trends Pharmacol. Sci*. 20: 59-61.

Amadei, A., M. A. Ceruso and A. Di Nola. 1999. On the convergence of the conformational coordinates basis set obtained by the essential dynamics analysis of proteins' molecular dynamics simulations. *Proteins.* 36:419-424.

Amadei, A., A.B.M. Linssen, H. J. C. Berendsen.1993. Essential dynamics of proteins, *Proteins: Struct. Funct. Genet.* 17:412-425.

Antonyuk, S. V., C. R. Trevitt, R. W. Strange, G. S. Jackson, D. Sangar, M. Batchelor, S. Cooper, C. Fraser, S. Jones, T. Georgiou, A. Khalili-Shirazi, A. R. Clarke, S. S. Hasnain and J. Collinge. 2009. Crystal structure of human prion protein bound to therapeutic antibody. *Proc. Natl. Acad. Sci. USA*. 106:2554-2558.

Apfel, S. C. 2002. Nerve growth factor for the treatment of diabetic neuropathy: what went wrong, what went right, and what does the future hold? *Int Rev Neurobiol*. 50:393-413.

Arcangeli, C., A. R. Bizzarri and S. Cannistraro. 2001. Concerted motions in copper plastocyanin and anuri: an essential dynamics study. *Biophysical Chemistry.* 90:45-56.

Arenas, E. and H. Persson. 1994. Neurotrophin-3 prevents the death of adult central noradrenergic neurons in vivo. *Nature*. 367:368-371.

Aurikko, J. P., B. T. Ruotolo, J. G. Grossmann, M. C. Moncrieffe, E. Stephens, V. M. Leppänen, C. V. Robinson, M. Saarma, R. A. Bradshaw and T. L. Blundell. 2005. Characterization of symmetric complexes of nerve growth factor and the ectodomain of the pan-neurotrophin receptor, p75NTR. *J. Biol. Chem*. 280:33453-33460.

Balbirnie, M., R. Grothe, and D. Eisenberg. 2001. An amyloid-forming peptide from the yeast prion Sup35 reveals a dehydrated β-sheet structure for amyloid. *Proc. Natl. Acad. Sci. USA.* 435:773-778.

Banfield, M. J., R. L. Naylor, A. G. Robertson, S. J. Allen, D. Dawbarn, and R. L. Brady. 2001. Specificity in Trk receptor:neurotrophin interactions: the crystal structure of TrkB-d5 in complex with neurotrophin-4/5. *Structure.* 9:1191-1199.

Barbacid, M. 1994. The Trk family of neurotrophin receptors. *J. Neurobiol.* 25:1386-1403.

Barde, Y. A., D., Edgar and H. Thoenen. 1982. Purification of a new neurotrophic factor from mammalian brain. *EMBO J.* 1:549-53.

Bax, B., T. L. Blundell, J. Murray-Rust, and N. Q. McDonald. 1997. Structure of mouse 7S NGF: a complex of nerve growth factor with four binding proteins. *Structure.* 5:1275-1285.

Beebe, D. J., J. S. Moore, J. M. Bauer, Q. Yu, R. H. Liu, C. Devadoss et al., 2001. Functional hydrogel structures for autonomous flow control inside microfluidic channels. *Nature.* 588-590.

Beglova, N., S. Maliartchouk, I. Ekiel, M. C. Zaccaro, H. U. Saragovi, and K. Gehring. 2000. Design and solution structure of functional peptide mimetics of nerve growth factor. *J. Med. Chem*. 43:3530-3540.

Berendsen, H. J. C., J. R. Grigera and T. P. Straatsma. 1987. The Missing Term in Effective Pair Potentials. *J. Phys. Chem.* 91:6269-6271.

Berrera, M., A. Cattaneo, and P. Carloni. 2006. Molecular simulation of the binding of nerve growth factor peptide mimics to the receptor tyrosine kinase A. *Biophys. J*. 91:2063-2071.

Best, R. B., N. V. Buchete, and G. Hummer. 2008. Are Current Molecular Dynamics Force Fields too Helical? *Biophys. J*. 95:L07-L09 and Erratum in *Biophys. J*. 95:4494.

Boehr, D. D., R. Nussinov, and P. E. Wright. 2009. The role of dynamic conformational ensembles in biomolecular recognition. *Nat. Chem. Biol*. 5:789-796.

Bradshaw, R. A., J. Murray-Rust, C. F. Ibanez, N. Q., McDonald, R. Lapatto and T. L. Blundell. 1994. Nerve growth factor: structure/function relationships. *Protein Sci*. 3:1901-1913.

Bruno, M. A., P. B. Clarke, A. Seltzer, R. Quirion, K. Burgess, A. C. Cuello, and H. U. Saragovi. 2004. Long-lasting rescue of age-associated deficits in cognition and the CNS cholinergic phenotype by a partial agonist peptidomimetic ligand of TrkA. *J. Neurosci*. 24:8009-8018.

Buxbaum, J. N. 2003 Diseases of protein conformation: what do in vitro experiments tell us about in vivo diseases? *Trends Biochem Sci*, 28:585.

Casaccia-Bonnefil, P., C. Gu, G. Khursigara, and M.V. Chao. 1999. p75 neurotrophin receptor as a modulator of survival and death decisions. *Microsc. Res. Tech*. 45:217-224.

Ceruso, M. A., A. Amadei and A. Di Nola. 1999. Mechanics and dynamics of B domain of protein G: role of packing and surface hydrophobic residues. *Protein Sci.* 8:147-160.

Chao, M. V.1994. The p75 neurotrophin receptor. *J. Neurobiol.* 25:137-1385.

Chao, M. V. and B.L. Hempstead 1995. p75 and Trk: a two-receptor system. *Trends Neurosci.*18:321-326.

Chiti, F. and C. M. Dobson. 2006. Protein misfolding, functional amyloid, and human disease. *Annu. Rev. Biochem.* 75:333-366.

Colangelo A. M., M. R.,Bianco, L. Vitagliano, C. Cavaliere, G. Cirillo, L. De Gioia, D. Diana, D. Colombo, C. Redaelli, L. Zaccaro, G. Morelli, Papa M, P. Sarmientos, L. Alberghina, and E. Martegani. 2008. A new nerve growth factor-mimetic peptide active on neuropathic pain in rats. *J. Neurosci*. 28:2698-2709.

Colombo, G., M. Meli, and A. De Simone. 2008. Computational studies of the structure, dynamics and native content of amyloid-like fibrils of ribonuclease A. *Proteins.* 70:863-72.

Connor, B., D. Young, Q. Yan, R. L. Faull, B. Synek and M. Dragunow. 1997. Brain-derived neurotrophic factor is reduced in Alzheimer's disease. *Brain. Res. Mol. Brain Res*. 49:71-81.

Covaceuszach, S., S. Capsoni, G. Ugolini, F. Spirito, D. Vignone, and A. Cattaneo. 2009. Development of a non invasive NGF-based therapy for Alzheimer's disease. *Curr Alzheimer Res*. 6:158-170.

D'Andrea, L. D., G. Iaccarino, R. Fattorusso, D. Sorriento, C. Carannante, D. Capasso, B. Trimarco, and C. Pedone. 2005. Targeting angiogenesis: structural characterization and biological properties of a de novo engineered VEGF mimicking peptide. *Proc. Natl. Acad. Sci. USA*. 102:14215-14220.

Darden, T., D. York and L. Pedersen. 1993. Particle mesh Ewald: an H log method for Ewald sums in large systems. *J. Chem. Phys.* 98:10089-10092.

Daura, X., A. E. Mark, and W. F. Van. Gunsteren. 1998. Parametrisation of aliphatic CH_n united atoms of GROMOS96 force field. *J. Comput. Chem.*19:535–547.

Dechant, G., and H. Neumann. 2002. Neurotrophins. *Adv. Exp. Med. Biol.* 513:303-334.

DeLano, W.L. 2002. The PyMOL Molecular Graphics System. DeLano Scientific, San Carlos, CA, USA

De Simone, A., L. Esposito, C. Pedone and L. Vitagliano. 2008. Insight into stability and toxicity of amyloid-like oligomers by replica exchange molecular dynamics analyses. *Biophys. J.* 95:1965-1973.

De Simone, A., C. Pedone and L. Vitagliano. 2008. Structure, dynamics, and stability of assemblies of the human prion fragment SNQNNF *Biochem. and Biophys. Comm.* 366:800-806.

De Simone, A., A. Zagari and P. Derreumaux. 2007. Structural and hydration properties of the partially unfolded states of the prion protein. *Biophys. J.* 93:1284-1292.

Diana, D., B. Ziaco, G. Colombo, G. Scarabelli, A. Romanelli, C. Pedone, R. Fattorusso, and L. D. D'Andrea. 2008. Structural determinants of the unusual helix stability of a de novo engineered vascular endothelial growth factor (VEGF) mimicking peptide. *Chemistry*. 14:4164-4166.

Duan, Y., C. Wu, S. Chowdhury, M. C. Lee, G. Xiong, W. Zhang, R. Yang, P. Cieplak, R. Luo, T. Lee, J. Caldwell, J. Wang, and P. Kollman. 2003. A point-charge force field for molecular mechanics simulations of proteins based on condensed-phase quantum mechanical calculations. *J. Comput. Chem*. 24:1999-2012.

Eanes, E. D. and G.G. Glenner.1968. X-ray diffraction studies on amyloid filaments. *J. Histochem. Cytochem.* 16:673-677.

Edwards, R. H., M. J. Selby, P. D. Garcia and W. J. Rutter. 1988. Processing of the native nerve growth factor precursor to form biologically active nerve growth factor. *J.Biol.Chem*.263:6810-6815.

Eisenberg, D., R. Nelson, M. R. Sawaya, M. Balbirnie, S. Sambashivan, M. I. Ivanova, A. O. Madsen, and C. Riekel. 2006. The structural biology of protein aggregation diseases: Fundamental questions and some answers. *Acc. Chem. Res*. 39:568-75.

Esposito, L., A. Paladino, C. Pedone and L. Vitagliano. 2008. Insight into structure, stability and toxicity of monomeric and aggregated polyglutamine models from molecular dynamics simulations. *Biophys. J.* 94:4031-4040.

Esposito, L., C. Pedone and L. Vitagliano. 2006. Molecular dynamics analyses of cross-beta-spine steric zipper models: beta-sheet twisting and aggregation. *Proc. Natl. Acad. Sci. USA.* 103:11533-11538.

Feng, D., T. Kim, E. Özkan, M. Light, R. Torkin, K. K. Teng, B. L. Hempstead and K. C. Garcia. 2010. Molecular and structural insight into proNGF engagement of p75NTR and Sortilin. *J. Mol. Biol.*396:967-984.

Gallicchio, E., M. Andrec, A. K. Felts and R. M. Levy. 2005. Temperature weighted histogram analysis method, replica exchange, and transition paths. *J. Phys. Chem. B.* 109:6722-6731.

Garcia, A.E. 1992. Large-amplitude nonlinear motions in proteins, *Phys. Rev. Lett*. 68:2696-2699.

Gong, Y., P. Cao, H. J. Yu, and T. Jiang. 2008. Crystal structure of the neurotrophin-3 and p75NTR symmetrical complex. *Nature.* 454:789-793.

Gotz, R., R. Koster, C. Winkler, F. Raulf, F. Lottspeich, M. Schartl and H. Thoenen. 1994. Neurotrophin-6 is a new member of the nerve growth factor family. *Nature*. 372: 266-269.

Granata, V., G. Graziano, A. Ruggiero, G. Raimo, M. Masullo, P. Arcari, L. Vitagliano, and A. Zagari. 2006. Chemical denaturation of the elongation factor 1alpha isolated from the hyperthermophilic archaeon Sulfolobus solfataricus. *Biochemistry*. 45:719-726.

Gsponer, J., U. Haberthur, and A. Caflisch. 2003. The role of side-chain interactions in the early steps of aggregation: Molecular dynamics simulations of an amyloid-forming peptide from the yeast prion Sup35. *Proc. Natl. Acad. Sci. USA.* 100:5154-9.

Gunasekaran, K., B. Ma, and R. Nussinov. 2004. Is allostery an intrinsic property of all dynamic proteins? *Proteins.* 57:433-443.

Haire, L. F., S. M. Whyte, N. Vasisht, A. C. Gill, C. Verma, E. J. Dodson, G. G. Dodson, P. M. Bayley. 2004. The crystal structure of the globular domain of the sheep prion protein. *J. Mol. Biol.* 336:1175-1183.

Hallbook, F. 1999. Evolution of the vertebrate neurotrophin and Trk receptor gene families. *Curr Opin Neurobiol*. 9:616-621.

Haniu, M., S .Montestruque, E. J. Bures, J .Talvenheimo, R. Toso, S. Lewis-Sandy, A. A. Welcher and M. F. Rohde. 1997. Interactions between brain-derived neurotrophic factor and the TrkB receptor. Identification of two ligand binding domains in soluble TRKB by affinity separation and chemical cross-linking. *J. Biol. Chem.* 272:25296–303.

He, X. L., and K. C. Garcia. 2004. Structure of nerve growth factor complexed with the shared neurotrophin receptor p75. *Science.* 304:870-875.

Heise, H. 2008. Solid-state NMR spettroscopy of amyloid proteins. *Chembiochem.* 9:179-189.

Hellweg, R., C. A. Gericke, K. Jendroska, H. D. Hartung and J. Cervos-Navarro. 1998. NGF content in the cerebral cortex of non-demented patients with amyloid-plaques and in symptomatic Alzheimer's disease. *Int. J. Dev. Neurosci*. 16: 787-794.

Hess, B., H. Bekker, H. J. C. Berendsen and J. Fraaije. 1997. LINCS: a linear constraint solver for molecular simulations. *J. Comput. Chem.* 18:1463-1472.

Holland, D. R., L. S. Cousens, W. Meng, and B. W. Matthews. 1994. Nerve growth factor in different crystal forms displays structural flexibility and reveals zinc binding sites. *J. Mol. Biol*. 239:385-400.

Holmes, T. C. 2002. Novel peptide-based biomaterial scaffolds for tissue engineering. *Trends. Biotechnol.* 20:16-21.

Holmes, T. C., S. Lacalle, X. Su, G. S. Liu, A. Rich and S. G. Zhang. 2000. Extensive neurite outgrowth and active synapse formation on self-assembling peptide scaffolds. *Proc. Natl. Acad. Sci. USA.* 97:6728-6733.

Hoppener, J. W., B. Ahren, and C. J. Lips. 2000. Islet amyloid and type 2 diabetes mellitus. *N. Engl. J. Med.* 343:411-9.

Hosszu, L. S. P., G. S. Jackson, C. R. Trevitt, S. Jones, M. Batchelor, D. Bhelt, K. Prodromidou, A. R. Clarke, J. P. Waltho and J. Collinge. 2004. The residue 129 polymorphism in human prion protein does not confer susceptibility to Creutzfeldt-Jakob disease by altering the structure of global stability of PrP^{C}. *J. Biol. Chem.* 279:28515-28521.

Howells, D. W., M. J. Porritt, J. Y. Wong, P. E. Batchelor, R. Kalnins, A. J. Hughes and G. A. Donnan. 2000. Reduced BDNF mRNA expression in the Parkinson's disease substantia nigra. *Exp. Neurol*. 166:127-135.

Humphrey, W., A. Dalke, and K. Schulten. 1996. VMD: visual molecular dynamics. *J. Mol. Graph*. 14:33-38, 27-28.

Hyman, C., M. Juhasz, C. Jackson, P. Wright, N. Y. Ip and R. M. Lindsay. 1994. Overlapping and distinct actions of the neurotrophins BDNF, NT-3, and NT-4/5 on cultured dopaminergic and GABAergic neurons of the ventral mesencephalon. *J. Neurosci*. 14:335-347.

Ip, N. Y., C. F. Ibáñez, S. H. Nye, J. McClain, P. F. Jones, D. Gies, L. Belluscio, M. M. Le Beau, R Espinosa, S. P. Squinto, et al. 1992. Mammalian neurotrophin-4: Structure, chromosomal localization, tissue distribution and receptor specificity. *Proc Natl Acad Sci USA.* 89:3060–3064.

Ip, N. Y., and G. D. Yancopoulos. 1993. Similarities and differences in the way neurotrophins interact with the trk receptors in neuronal and nonneuronal cells. *Neuron*. 10:137–149.

Jorgensen, W. L.; J. Chandrasekhar, J. D. Madura, R. W. Impey and M. L. Klein. 1983 Comparison of simple potential functions for simulating liquid water. *J. Chem. Phys.* 79:926-935.

Jorgensen, W. L., D. S. Maxwell and J. Tirado-Rives. 1996. Development and testing of the OPLS all-atom force field on conformational energetics and properties of organic liquids. *J. Am. Chem. Soc.* 118:11225-11236.

Kisiday, J., M. Jin, B. Kurz., H. Hung., C. Semino, S. Zhang et al., 2002. Self-assembling peptide hydrogel fosters chondrocyte extracellular matriz production and cell division: implications for cartilage tissue repair. *Proc. Natl. Acad. Sci. USA.* 99:9996-10001.

Klein, R., F. Lamballe, S. Bryant and M. Barbacid.1992. The trkB tyrosine protein-kinase is a receptor for neurotrophin-4. *Neuron.* 8:947–956.

Lamballe, F., R. Klein and M. Barbacid. 1991. TrkC, a new member of the trk family of tyrosine protein-kinases, is a receptor for neurotrophin-3. *Cell.* 66: 967–979.

Lambiase, A., P. Rama, S. Bonini, G. Caprioglio, and L. Aloe. 1998. Topical treatment with nerve growth factor for corneal neurotrophic ulcers. *N. Engl. J. Med.* 338:1174-1180.

Lanave, C., A. M. Colangelo, C. Saccone, and L. Alberghina. 2007. Molecular evolution of the neurotrophin family members and their Trk receptors. *Gene.* 394:1-12.

Lee, K. Y. and D. J. Mooney. 2001. Hydrogels for tissue engineering. *Chem. Rev.* 101:1869-1880.

Lee, S., L. Antony, R. Hartmann, K. J. Knaus, K. Surewicz, W. K. Surewicz and V. C. Yee. 2010. Conformational diversity in prion protein variants influences intermolecular β-sheet formation. *EMBO J.* 29:251-262.

Levi-Montalcini, R.1964. The nerve-growth factor. *Ann. N. Y. Acad. Sci.* 118:149-70.

Levivier, M., S. Przedborski, C. Bencsics and U. J. Kang 1995. Intrastriatal implantation of fibroblasts genetically engineered to produce brain-derived neurotrophic factor prevents degeneration of dopaminergic neurons in a rat model of Parkinson's disease. *J. Neurosci*. 15:7810-7820.

Ma, N., S. S. Wu, Y. X. Ma, X. Wang, J. Zeng, G. Tong, Y. Huang, and S. Wang. 2004. Nerve growth factor receptor-mediated gene transfer. *Mol. Ther*. 9:270-281.

Maisonpierre, P. C., L. Belluscio, S. Squinto, N. Y. Ip, M. E., Furth, R. M. Lindsay and G. D. Yancopoulos. 1990. Neurotrophin-3: a neurotrophic factor related to NGF and BDNF. *Science*. 247:1446-1451.

Makin, O. S. and L. C. Serpell, 2004. Structural insight into a yeast prion illuminate nucleation and strain diversity. *Nature.* 435:765-772.

Massa, S. M., Y. Xie, and F. M. Longo. 2002. Alzheimer's therapeutics: neurotrophin small molecule mimetics. *J. Mol. Neurosci*. 19:107-111.

McDonald, N. Q., R. Lapatto, J. Murray-Rust, J. Gunning, A. Wlodawer, and T. L. Blundell. 1991. New protein fold revealed by a 2.3-A resolution crystal structure of nerve growth factor. *Nature.* 354:411-414.

Merlino, A, M. A. Ceruso, L. Vitagliano and L. Mazzarella. 2005. Open interface and large quaternary structure movements in 3D domain swapped proteins: insights from molecular dynamics simulations of the C-terminal swapped dimer of ribonuclease A.
Biophys. J. 88:2003-2112.

Merlino, A, L. Vitagliano, M. A. Ceruso and L. Mazzarella.2004. Dynamic properties of the N-terminal swapped dimer of ribonuclease A. *Biophys. J.* 86:2383-2391.

Merlino, A., L. Vitagliano, M. A. Ceruso and L. Mazzarella. 2003. Subtle functional collective motions in pancreatic-like Ribonucleases: from Ribonuclease A to Angiogenin. *Proteins.* 53:101-110.

Michalski, B. and M. Fahnestock. 2003. Pro-brain-derived neurotrophic factor is decreased in parietal cortex in Alzheimer's disease. *Brain Res. Mol. Brain Res.* 111:148-154.

Neet, K. E. and R. B. Campenot. 2001. Receptor binding, internalization and retrograde transport of neurotrophic factors. *Cell Mol. Life Sci*. 58:1021-1035.

Nelson, R., M. R. Sawaya, M. Balbirnie, A. O. Madsen, C. Riekel, R. Grothe, D. Eisenberg. 2005. Structure of the cross-beta spine of amyloid-like fibrils. *Nature.* 435:1172-1184.

Nose, S. 1984. A Molecular-Dynamics Method for Simulations in the Canonical Ensemble. *Molecular Physics.* 52:255-268.

Nose, S. and M. L. Klein. 1983. Constant Pressure Molecular-Dynamics for Molecular-Systems. *Molecular Physics* 50:1055-1076.

O'Leary, P. D., and R. A. Hughes. 2003. Design of potent peptide mimetics of brain-derived neurotrophic factor. J. Biol. Chem. 278:25738-25744.

Peleshok, J., and H. U. Saragovi. 2006. Functional mimetics of neurotrophins and their receptors. *Biochem. Soc. Trans.* 34:612-617.

Peppas, N. A., P. Bures, W. Leobandung and H. Ichikawa. 2000. Hydrogels in pharmaceutical formulations. *Eur. J. Biopharm.* 50:27-46.

Periole, X., A. Rampioni, M. Vendruscolo, and A. E. Mark. 2009. Factors that affect the degree of twist in beta-sheet structures: a molecular dynamics simulation study of a cross-beta filament of the GNNQQNY peptide. *J. Phys. Chem. B*. 113:1728-37.

Perutz, M. F. 1995. Polar zippers: their role in human disease. *Pharma. Acta. Helv.* 69:213-224.

Perutz, M. F., B. J. Pope, D. Owen, E. E. Wanker and E. Scherzinger. 2002. Aggregation of proteins with expanded glutamine and alanine repeats of the glutamine-rich and asparagine-rich domains of Sup35 and of the amyloid beta-peptide of amyloid plaques. *Proc. Natl. Acad. Sci. USA*. 99:5596-5600.

Petkova, A. T., Y. Ishii, J. J. Balbach, O. N. Antzutkin, R. D. Leapman, F. Delaglio and R. Tycko. 2002. A structural model for Alzheimer's β-amyloid fibrils based on experimental constraints from solid state NMR. *Proc. Natl. Acad. Sci. USA.* 99:16742-16747.

Petruska, J. C. and L. M. Mendell. 2004. The many functions of nerve growth factor: multiple actions on nociceptors. *Neurosci. Lett*. 361:168-171.

Reches, M. and E. Gazit. 2003. Casting metal nanowires within discrete self-assembled peptide nanotubes. *Science.* 625-627.

Riek, R., S. Homemann, G. Wider, M. Billeter, R. Glockshubert and K. Wütrick. 1996. NMR structure of the mouse prion protein domain PrP(121-321). *Nature*. 382:180-182.

Robertson, A. G. S., M. J. Banfield, S. J. Allen, J. A. Dando, G. G. F. Mason, S. J. Tyler, G. S. Bennett, S. D. Brain, A. R. Clarke, R. L. Naylor, G. K. Wilcock, R. L. Brady and D. Dawbarn. 2001. Identification and structure of the nerve growth factor binding site on TrkA. *Biochem. Biophys. Res. Commun*. 282:131-141.

Roosen, A., A. Schober, J. Strelau, M. Bottner, J. Faulhaber, G. Bendner, S.L. McIlwrath, H. Seller, H. Ehmke, G.R. Lewin, and K. Unsicker. 2001. Lack of neurotrophin-4 causes selective structural and chemical deficits in sympathetic ganglia and their preganglionic innervation. *J. Neurosci*. 21:3073-3084.

Rousseau, F., J. Schymkowitz and L. Serrano. 2006. Protein aggregation and amyloidosis: confusion of the kinds? *Curr. Opin. Struct. Biol.*16:118-126.

Rueda, M., P. Chancón and M. Orozco. 2007. Through validation of protein normal mode analysis: a comparative study with essential dynamics. *Structure*.15:565-575.

Santini, S., J. B. Claude, S. Audic and P. Derreumaux. 2003. Impact of the tail and mutations G131V and M129V on prion protein flexibility. *Proteins.* 51:258-265.

Saragovi, H. U., E. Hamel, and A. Di Polo. 2009. A neurotrophic rationale for the therapy of neurodegenerative disorders. *Curr. Alzheimer Res.* 6:419-423.

Saragovi, H. U. and M. C. Zaccaro. 2002. Small molecule peptidomimetic ligands of neurotrophin receptors, identifying binding sites, activation sites and regulatory sites. *Curr. Pharm. Des.* 8:2201-2216.

Sawaya, M. R., S. Sambashivan, R. Nelson, M. I. Ivanova, S. A. Sievers, M. I. Apostol, M. J. Thompson, M. Balbirnie, J. J. W. Wiltzius, H. T. McFarlane, A. O Madsen, C. Riekel and D. Eisenberg. 2007. Atomic structures of amyloid cross-β spines reveal varied steric zippers. *Nature.* 447:453-457.

Schneider, R. and M. Schweiger. 1991. A novel modular mosaic of cell adhesion motifs in the extracellular domains of the neurogenic trk and trkB tyrosine kinase receptors. *Oncogene.* 6:1807-1811

Seibert, M. M., A. Patriksson, B. Hess, and D. van der Spoel. 2005. Reproducible polypeptide folding and structure prediction using molecular dynamics simulations. *J. Mol. Biol.* 354:173–183.

Settanni, G., A. Cattaneo, and P. Carloni. 2003. Molecular dynamics simulations of the NGF-TrkA domain 5 complex and comparison with biological data. *Biophys. J.* 84:2282-2292.

Sheibel, T, R. Parthasarathy, G. Sawicki, X. M. Lin, H. Jaeger and S. L. Lindquist. 2003. Conducting nanowires built by controlled self-assembly of amyloid fibers and dìselective metal deposition. *Proc. Natl. Acad. Sci. USA.*100:4527-4532.

Shimizu, E., K. Hashimoto, H. Watanabe, N. Komatsu, N. Okamura, K. Koike, N. Shinoda, M. Nakazato, C. Kumakiri, S. Okada and M. Iyo. 2003. Serum brain-derived neurotrophic factor (BDNF) levels in schizophrenia are indistinguishable from controls. *Neurosci. Lett*. 351:111-114.

Siegel, G. J. and N. B. Chauhan. 2000. Neurotrophic factors in Alzheimer's and Parkinson's disease brain. *Brain Res. Rev*. 33:199-227.

Sikorski P. and E. Atkins 2005. New model for crystalline polyglutamine assemblies and their connection with amyloid fibrils. *Biomacromolecules.* 6:425-432.

Soppet, D., E. Escandon, J. Maragos, D. S. Middlemas, S. W. Reid, J. Blair, L. E. Burton, B. R. Stanton, D. R. Kaplan, T. Hunter, K. Nikolics and L. F. Parada. 1991. The neurotrophic factors brain-derived neurotrophic factor and neurotrophin-3 are ligands for the trkB tyrosine kinase receptor. *Cell*. 65: 895–903.

Stanzione, F., L., Esposito, A. Paladino, C. Pedone, G. Morelli and L. Vitagliano. 2010. Role of the conformational versatility of the neurotrophin N-terminal regions in their recognition by Trk receptors. *Biophys. J.*99:2273-2278.

Strodel, B., C. S. Whittleston, and D. J. Wales. 2007. Thermodynamics and kinetics of aggregation for the GNNQQNY peptide. *J. Am. Chem. Soc.* 129:16005-14.

Sugita, Y. and Y. Okamoto. 1999. Replica-Exchange molecular dynamics method for protein folding. *Chem. Phys. Lett.* 314:141-151.

Sunde, M. and C. Blake. 1997. The structure of amyloid fibrils by electron microscopy and X-ray diffraction. *Adv. Protein Chem.* 50:123-159.

Sunde, M., L. C. Serpell, M. Bartlam, P. E. Fraser, M. B. Pepys, C. C. Blake.1997. Common core of amyloid fibrils by synchrotron X-ray diffraction. *J. Mol. Biol.* 273:729-739.

Tycko, R. 2006. Molecular structure of amyloid fibrils: insight from solid-state NMR. *A. Rev. Biophys.* 39:1-55.

Van Der Spoel, D., E. Lindahl, B. Hess, G. Groenhof, A. E. Mark, and H. J. Berendsen. 2005. GROMACS: fast, flexible, and free. *J. Comput. Chem*. 26:1701-1718.

Van Gunsteren, W. F. and H. J. C. Berendsen. 1977. Algorithms for macromolecular Dynamics and Constraint Dynamics. *Molecular Physics* 34:1311-1327.

Vilar, M., I. Charalampopoulos, R. S. Kenchappa, A. Simi, E. Karaca, A. Reversi, S. Choi, M. Bothwell, I. Mingarro, W. J. Friedman, G. Schiavo, P. I. Bastiaens, P. J. Verveer, B. D. Carter, and C. F. Ibanez. 2009. Activation of the p75 neurotrophin receptor through conformational rearrangement of disulphide-linked receptor dimers. *Neuron*.62:72-83.

Vitagliano, L., Esposito L., C. Pedone and A. De Simone. 2008. Stability of single sheet GNNQQNY aggregates analyzed by replica exchange molecular dynamics: Antiparallel versus parallel association. *Biochem. and Biophys. Comm.* 377:1036-1041.

Vitagliano, L., F. Stanzione, A. De Simone, and L. Esposito. 2009. Dynamics and stability of amyloid-like steric zipper assemblies with hydrophobic dry interfaces. *Biopolymers.* 91:1161-71.

Walensky, L. D., A. L. Kung, I. Escher, T. J. Malia, S. Barbuto, R. D. Wright, G. Wagner, G. L. Verdine, and S. J. Korsmeyer. 2004. Activation of apoptosis in vivo by a hydrocarbon-stapled BH3 helix. *Science.* 305:1466-1470.

Walsh, D. M., and D. J. Selkoe. 2007. A beta oligomers-a decade of discovery. *J. Neurochem.* 101:1172-1184.

Walsh P., K. Simonetti and S. Sharpe. 2009. Core structure of amyloid fibrils formed by residues 106-126 of the human prion protein. *Structure*. 17:417-26.

Wasmer, C., A. Lange, H. Van Melckebeke, A. B. Siemer, R. Riek, B. H. Meier. 2008. Amyloid fibrils of the HET-s(218-289) prion form a beta solenoid with a triangular hydrophobic core. *Science.* 319:1523-1526.

Wehrman, T., X. He, B. Raab, A. Dukipatti, H. Blau, and K. C. Garcia. 2007. Structural and mechanistic insights into nerve growth factor interactions with the TrkA and p75 receptors. *Neuron.* 53:25-38.

Westermark, P. 2005. Aspects on human amyloid forms and their fibril polypeptides. *FEBS J.* 272:5942-5949.

Wiesmann, C., and A. M. de Vos. 2001. Nerve growth factor: structure and function. *Cell. Mol. Life Sci*. 58:748-759.

Wiesmann, C., M. H. Ultsch, S. H. Bass, and A. M. de Vos. 1999. Crystal structure of nerve growth factor in complex with the ligand-binding domain of the TrkA receptor. *Nature.* 401:184-188.

Wilcox, B. J., M. D. Applegate, C. Portera-Cailliau, and V.E. Koliatsos. 1995. Nerve growth factor prevents apoptotic cell death in injured central cholinergic neurons. *J Comp. Neurol.* 359:573-585.

Williams, B. J., M. Eriksdotter-Jonhagen, and A. C. Granholm. 2006. Nerve growth factor in treatment and pathogenesis of Alzheimer's disease. *Prog Neurobiol.* 80:114-128.

Wiltzius, J. J., M. Landau, R. Nelson, M. R. Sawaya, M. I. Apostol, L. Goldschmidt, A. B. Soriaga, D. Cascio, K. Rajashankar and D. Eisenberg. 2009. Molecular mechanisms for protein-encoded inheritance. *Nature Structural & Molecular Biology*. 16:973–978.

Wiltzius, J. J., S. A. Sievers, M. R. Sawaya, D. Cascio, D. Popov, C. Riekel, and D. Eisenberg. 2008. Atomic structure of the cross-beta spine of islet amyloid polypeptide (amylin). *Protein Sci.* 17:1467-74.

Xie, Y., M. A. Tisi, T. T. Yeo, and F. M. Longo. 2000. Nerve growth factor (NGF) loop 4 dimeric mimetics activate ERK and AKT and promote NGF-like neurotrophic effects. *J. Biol. Chem*. 275:29868-29874.

Yamazaki, T., N. Blinov, D. Wishart and A. Kovalenko.2008. Hydration effects on the HET-s prion and amyloid-beta fibrillous aggregates, studied with three-dimensional molecular theory of salvation. *Biophys. J.* 95:4540-4548.

Zampieri, N., and M. V Chao. 2004. Structural biology. The p75 NGF receptor exposed. *Science*. 304:833-834.

Zanuy, D., B. Ma and R. Nussinov. 2003. Short peptide amyloid organization: stabilities and conformations of the islet amyloid peptide NFGAIL. *Biophys. J.* 84:1884-1894.

Zheng, J., B. Ma, C. J. Tsai, and R. Nussinov. 2006. Structural stability and dynamics of an amyloid-forming peptide GNNQQNY from the yeast prion sup-35. *Biophys. J.* 91:824-833.

Zheng, J., B. Ma, and R. Nussinov. 2006. Consensus features in amyloid fibrils: sheet-sheet recognition via a (polar or nonpolar) zipper structure. *Phys. Biol.* 3:1-4.

PUBBLICATIONS

- Stanzione F., Esposito L., Paladino A., Pedone C., Morelli G., Vitagliano L. “Role of the conformational versatility of the neurotrophin N-terminal regions in their recognition by Trk receptors”. *Biophysical Journal* 2010, 99:2273-2278.

- Vitagliano L., Stanzione F., De Simone A. and Esposito L. “Dynamics and stability of amyloid-like steric zipper assemblies with hydrophobic dry interfaces”. *Biopolymers*. 2009, 91:1161-1171.

ORAL PRESENTATIONS

- Stanzione F., Paladino A., Pedone C., Morelli G., Esposito L. and Vitagliano L. “Riconoscimento molecolare tra le neurotrofine e i loro recettori: importanza della versatilità conformazionale della regione N-terminale”. *Bioinformatica e Biologia Computazionale in Campania BBCC2008, Avellino December 12th 2008.*

POSTER PRESENTATIONS

- Stanzione F., De Simone A., Esposito L. and Vitagliano L. “Structural stability and dynamical properties of steric zipper polymorphs formed by a IAPP-derived peptide.” *NETTAB-BBCC 2010, Napoli November 29th to December 1th 2010.*

- Vitagliano L., De Simone A., Pedone C., Stanzione F. and Esposito L. *“*Computational approaches for unveiling the molecular basis of amyloid-related diseases.” *12th Naples Workshop on Bioactive Peptides, Napoli June 4-7th 2010.*

- De Simone A., Esposito L., Stanzione F., Scognamiglio P.L., Marasco D. and Vitagliano L. “Unveiling analogies between amyloid-based diseases and serpinopathies: an integrated computational/experimental approach.” *Winter Modeling 2010, Pisa February 26th 2010.*

- L. Esposito, A. De Simone, F. Stanzione, C. Pedone, L. Vitagliano.”Amyloid fibers and their toxic precursors: insights from molecular dynamics simulations.” *XXXVIII Congresso Nazionale dell'Associazione Italiana di Cristallografia, Salerno September 20-23th 2009*.

- L. Esposito, A. De Simone, F. Stanzione, C. Pedone, L. Vitagliano.”Modeling of amyloid fibers and their toxic precursors: insights from molecular dynamics simulations.” *VIII European Symposium of the Protein Society, Zurich (CH) June 14-18th 2009.*

- Esposito L., De Simone A., Stanzione F., Pedone C., Vitagliano L., “Amyloid fibers: insights from molecular dynamics simulations”. *Winter Modeling 2008, Pisa December 19th 2008.*

- Stanzione F., Esposito L., Paladino A., Morelli G., Pedone C. and Vitagliano L. “Molecular recognition between neurotrophins and their receptors: role of N-teminal region.” *Scuola nazionale di chimica bioinorganica, Napoli September 14-16th 2008.*

- Stanzione F., Esposito L., Paladino A., Morelli G., Pedone C. and Vitagliano L. “Molecular recognition between neurotrophins and their receptors: a molecular dynamics approach.”*11th Naples Workshop on Bioactive Peptides, Napoli May 24-27th 2008.*

ATTENDED COURSES ANS SCHOOLS

- "CECAM-PLUMED Tutorial 2010", *Lausanne (CH) September 28th to October 1th 2010.*
- "Bioinformatica per la Proteomica (B4P)", *Avellino November 10-13th 2009.*

RESEARCH ACTIVITY IN SCIENTIFIC INSTITUTIONS ABROAD

From April 6th to May 5th 2010, the research activity of Francesca Stanzione has been carried out at the Department of Chemistry of University of Cambridge, Cambridge, United Kingdom.